Sociedade Brasileira de Vácuo

XLVII CBrAVIC
30 de Maio a 3 de Junho
Toledo - Paraná 2026

Caderno de Resumos

XLVII Congresso Brasileiro de Aplicações de Vácuo na Indústria e na Ciência

Toledo - PR

30 de maio a 3 de junho de 2026



EDITORA Donaduzzi

Dados Internacionais de Catalogação na Publicação (CIP)

C749 Congresso Brasileiro de Aplicações de Vácuo na Indústria e na Ciência (47: 2026: Toledo, PR).

Caderno de resumos do XLVII CBrAVIC [recurso eletrônico] / organizadores: Sociedade Brasileira de Vácuo, Biopark Educação. – Toledo: Editora Donaduzzi, 2026.

65 p. : il.
ISBN: 978-65-02-49100-3
DOI: 10.17563/cbravic.2026

1. Ciências aplicadas. 2. Indústria. 3. Tecnologia. I. Sociedade Brasileira de Vácuo. II. Biopark Educação. III. Título.

CDU 6
CDD 60

Ficha elaborada pela bibliotecária Priscila Rodrigues dos Santos CRB1/3381

Apresentação

O XLVII Congresso Brasileiro de Aplicações de Vácuo na Indústria e na Ciência — CBrAVIC 2026 — foi realizado em Toledo, Paraná, de 30 de maio a 3 de junho de 2026. Organizado por representantes da Sociedade Brasileira de Vácuo (SBV) e do Biopark Educação, o encontro reuniu as comunidades acadêmica, industrial e estudantil em torno da ciência e tecnologia do vácuo, dos plasmas e de suas aplicações.

A programação combinou formação técnica, conferências convidadas, sessões orais, apresentações de pôsteres e atividades voltadas à aproximação entre universidades, institutos de pesquisa, laboratórios e empresas. Os temas contemplaram superfícies, interfaces e filmes finos; ciência e tecnologia dos materiais; biomateriais; sensores e dispositivos; metrologia de vácuo; nanociência e nanotecnologia; diagnóstico de plasmas; revestimentos funcionais; e aplicações industriais, biomédicas, ambientais e agroalimentares. Duas das dez atividades formativas ocorreram em 29 de maio, antecedendo o período formal do congresso.

A edição de Toledo fortaleceu o papel do CBrAVIC como espaço de intercâmbio científico e tecnológico, formação de estudantes e profissionais e construção de redes colaborativas. O evento contou com contribuições de pesquisadores e professores vinculados a instituições brasileiras e estrangeiras, promovendo o diálogo entre conhecimento fundamental, desenvolvimento tecnológico e demandas do setor produtivo.

Estes Anais registram as contribuições técnico-científicas apresentadas no evento e preservam a memória de uma edição marcada pela internacionalização, pela diversidade temática e pela integração entre ciência, inovação e indústria.

Coordenação e comissões

Coordenação geral

Francisco Alfaro — coordenador local do CBrAVIC 2026; tesoureiro da Sociedade Brasileira de Vácuo (SBV); pesquisador do Biopark Educação.

Comitê organizador local

Integrante	Instituição / atuação
Francisco Alfaro	coordenação geral · Biopark Educação
Helton José Wiggers	Biopark Educação
Cecília Zorzi Bueno	Biopark Educação
Fernanda Heloísa Simch Guimarães	Biopark Educação
Tiago Antônio de Oliveira Mendes	Biopark Educação
Rosilei Heck Schmidt	Biopark Educação
Carla Catharina Joner Heck	Biopark Educação
Vinicius Luiz Ruschel	Biopark Educação
Andressa Caroline Simões do Nascimento	Biopark Educação
Cassia da Silva Cerri	Biopark Educação
Claudia da Silva Marques	UNIOESTE
Douglas Cardoso Dragunski	UNIOESTE

Comissão de minicursos

- Francisco Tadeu Degasperi — FATEC-SP
- Julio César Sagás — UDESC
- Francisco Alfaro — Biopark Educação

Comitê científico

Ciência e Tecnologia do Vácuo

- Marcelo Juni Ferreira — European Spallation Source (ESS)
- Francisco Tadeu Degasperi — FATEC-SP
- Denize Kalempa — USP
- Luciano do Nascimento Batista — INMETRO

Ciência e Tecnologia de Plasma

- Nilson Cristino da Cruz — UNESP
- Julio César Sagás — UDESC
- Julia Karnopp — UDESC

Ciência e Tecnologia dos Materiais

- Felipe Carneiro da Silva — FATEC-Cotia
- Álvaro José Damião — ITA
- Diego Alexandre Duarte — UFSC

Superfícies, Interfaces e Filmes Finos

- Nilson Cristino da Cruz — UNESP
- Mariana Amorim Fraga — Universidade Presbiteriana Mackenzie
- Nazir Monteiro dos Santos — pesquisador associado

Biomateriais

- Carlos Roberto Grandini — UNESP
- Mariana Amorim Fraga — Universidade Presbiteriana Mackenzie
- Diego Rafael Nespeque Corrêa — UNESP

Sensores e Dispositivos

- Álvaro José Damião — ITA
- Francisco Tadeu Degasperi — FATEC-SP
- Luciana Sgarbi Rossino — FATEC-SP
- Luciano do Nascimento Batista — INMETRO

REALIZAÇÃO E ORGANIZAÇÃO

BIOPARK EDUCAÇÃO

Sociedade Brasileira de Vácuo

FINANCIAMENTO

ARAUCÁRIA
CIÊNCIA, TECNOLOGIA E INOVAÇÃO PARA O PARANÁ

CNPq

PATROCÍNIO

HSENSOR

FCA BRASIL
SOLUÇÕES EM VÁCUO

ohmini®

NITRETAÇÃO A PLASMA

Quantum Design

Inergiae

Advancing Plasma-Based Technologies
PLASMIONIQUE
À l'Avant-Garde de Technologies Plasma

Cronologia do congresso

Data	Núcleo da programação
29 de maio	Dois minicursos para estudantes e professores de ensino médio: História da Ciência do Vácuo e Demonstrações (08h–11h) e Ensinando Ciência do Vácuo por meio da Aprendizagem Baseada em Investigação (13h30–17h)
30 e 31 de maio	Minicursos de caráter científico, tecnológico e industrial
1º de junho	Abertura, palestras convidadas e sessão de pôsteres 1
2 de junho	Sessões de vácuo na indústria e metrologia, sessão oral 1, pôsteres 2 e palestras convidadas
3 de junho	Sessão oral 2, palestras convidadas, Assembleia da SBV e encerramento

Palestras convidadas

Data	Palestrante	Instituição
01/06	Diego Mantovani	Université Laval
01/06	Mônica Alonso Cotta	UNICAMP
01/06	Rodrigo Sávio Pessoa	ITA
01/06	Sandra Rodil	UNAM
01/06	Holger Kersten	Kiel University
02/06	Elidiane Cipriano Rangel	UNESP Sorocaba
02/06	Naoya Nishi	Kyoto University
03/06	Filipe Ferreira da Silva	NOVA University Lisbon
03/06	Carlo Paternoster	Université Laval

Minicursos

Data e horário	Minicurso e ministrantes	Local
29/05 · 08h–11h	História da Ciência do Vácuo e Demonstrações Ministrantes: Álvaro José Damião; Sarah Helem Tschá	Auditório da UFPR em Toledo
29/05 · 13h30–17h	Ensinando Ciência do Vácuo por meio da Aprendizagem Baseada em Investigação Ministrantes: Álvaro José Damião; Sarah Helem Tschá	Faculdade Donaduzzi
30/05 · 08h–12h	Introdução às Tecnologias de Infravermelho para Agricultura e Biotecnologia Ministrantes: Álvaro José Damião	Faculdade Donaduzzi
30/05 · 08h30–11h30	Modelagem e cálculo de sistemas de vácuo Ministrantes: Nilberto Heder Medina; Francisco Tadeu Degasperi	Faculdade Donaduzzi
30/05 · 13h–18h	Introdução à ciência e tecnologia do vácuo Ministrantes: Francisco Tadeu Degasperi; Marcelo Juni Ferreira	Faculdade Donaduzzi
30/05 · 13h30–17h30	Vacuum Processes for Enhancing the Performances and Value to Biomaterials, Medical Devices and Pharmaceutical Products Ministrantes: Carlo Paternoster; Diego Mantovani	Faculdade Donaduzzi
31/05 · 08h–12h	Ciência e Tecnologia de Filmes Finos Ministrantes: Julio César Sagás	Faculdade Donaduzzi
31/05 · 08h30–11h30	Introdução à metrologia do vácuo com cálculo de incertezas Ministrantes: Francisco Tadeu Degasperi; Luciano do Nascimento Batista	Faculdade Donaduzzi
31/05 · 13h30–17h30	Determination of Particle-, Momentum-, and Energy-fluxes Toward Surfaces in Plasma Processing Ministrantes: Holger Kersten	Faculdade Donaduzzi
31/05 · 13h30–17h30	Introdução à dinâmica dos gases rarefeitos: teoria e aplicações aos sistemas de vácuo Ministrantes: Felix Sharipov; Francisco Tadeu Degasperi	Faculdade Donaduzzi

Sessão especial

Vácuo na Indústria e Metrologia do Vácuo

Realizada na manhã de 2 de junho de 2026, a sessão temática foi organizada em duas partes e reuniu docentes, pesquisadores e profissionais de empresas, laboratórios e centros de metrologia. As apresentações abordaram detecção de vazamentos, metrologia aplicada, dinâmica de gases rarefeitos, liofilização, sistemas com alta pressão parcial de água, práticas metrológicas e desenvolvimento de câmaras de vácuo para aplicações industriais.

A atividade evidenciou a articulação entre fundamentos científicos, rastreabilidade metrológica, instrumentação e demandas do setor produtivo, reforçando a aproximação entre universidade, centros de pesquisa, laboratórios e indústria.

Horário	Tema	Participantes e instituições
PARTE I 08h30	A detecção de vazamentos aplicada às atividades industriais e de serviços	Fernando Zappellini — Haretest
08h50	Metrologia: importância para a indústria, os serviços e a pesquisa	Luciano Batista Nascimento — LAPRE/Inmetro
09h10	Metrologias térmica e de pressão para a indústria e os serviços	Rodrigo Cordeiro; André Chaves — Grupo Elus – Metrologia
PARTE II 10h00	Como a dinâmica dos gases rarefeitos pode potencializar o cálculo e os projetos de sistemas de vácuo industriais?	Denize Kalempa — EEL/USP; Francisco Tadeu Degasperi — Fatec-SP/CEETEPS
10h30	Aplicações da liofilização nos sistemas biológicos e o processo de dessalinização com térmica e vácuo	Sílvia Pierre Irazusta — Fatec-Sorocaba/CEETEPS
10h50	Sistemas de vácuo industriais com alta pressão parcial de água: soluções com métodos e instrumentação	Fernando Schneider — Busch do Brasil
11h10	Práticas e necessidades da metrologia de vácuo: indústria e centros de pesquisa	Hugo A. Garrido Aguiar — Centro Tecnológico de Metrologia (CTM Ltda.)
11h30	Câmaras de vácuo especiais para o setor industrial	Fernando Arroyo — FCA – Usinagem Brasil Ltda.
11h50	Encerramento da sessão	Francisco Tadeu Degasperi — Fatec-SP/CEETEPS

Relação dos resumos publicados

Comunicações orais — 6 trabalhos

Identif.	Título do resumo	Página
1	EVAPORATION OF A COPPER DROPLET IN ARGON GAS	12
2	Comparative Effects of Surfatron-Generated Plasma-Activated Water and Hydrogen Peroxide on Growth Kinetics and the Saccharidic Fraction of EPS in Escherichia coli ATCC 25922	13
4	INFLUENCE OF APPLIED VOLTAGE IN THE PEO PROCESS ON THE THICKNESS AND MICROHARDNESS OF AZ31 AND TI25TA35NB3SN ALLOYS	14
5	INFLUENCE OF APPLIED VOLTAGE ON ELECTROLYTE TEMPERATURE, COATING THICKNESS AND MICROHARDNESS OF PEO COATINGS ON AZ31 ALLOY	15
27	CONTROL OF INTERFACIAL CONTACT RESISTANCE AND WETTABILITY IN TIN FILMS BY ION ENERGY AND NITROGEN SUPPLY FOR PEMFC APPLICATIONS	16
57	DEVELOPMENT OF PH-RESPONSIVE HYDROGELS	18

Pôsteres — 46 trabalhos

Identif.	Título do resumo	Página
3	MODULATING ZnO THIN FILM STOICHIOMETRY AND CORROSION DYNAMICS: LINKING OXYGEN-TO-ARGON GAS RATIOS TO ELECTROCHEMICAL STABILITY	20
6	CHANGES IN THE SHAPE OF THE NbN REACTIVE SPUTTERING HYSTERSIS CURVE WITH THE CONTROL PARAMETER OF THE DISCHARGE	21
7	IMPLEMENTATION OF DYNAMIC SPUTTER YIELDS FOR REACTIVE MAGNETRON SPUTTERING MODELING OF NbN DEPOSITION	22
8	PLASMA NITRIDING WITH CATHODIC CAGE OF SS 304 ON CORROSION AND WEAR PROPERTIES	23
9	STERILIZATION OF DENTAL IMPLANTS USING PLASMA-ACTIVATED WATER (PAW) WITH ANTIMICROBIAL ACTIVITY GENERATED BY NON-THERMAL ATMOSPHERIC PLASMA	24
10	On the Adhesion of a-C:H Coatings Deposited by PECVD on PDMS for Biomedical Applications	25
12	CORRELATION BETWEEN PLASMA CHARACTERISTICS AND OIL-METHANOL EMULSION IN DBD REACTOR FOR BIODIESEL PRODUCTION	26
13	EVALUATION OF DYE-SENSITIZED SOLAR CELLS WITH Nb2O5-TiO2 SINGLE-LAYER PHOTOANODES	27
14	TAILORING MG-BASED ALLOYS VIA SURFACE FINISHING AND PLASMA PROCESSING FOR BIOMEDICAL APPLICATIONS	28
15	OPTICAL AND SURFACE PROPERTIES OF Nb2O5 THIN FILMS GROWN BY DC-PULSED MAGNETRON SPUTTERING	29
16	POROSITY MEASUREMENTS IN 316L STEEL SINTERED BY ADDITIVE MANUFACTURING	30
17	DESIGN AND CHARACTERIZATION OF A 4 LAYERS TIO2/SIO2 OPTICAL COATING USING THE OPTILAYER SOFTWARE	31
18	PROCESS OPTIMIZATION FOR THE DEVELOPMENT OF ZnO THIN FILM RESISTORS WITHOUT PHOTOLITHOGRAPHY	32
19	AUTOMATED RADIOMETRIC CHARACTERIZATION OF INFRARED SENSORS USING THE RADIOMÉTRICA SOFTWARE	33
21	INFLUENCE OF ELECTRODEPOSITION TIME OF THE NiCoFeCrMn ALLOY ON THE MORPHOLOGY OF SAE 1020 STEEL	34
22	STUDY OF DIFFERENT POWDERS FOR THE BORONIZATION OF AISI 304 STAINLESS STEEL	35
24	DESIGN AND DEVELOPMENT OF A DIDACTIC PLASMA NITRIDING CHAMBER	36
26	HIGH-HEAT-FLUX PERFORMANCE OF THERMAL BARRIER COATINGS FOR ATMOSPHERIC REENTRY	37
28	SMART CHITOSAN FILMS WITH ALGINATE NANOPARTICLES FOR ON-DEMAND GENTAMICIN RELEASE	38
29	SUBSTRATE-DEPENDENT WETTABILITY AND HYDROPHOBIC RECOVERY OF PE AND PDMS UNDER IDENTICAL PLASMA TREATMENT	39
31	EXPLORING THE POTENTIAL OF OIL AND GAS DRILLING TECHNOLOGIES IN NATURAL HYDROGEN EXTRACTION	40
32	EFFECT OF APPLIED FREQUENCY ON THE FORMATION OF REACTIVE SPECIES AND THE PHYSICOCHEMICAL PROPERTIES OF PLASMA-ACTIVATED WATER	41
33	POTENTIAL ANTIMICROBIAL ACTIVITY OF MULTI-WALLED CARBON NANOTUBES (MWCNTs) OBTAINED BY DIFFERENT SYNTESIS METHODS: A COMPARATIVE STUDY	42
35	Modification of the Structure and Properties of TiN_x Films with Nitrogen Concentration	43
36	COMPARATIVE EFFICIENCY OF PIN AND DBD PLASMA REACTORS IN THE DEGRADATION OF RHODAMINE B AND METHYLENE BLUE	44
37	BIOPOLYMER NANOPARTICLES WITH HIGH MUCOADHESION TO IMPROVE ANTIBIOTIC RETENTION IN MUCOSAL INFECTIONS	45

Identif.	Título do resumo	Página
38	CONTROLLING ANTIBIOTIC RELEASE IN CHITOSAN FILMS: FROM MOLECULAR INTERACTIONS TO LONG-TERM PERFORMANCE	46
40	CHARACTERIZATION OF A REMOTE PLASMA JET USING LISSAJOUS FIGURES	47
41	INFLUENCE OF HEAT FLUX AND EXPOSURE TIME ON SURFACE ROUGHNESS OF YSZ THERMAL BARRIER COATINGS	48
42	INFLUENCE OF THERMAL ANNEALING ON THE MORPHOLOGICAL AND OPTICAL PROPERTIES OF Nb2O5 THIN FILMS DEPOSITED BY PULSED DC MAGNETRON SPUTTERING	49
43	PLASMA-ASSISTED SURFACE FUNCTIONALIZATION OF THERMOPLASTIC STARCH FILMS FOR NISIN-BASED ANTIMICROBIAL APPLICATIONS	50
44	Optimization of $CaCl_2$ Concentration in Edible Film Formation	51
45	CONTROLLED SYNTHESIS OF SILVER NANOPARTICLES VIA DIELECTRIC BARRIER DISCHARGE PLASMA–LIQUID INTERACTION	52
46	GRAPHENE: NANOMATERIAL SYNTHESIS IN CONNECTION WITH THE LOCAL PRODUCTIVE ARRANGEMENT	53
47	ENGINEERING ELECTROSPUN PVA NANOFIBERS WITH PORCINE LIVERBIOACTIVES FOR ANTIMICROBIAL DRESSINGS AND CHRONIC WOUND HEALING	54
48	FROM PATENT TO PRODUCTION: THE CIMENT COMPOSITE DEVELOPMENT CASE	55
49	TRANSESTERIFICATION REACTION CATALYZED BY NANOPOWDER CALCIUM OXIDE ASSISTED BY PLASMA	56
50	ELECTROSTATIC STUDY OF CAPACITIVE COUPLING IN REMOTE PLASMA JET SYSTEMS	57
51	PLASMA-SUBSTRATE INTERACTIONS DURING LOW-VACUUM PLASMA TREATMENT OF THERMOPLASTIC STARCH FILMS FOR CHITOSAN COATING RETENTION	58
52	MODELING OF A HIGH-VACUUM SYSTEM WITH CUBOID GEOMETRY USING THE MONTE CARLO METHOD	59
53	METHOD-DEPENDENT ANTIMICROBIAL EVALUATION OF PLASMA-TREATED SURFACES	60
54	ANTIMICROBIAL ACTIVITY OF CARVACROL AND ZINC NANOPARTICLES IN POLYLACTIC ACID AND STARCH BLENDS	61
55	METROLOGICAL PRESSURE SYSTEM: MERCURY MANOMETER, VACUSTAT™, BOURDON PRESSURE GAUGE, CAPACITIVE MEMBRANE PRESSURE AND MICRO PIRANI™VACUUM TRANSDUCER.	62
56	CUSTOM-DESIGNED PERMEABILITY APPARATUS FOR GAS BARRIER CHARACTERIZATION UNDER CONTROLLED VACUUM-ATMOSPHERE CONDITIONS	63
58	LOW PRESSURE PLASMA FOR FABRIC DESINFECTION	64
59	POTENTIAL DISINFECTION OF FABRICS IN LOW-PRESSURE PLASMAS USING SODIUM CHLORITE AS A CHLORINE SOURCE	65

Comunicações orais

EVAPORATION OF A COPPER DROPLET IN ARGON GAS

Denize Kalempa[1]*, Felix Sharipov[2]
[1] *Escola de Engenharia de Lorena, Universidade de São Paulo, Lorena, 12602-810l*
[2]*Departamento de Física, Universidade Federal do Paraná, Caixa Postal 19044, Curitiba, 81531-980*

1. Introduction

Modeling evaporation of metal droplets in a rarefied gas is very important for accurately describing processes involving molten metals. In this kind of system, the metal evaporates into a mixture consisting of its own vapor and a background non-condensable gas. The evaporation rate and the energy flux depend on several parameters, e.g. temperature, mixture pressure, gas composition, and droplet radius. Non-equilibrium phenomena arising in the vicinity of the droplet, i.e. in the Knudsen layer, can be properly described by methods of rarefied gas dynamics based on either the Direct Simulation Monte Carlo method or solution of kinetic models for the Boltzmann equation. In the framework of rarefied gas dynamics, there are many papers in the literature concerning evaporation and condensation phenomena in a pure vapor or in a vapor with a non-condensable gas, e.g. Refs. [1-3]. However, the hard-spheres model of intermolecular interaction and hypothetical molecular masses are usually used, which may not accurately capture the complexities of real molecular interactions. In the present work, the evaporation of a copper droplet in argon gas at the temperature 2000 K is modeled with basis on a kinetic model for the linearized Boltzmann equation. The mass and energy flow rates are calculated numerically for various values of gas rarefaction parameter and molar fraction of argon in the vapor–gas mixture.

2. Method of solution

Similarly to our previous paper [4], the model proposed by McCormack [5] for the linearized Boltzmann equation is used, with the assumption of complete evaporation at the surface as the boundary condition. The interatomic interactions are simulated using *ab-initio* potentials argon-argon, copper-copper and copper-argon collisions. The macroscopic quantities of interest are calculated in terms of the distribution function of molecular velocities. The discrete velocity method is the numerical technique used to solve the system of kinetic equations numerically. The calculations are carried out in a wide range of the gas rarefaction degree, which depends on the gas pressure and temperature, and droplet radius, so that the free molecular, transitional and slip flow regimes are covered. The influence of molar fraction of argon in the mixture on the solution of the problem is carefully analyzed.

2. Results and Discussions

The dimensional mass and energy flow rates are obtained assuming a small temperature difference of 0.1 K between the spherical surface and the surrounding equilibrium gas. Under this condition, the mass flux is always positive, indicating a net transfer of mass from the sphere to the gaseous phase. This corresponds to evaporation being the dominant process. The heat flux, however, may be either positive or negative. This means that thermal energy can flow either from the sphere to the gas or from the gas toward the sphere, depending on the combined effects of thermal gradients, rarefaction, and mixture composition. Despite this, the total energy flux is always positive, i.e., it is directed outward from the spherical surface. Therefore, energy is consistently transferred from the hotter region (the sphere) to the colder region in the surrounding gas medium. The calculated mass and energy flow rates depend strongly on both the rarefaction parameter and the molar fraction of the gas mixture. For a fixed rarefaction parameter, increasing the molar fraction of argon reduces both the mass flux and the total energy flux at the spherical surface. These results indicate that the evaporation of a metal droplet in a rarefied gas can be enhanced or even controlled by adjusting the molar fraction of the background gas..

4. References

[1] P. Pao, Phys. Fluids 14, 306–312 (1971).
[2] K. Aoki, S. Takata, S. Kosuge, Phys. Fluids 10, 1519–1533 (1998).
[3] C. E. Siewert, Eur. J. Mech. B/Fluids 22, 391–408 (2003).
[4] D. Kalempa, F. Sharipov, I. Graur, Int. J. Heat and Mass Transfer 256, 128021 (2026).
[5] F. J. McCormack, Phys. Fluids 16, 2095–2105 (1973).98).

Acknowledgments

D. Kalempa acknowledges FAPESP (Fundação de Amparo à Pesquisa do Estado de São Paulo), Brazil for the support of the research, grant 2022/10476-1. F. Sharipov acknowledges CNPq (Conselho Nacional de Desenvolvimento Científico e Tecnológico), Brazil , grant 303429/2022-4.

*Corresponding author: kalempa@usp.br

Comparative Effects of Surfatron-Generated Plasma-Activated Water and Hydrogen Peroxide on Growth Kinetics and the Saccharidic Fraction of EPS in *Escherichia coli* ATCC 25922

Eduardo Ferreira Martins[1], Marina Clara Ribeiro dos Santos[1], Alvaro Busquet de Sant'Anna Junior[1], Jade Helena Campos Augustroze[1], Alice Loureiro Martins[2], Michael dos Santos Brito[2], Sonia Khouri Sibelino[1], Argemiro Soares da Silva Sobrinho[1], Rodrigo Sávio Pessoa[1]

[1]Plasmas and Processes Laboratory (LPP), Aeronautics Institute of Technology (ITA), 12228-900, São José dos Campos-SP, Brazil.

[2]Plant Biotechnology Laboratory (Plantech), Institute of Science and Technology of the Federal University of São Paulo (ICT-UNIFESP), 12231-280, São José dos Campos-SP, Brazil.

1. Introduction

Plasma-activated water (PAW) has attracted increasing attention as an antimicrobial medium due to the formation of reactive oxygen and nitrogen species (RONS) during plasma–liquid interactions. These species can induce oxidative stress and affect bacterial physiology and survival. Although hydrogen peroxide (H_2O_2) is often one of the major long-lived species present in PAW, its antimicrobial activity is thought to result from the combined action of multiple oxidizing agents rather than a single compound [1,2]. In this study, we investigated the effects of PAW generated by a microwave plasma Surfatron reactor on the growth dynamics of *Escherichia coli* and compared these effects with those produced by defined concentrations of hydrogen peroxide.

2. Experimental or Theory depending on the paper's subject

E. coli cultures were grown in liquid medium and exposed to PAW or to H_2O_2 solutions prepared at concentrations comparable to those measured in PAW. Bacterial growth was monitored by spectrophotometric measurements of optical density at 600 nm (OD_{600}), allowing the construction of detailed growth curves and evaluation of the lag, exponential, and stationary phases [3,4]. Optical density data were interpreted considering established relationships between OD measurements and microbial population density [5,6]. In parallel, viable cell counts were determined by plating serial dilutions to quantify colony forming units ($CFU \cdot mL^{-1}$). Extracellular polymeric substances (EPS) production was also quantified using a colorimetric carbohydrate assay following EPS extraction from the cultures.

3. Results and Discussions

Exposure to PAW resulted in a measurable delay in the onset of the exponential growth phase and a reduction in bacterial growth rate compared with untreated controls. Viable cell quantification showed a decrease in $CFU \cdot mL^{-1}$ during the early growth stages under PAW treatment. Furthermore, EPS production was significantly affected, suggesting that oxidative stress induced by plasma-generated species interferes with metabolic pathways related to extracellular matrix formation. In several experimental conditions, PAW exhibited stronger inhibitory effects than equivalent concentrations of hydrogen peroxide alone.

These results indicate that the antimicrobial activity of PAW cannot be explained solely by hydrogen peroxide and likely involves the synergistic action of multiple plasma-generated reactive species. The findings contribute to the understanding of how plasma-treated liquids influence bacterial growth dynamics and extracellular polymer production.

4. References

[1] Imlay, J.A. *The molecular mechanisms and physiological consequences of oxidative stress: lessons from a model bacterium.* **Nat. Rev. Microbiol.** (2013).

[2] Wong, K.S. et al. *Plasma-Activated Water: Physicochemical Properties and Applications.* **Processes** (2023).

[3] Pletnev, P. et al. *Survival guide: Escherichia coli in the stationary phase.* **Microbiology** (2015).

[4] Rolfe, M.D. et al. *Lag Phase Is a Distinct Growth Phase That Prepares Bacteria for Exponential Growth.* **mBio** (2012).

[5] Mira, P.M. et al. *Estimating microbial population data from optical density.* **PLOS ONE** (2022).

[6] Stevenson, K. et al. *General calibration of microbial growth in microplate readers.* **Sci. Rep.** (2016).

Acknowledgments

CAPES (Code 001) and FAPESP (Process: 19/05856-7)

* Corresponding author: eduardomartins@ita.br

INFLUENCE OF APPLIED VOLTAGE IN THE PEO PROCESS ON THE THICKNESS AND MICROHARDNESS OF AZ31 AND TI25TA35NB3SN ALLOYS

Juliana Layber Mota Engelhardt[1,2], Henrique Engelhardt[1,2], Rafael Resende Lucas[1], André Luiz Reis Rangel[1], Ana Paula Rosifini Alves Claro[1], Rogério Pinto Mota[1]

[1]*São Paulo State University (UNESP), School of Engineering and Sciences, São Paulo, Brazil*
[2]*Fluminense Federal Institute of Education, Science and Technology (IFF), Campos dos Goytacazes, Brazil.*

1. Introduction

Plasma Electrolytic Oxidation (PEO) produces adherent and porous ceramic coatings that improve corrosion resistance, wear resistance, and bioactivity [1]. The process is governed by applied voltage, which controls microdischarges and coating properties. AZ31 magnesium alloys exhibit biodegradability but high corrosion, while β-type Ti25Ta35Nb3Sn alloys show high corrosion resistance but lower bioactivity [2,3]. Thus, this study evaluates the effect of applied voltage on coating thickness and microhardness, comparing both substrates.

2. Experimental

Commercial AZ31 alloy (10 × 10 mm, ground to 320 mesh) and Ti25Ta35Nb3Sn discs (10 mm × 4 mm, 80–800 mesh) were treated by PEO using the same pulsed DC source (T2S PS-2, duty cycle 60%). AZ31 was processed at 260, 320, and 460 V for 180 s in calcium glycerophosphate (0.07 $g \cdot L^{-1}$), while Ti was treated at 350, 450, and 550 V for 360 s in an electrolyte containing calcium glycerophosphate (0.0042 $g \cdot L^{-1}$), calcium acetate (0.0316 $g \cdot L^{-1}$), and sodium phosphate (1.56 $g \cdot L^{-1}$). Microhardness (Vickers) was measured at 5 N (AZ31) and 10 N (Ti) for 10 s, and thickness by eddy current.

3. Results and Discussions

The thickness (μm) and microhardness (HV) results as a function of the applied voltage (V) are shown in figures 1 (Ti25Ta35Nb3Sn) and 2 (AZ31). The applied voltage controls the energy of microdischarges and, consequently, the coating growth and properties [4,5]. For AZ31 (Fig. 2), thickness increased from 71.6 to 148.8 μm (260–320 V) and decreased to 118.1 μm at 440 V ($p < 0.05$), indicating greater stability at intermediate voltages. For Ti25Ta35Nb3Sn (Fig. 1), thickness increased with voltage, reaching 295.1 μm at 550 V ($p < 0.001$), evidencing higher process stability in Ti alloys [3]. Microhardness also varied with voltage: for AZ31, it reached 220.8 HV at 440 V, while for Ti the maximum value occurred at 450 V (388.6 HV), decreasing at 550 V, likely due to increased porosity and defects at higher voltages [5]. These differences are related to the higher reactivity of Mg, which requires lower voltages, and the higher stability of Ti, which supports higher voltages. Therefore, the applied voltage is a key parameter in PEO, influencing thickness and microhardness depending on the substrate.

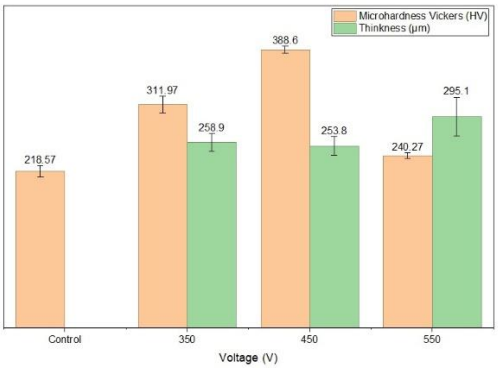


Fig. 1. *Effect of applied voltage on coating thickness and microhardness of Ti25Ta35Nb3Sn alloy.*

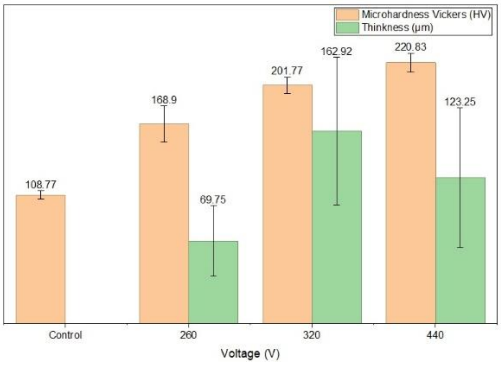


Fig. 2. *Effect of applied voltage on coating thickness and microhardness of AZ31 alloy.*

4. References

[1]- G. Giavaresi et al., *Int. J. Mol. Sci.*, 25, 282, (2023).
[2]- M. Rizwan et al., *J. Biomed. Mater. Res. A*, 106, 590–605, (2018).
[3]- S. Bahl, S. Suwas and K. Chatterjee, *Int. Mater. Rev.*, 66, 114–139, (2021).
[4]- T. Hryniewicz, *Metals*, 8, 1058, (2018).
[5]- L. Fu et al., *Coatings*, 9, 826, (2019).

Acknowledgments
The authors thank IFF, UNESP-FEG, and the Graduate Program in Engineering for their support.

*Corresponding author: juliana.mota@unesp.br

INFLUENCE OF APPLIED VOLTAGE ON ELECTROLYTE TEMPERATURE, COATING THICKNESS AND MICROHARDNESS OF PEO COATINGS ON AZ31 ALLOY

Henrique Engelhardt[1,2], Juliana Layber Mota Engelhardt[1,2], Rafael Resende Lucas[1], André Luiz Reis Rangel[1], Rogério Pinto Mota[1]

[1]*São Paulo State University (UNESP), School of Engineering and Sciences, São Paulo, Brazil*
[2]*Fluminense Federal Institute of Education, Science and Technology (IFF), Campos dos Goytacazes, Brazil.*

1. Introduction

Magnesium alloys, particularly AZ31, have attracted attention for structural and biomedical applications due to their low density and favorable mechanical properties. However, their high corrosion rate limits practical applications. Surface modification techniques, such as Plasma Electrolytic Oxidation (PEO), have been widely used to improve surface properties by forming ceramic coatings with enhanced mechanical performance [1]. The properties of PEO coatings are strongly influenced by processing parameters, especially the applied voltage, which directly affects plasma discharge behavior, thermal evolution, and coating growth mechanisms [1,2]. In this context, this study aims to evaluate the influence of applied voltage on electrolyte temperature evolution, coating thickness, and microhardness of PEO coatings formed on AZ31 alloy.

2. Experimental

AZ31 magnesium alloy samples were subjected to PEO treatment using a DC power supply under three voltage conditions: 260 V, 320 V, and 440 V, with a processing time of 180 s. The electrolyte consisted of a calcium glycerophosphate solution. The electrolyte temperature was monitored throughout the process. Coating thickness was measured using the eddy current technique, and microhardness was evaluated by Vickers microindentation. Statistical analysis was performed using ANOVA with a significance level of 5%.

3. Results and Discussions

The electrolyte temperature increased during the PEO process for all conditions (Fig. 1), with higher values at higher voltages. The 440 V condition showed the highest temperature variation, indicating a more energetic discharge regime [1,2]. As shown in Fig. 2, coating thickness exhibited a non-linear behavior, with maximum values at 320 V. At 440 V, no proportional increase in thickness was observed, likely due to competing effects such as localized dissolution [2]. Microhardness increased with applied voltage, reaching its highest values at 440 V, due to enhanced coating densification under more energetic conditions [3]. Overall, 320 V provides the best balance between thickness and stability, while 440 V favors higher microhardness.

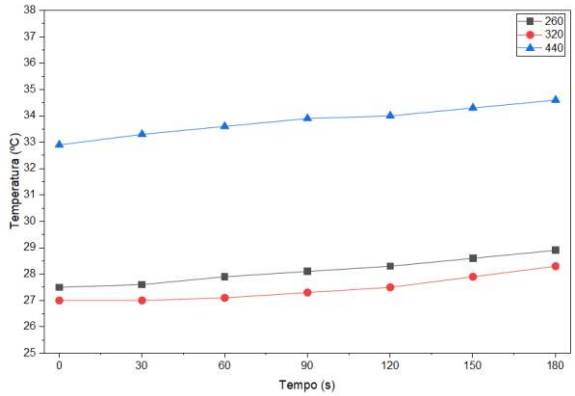


Fig. 1. *Electrolyte temperature evolution as a function of time during the plasma electrolytic oxidation (PEO) process under different applied voltages (260 V, 320 V, and 440 V).*

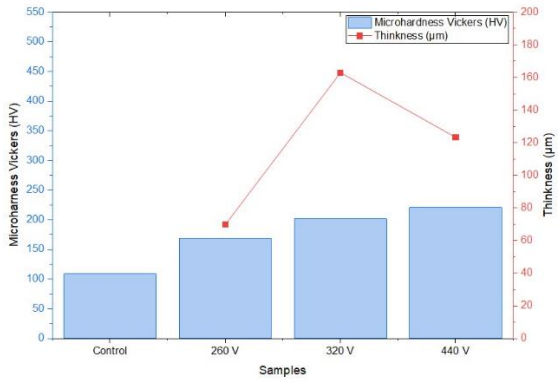


Fig. 2. *Variation of coating thickness and microhardness as a function of applied voltage, showing non-linear thickness behavior and increased hardness with higher energy input during the PEO process.*

4. References

[1] Simchen et al., *Coatings,* 10, 628 (2020).
[2] Mohedano and Mingo, *Coatings,* 11, 111 (2021).
[3] Rizwan et al., J. *Biomed. Mater. Res.,* 106, 590 (2018)

Acknowledgments

The authors thank IFF, UNESP-FEG, and the Graduate Program in Engineering for their support.

*Corresponding author: h.engelhardt@unesp.br

CONTROL OF INTERFACIAL CONTACT RESISTANCE AND WETTABILITY IN TIN FILMS BY ION ENERGY AND NITROGEN SUPPLY FOR PEMFC APPLICATIONS

*Felipe Carneiro da Silva**[1,2], Julio César Sagás[3], Mengying Wang[4], Cláudio Geraldo Schön[2], Xungang Diao[4], Luis Cesar Fontana[3]

[1]*State Center of Technological Education Paula Souza, São Paulo State Technological College, Department of Production Management, Brazil*

[2]*Universidade de São Paulo (USP), Department of Metallurgical and Materials Engineering, São Paulo, Brazil*

[3]*UDESC, Santa Catarina State University, Laboratory of Plasmas, Films and Surfaces, Joinville, SC, Brazil*

[4]*School of Energy and Power Engineering, Beihang University, Beijing 100191, PR China*

1. Introduction

The development of cost-effective and lightweight bipolar plates is essential for the large-scale application of proton exchange membrane fuel cells (PEMFCs). Bipolar plates account for approximately 70% of the total system weight and about 40% of the overall production cost, making material selection a critical factor their widespread commercialization [1]. The use of transition metal nitride coatings, such as titanium nitride (TiN), has been widely investigated due to their excellent chemical stability, corrosion resistance, and electrical conductivity under harsh PEMFC operating conditions (pH 2-4, working temperature ~ 70^{0}C) [2]. This work investigates the effect of substrate bias voltage and nitrogen supply mode (homogeneous and graded) on the interfacial contact resistance and wettability of TiN films deposited on AA5052 aluminum, aiming to optimize their performance for PEMFC bipolar plate applications.

2. Experimental

AA5052 aluminum substrates were mechanically ground and subsequently polished with 1 µm diamond paste. Prior to TiN deposition, a titanium interlayer (Ti) was applied to enhance adhesion at the film/substrate interface. TiN coatings were deposited by grid-assisted magnetron sputtering (GAMS) under different substrate bias voltages (Ub = -40 V and -100 V) and nitrogen supply modes, namely homogeneous (constant flow 8 sccm) and graded (increasing nitrogen flow during deposition until achiebe 8 sccm), producing films with distinct compositional profiles. The interfacial contact resistance (ICR) was measured under a compressive load of 150 $N \cdot cm^{-2}$ after corrosion testing performed in a 0.5 M H_2SO_4 solution at 70 °C for 1 h, simulating PEMFC operating conditions. Wettability was evaluated by water contact angle measurements using the sessile drop method. Film morphology and thickness were analyzed by scanning electron microscopy (SEM).

3. Results and Discussions

SEM images (Fig1) revealed a dense and homogeneous TiN coatings with thicknesses ranging from approximately 1.5 to 2 µm. The grain size was approximately 100 nm for all deposition conditions.The interfacial contact resistance (ICR) results demonstrated a clear dependence on both substrate bias voltage (Ub) and nitrogen supply mode. Homogeneous TiN coatings consistently exhibited lower ICR values compared to graded films. The best performance was obtained for the homogeneous film deposited at Ub = -100 V, reaching 13.7 $m\Omega \cdot cm^2$ (Table 1). This behavior is attributed to enhanced ion bombardment energy, which promotes film densification and improves the effective contact area at the interface. In contrast, graded TiN coatings showed higher ICR values, suggesting that compositional gradients may introduce heterogeneities that reduce the effective electrical contact. These findings indicate that, under the investigated conditions, electrical performance is primarily governed by film densification rather than compositional grading.

*Corresponding author: felipe.carneiro01@fatec.sp.gov.br

Table 1: Interfacial contact resistance (ICR) values for TiN films obtained under different deposition parameters

U_b (V)	nitrogen supply mode	ICR (mΩ·cm²)
- 40	graded	17.1 ± 0.7
- 100	graded	16.4 ± 0.9
- 40	homogeneous	15.5 ± 0.9
- 100	homogeneous	13.7 ± 0.8

Wettability measurements revealed a distinct trend compared to ICR (Table 2). Graded films exhibited higher hydrophobicity, with contact angles reaching approximately 104° (U_b = - 40 V). This suggests that nitrogen supply mode significantly affects surface energy and water management properties. Overall, an inverse relationship between ICR and wettability was observed, indicating a trade-off between electrical conductivity and hydrophobicity. These results highlight that substrate bias voltage and nitrogen supply mode can be used as effective tools to tailor the functional performance of TiN coatings depending on the specific requirements of PEMFC bipolar plates.

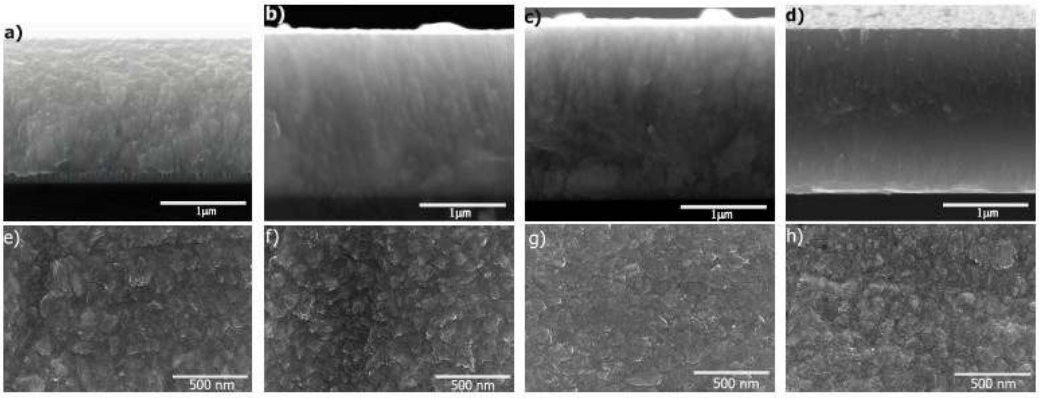


Figure 1: SEM images of cross-sectional morphology (a-d) and surface morphology (e-h) of TiN coatings deposited at different conditions: a-e: - 40 V homogeneous; b-f: - 100 V homogeneous;c-g: - 40 V graded; d-h: - 100 V graded

Table 2: Water contact angle measurements for TiN coatings.

Condition	Water Contact Angle (°)
Graded – 40 V	104.8 ± 0.2
Graded – 100 V	98.7 ± 0.5
Homogeneous – 40 V	88.8 ± 1.0
Homogeneous – 100 V	102.9 ± 0.2

4. References

[1]- F. C. Silva *et. al.* International Journal of Hydrogen Energy, 45, 33993–34010, (2020).

[2]- J. Lin, *et. al.* Journal of Power Sources, 662, 238701, (2026)

Acknowledgments

FCS would like to thank the National Council for Scientific and Technological Development – CNPq for the grant 405196/2023-7 and FAPESP for the grant 2025/07129-6. The authors are thankful for the Multi-User Facility infrastructure from Santa Catarina State University's Technological Sciences Center.

*Corresponding author: felipe.carneiro01@fatec.sp.gov.br

DEVELOPMENT OF PH-RESPONSIVE HYDROGELS

Thomas Lima Albuquerque[1]*, Schirlei Diana Kleinubing Silva[1], Hugo Mauricio Tiggemann[1]
[1]*Pharmacy course, Faculdade Donaduzzi – Toledo-PR*

1. Introduction

PH-responsive hydrogels have attracted increasing interest in the field of biomaterials due to their ability to modify physicochemical properties according to environmental pH variations, enabling applications focused on controlled drug delivery. These systems show potential for the treatment of pressure ulcers, chronic lesions that represent an important public health issue, especially in elderly and bedridden patients [1,2]. Under physiological conditions, skin pH presents a slightly acidic character; however, in infected lesions, this value tends to increase, favoring bacterial proliferation and impairing the healing process. In this context, smart hydrogels have been investigated as promising systems for selective response to pH changes and controlled release of active substances. Previous studies have already described different formulations of pH-responsive hydrogels using bio-nanocomposites and ultrasensitive matrices [3,4]. Therefore, the present work proposes the development of a hydrogel formulated from chitosan, carboxymethylcellulose, sodium alginate, and hyaluronic acid associated with Clindamycin, aiming to obtain a system with potential for selective and controlled antibiotic release, promoting infection treatment and the healing process in pressure ulcers.

2. Experimental

Three pH-responsive hydrogel formulations were developed using chitosan, carboxymethylcellulose, and sodium alginate at a 0.2:4:1 ratio, varying the acetic acid concentration and the addition rate of the crosslinking agent. The formulations presented pH values between 4.8 and 4.9 and used sodium tripolyphosphate (TPP) as the crosslinking agent, incorporated by controlled dripping under mechanical stirring. After hydrogel formation, the samples were frozen in an ultra-freezer and subjected to lyophilization. Preliminary characterization was performed through swelling assays in distilled water, phosphate buffer solution (pH 7.2), and acidic buffer solution (pH 5.6) at intervals of 30 minutes, 1 hour, and 24 hours. In addition to mass variation, structural and visual changes in the formulations after exposure to the different media were also evaluated.

3. Results and Discussions

The developed hydrogels showed high water absorption capacity and porous structure after lyophilization. Hydrogel 01 presented low structural stability, undergoing disintegration after approximately 1 hour of testing, indicating insufficient crosslinking of the polymeric matrix. In contrast, Hydrogels 02 and 03 showed better homogeneity, lower formation of aggregates, and greater structural stability during the assays. In distilled water, both hydrogels demonstrated a high swelling degree, with maximum values exceeding 1600%, reaching approximately 1692% for Hydrogel 02 and 1923% for Hydrogel 03 after 24 hours. In neutral buffer solution (pH 7.2), Hydrogel 03 showed higher water absorption and better structural integrity, reaching a final mass of 30.56 g or 2350% after 24 hours. In acidic medium (pH 5.6), both hydrogels maintained high swelling capacity; however, Hydrogel 03 demonstrated greater firmness and stability of the polymeric network when compared to Hydrogel 02, indicating better pH-responsive behavior.

4. References

[1]- G. R. Alves, S. G. Malaquias and M. M. Bachion, Rev. Eletr. Enf., 20, (2018). https://doi.org/10.5216/ree.v20.49411
[2]- A. C. Oliveira, D. M. Rocha, S. M. G. Bezerra, E. M. L. R. Andrade, A. M. R. Santos and L. T. Nogueira, Acta Paul. Enferm., 32(2), 194-201, (2019). https://doi.org/10.1590/1982-0194201900027
[3]- P. Gupta et al., Drug Discovery Today, 7(10), 569-579, (2002). https://doi.org/10.1016/S1359-6446(02)02255-9
[4]- I. S. Bayer, Pharmaceutics, 15, 1364, (2023). https://doi.org/10.3390/pharmaceutics15051364

Acknowledgments
Faculdade Donaduzzi.

*Corresponding author: thomas.albuq.99@gmail.com

Pôsteres

MODULATING ZnO THIN FILM STOICHIOMETRY AND CORROSION DYNAMICS: LINKING OXYGEN-TO-ARGON GAS RATIOS TO ELECTROCHEMICAL STABILITY

CG Hynes[1], CHM Beraldo[1], C Paternoster[1], A Sarkissian[2], D Mantovani[1]

[1] *Laboratory for Biomaterials and Bioengineering (CRC-Tier 1), Dept. Min-Met Materials Eng, & Regenerative Medicine, CHU de Quebec, Laval University, & Plasmionique, Varennes, Canada*

1. Introduction

Zinc (Zn) and its oxides' (ZnO) inherent biodegradability and overall properties make them a promising material for biomedical applications. Reactive magnetron sputtering (RMS) is a versatile deposition technique that enables precise control over film composition and microstructure.[1] RMS allows for modulation of the plasma gas composition, which can significantly influence the resulting film properties.[2] It is hypothesised that controlled modulation of the reactive gas ratio can influence film structure, degradation behaviour, and Zn ion release. Understanding these relationships will provide a foundation for optimising Zn-based coatings for biomedical surfaces and future multi-component thin film systems.

2. Experimental

ZnO thin films were deposited via RMS on Si substrates under varying argon-to-oxygen ($Ar:O_2$) ratios. Four sample groups were produced: (1) ZnO from a Zn target with a continuous flow of A and O_2 gas, (2) ZnO with alternating $Ar:O_2$ flow (2s:60s), (3) ZnO with alternating $Ar:O_2$ flow (2s:30s), and (4) ZnO with alternating $Ar:O_2$ flow (2s:8s). Deposition was conducted at 125 W and a chamber pressure of 10 and 15 mTorr for Ar and O_2 respectively. Thickness was controlled by deposition time to 150 nm. Scanning electron microscopy (SEM), X-ray photoelectron spectroscopy (XPS), and atomic force microscopy (AFM) were employed to assess stoichiometry and surface morphology. Corrosion behavior was assessed via electrochemical tests.

3. Results and Discussions

Fig. 1 depicts SEM images of each of the 4 conditions with respect to a decrease in O_2 flowrate, the reduced O_2 results in increasing roughness of the films as measured by AFM and reported on Fig.1. Potentiodynamic curves for each of the 4 conditions are reported in Fig. 2. Corrosion currents for each of the 4 conditions are recorded as ($1.59x10^{-8}$, $6.53x10^{-8}$, $1.58x10^{-6}$, $3.9x10^{-6}$ A/cm^2) respectively, the reduction in O_2 gas in the deposition process results in an increase in corrosion rate which varies between that of a stoichiometric ZnO and that of metallic Zn. This work demonstrates that reducing the ratio of oxygen in reactive magnetron sputtering can increase the corrosion current density of ZnO films, it is proposed that changes in corrosion is due to changes in the film morphology and the stoichiometric make-up of the ZnO film surface Future work can examine the incorporation of other metallic elements as dopants to functionalize the film for biomedical purposes with the aim of providing an eluting film with tuneable corrosion properties.

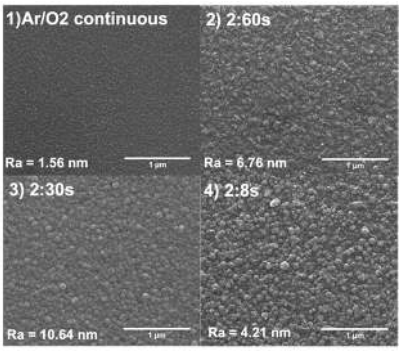


Fig. 1. *SEM Morphologies of ZnO films with roughness values as measured from Atomic Force Microscopy (AFM) reported.*

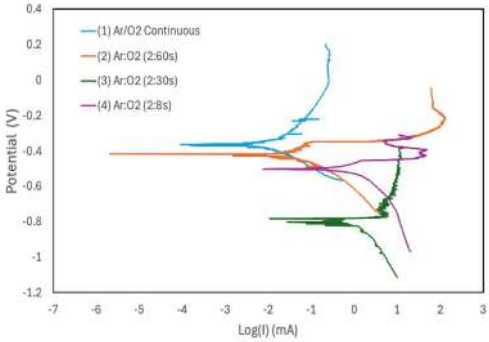


Fig. 2. *Corrosion resistance measured via potentiodynamic polarization measures.*

4. References

[1] Y. Deng, et al. Ceram. Int. 46 (2020) 18373–18390
[2] T. Angkuratipakorn et al. Ceram. Int. 49 (2023) 19102–19108

Acknowledgments

This research was partially supported by the Fonds de Recherche du Québec (Strategia), the Natural Science and Engineering Research Council of Canada, Prima Quebec, and the CHU de Quebec Research Centre.

*Corresponding author: Diego Mantovani, *diego.mantovani@gmn.ulaval.ca*

CHANGES IN THE SHAPE OF THE NbN REACTIVE SPUTTERING HYSTERSIS CURVE WITH THE CONTROL PARAMETER OF THE DISCHARGE

Kauã Pioli da Rosa*, Nathan Henrique de Melo Quintino da Silva, Josieli Honorato, and Julio César Sagás,

Universidade do Estado de Santa Catarina (UDESC), Laboratório de Plasmas, Filmes e Superfícies, Joinville-SC, Brazil

1. Introduction

Reactive magnetron sputtering is widely used for the deposition of compound thin films. However, the process commonly exhibits hysteresis, which affects deposition stability and process control [1]. Each target-reactive gas combination will exhibit a typical behavior depending on the chemical affinity between them, but it also depends on the control parameter of the discharge. Understanding the reactive deposition of NbN is particularly relevant due to its applications in superconducting and protective coatings [2]. In this work, we investigated the hysteresis curves of a reactive sputtering system using a Nb target in an Ar/N_2 atmosphere for different control parameters: current, voltage and power.

2. Experimental

The experimental trial was carried out in a DC grid-assisted magnetron sputtering system. The Ar flow rate kept constant while the N_2 flow rate was gradually increased and decreased to obtain the hysteresis curves. The pressure was monitored using a capacitive gauge. The discharge was generated at three different modes: constant current, constant voltage, and constant power. Besides the pressure, the free electrical parameters were also monitored. Optical emission spectra of the plasma were also acquired using an USB4000 spectrometer from Ocean Optics at different N_2 flow rates.

3. Results and Discussions

The shape of the hysteresis curve depends on the control parameter. When the voltage is fixed (fig. 1), the hysteresis curve (both for pressure and discharge current) have an abrupt transition between the metallic and compound modes. On the other hand, when the discharge current is fixed (fig. 2), the hysteresis curves show a smooth transition between the metallic and compound modes. This smooth transition is usually not observed (TiN deposition, for example), indicating a possible formation of intermediates nitrides. However, dependency with the control parameters highlights that this is not the only mechanism affecting the shape of the hysteresis curves.

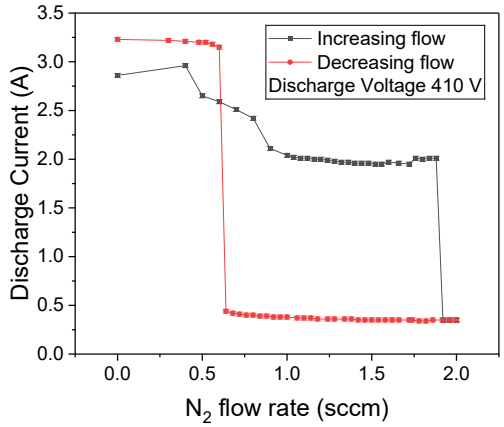


Fig. 1. *Discharge current hysteresis curve for constant voltage.*

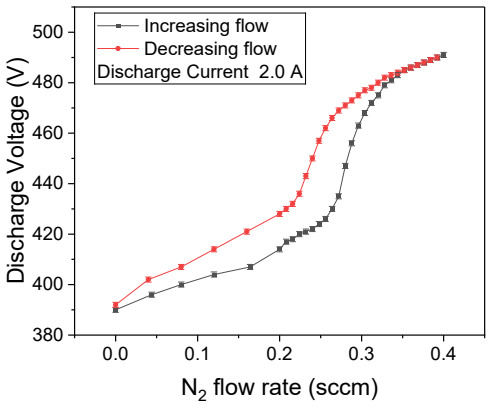


Fig. 2. *Discharge voltage hysteresis curve for constant current.*

4. References

[1] K. Strijckmans, R. Schelfhout e D. Depla, J. Appl. Física, 124, 241101, (2018).
[2] S. Berg, HO Särhammar e T. Nyberg, J. Phys. D: Appl. Phys., 22, 1788, (1989).

Acknowledgments

The authors acknowledge financial support from PIBIC-CNPq, PROBIC-UDESC and PROMOP/UDESC.

*Kauã Pioli da Rosa: kaua.rosa@edu.udesc.br

IMPLEMENTATION OF DYNAMIC SPUTTER YIELDS FOR REACTIVE MAGNETRON SPUTTERING MODELING OF NbN DEPOSITION

Nathan Henrique de Melo Quintino da Silva*, Julio Cesar Sagás

Universidade do Estado de Santa Catarina (UDESC), Laboratório de Plasmas, Filmes e Superfícies, Joinville-SC, Brazil

1. Introduction

Reactive magnetron sputtering is a well-known technique for thin film deposition. However, it exhibits a nonlinear relationship between reactive gas flow rate and the process parameters which lead to the hysteresis phenomenon. The use of phenomenological models is a powerful tool to understand the complexities of reactive deposition; however, most models do not implement the dynamic features of the process. In this work, we analyze the influence of electrical parameters, focusing on the modeling of dynamic sputtering yields as a function of discharge voltage.

2. Experimental setup

The simulation was developed based on the Updated Berg Model [1], utilizing specific parameters from the magnetron sputtering reactor at UDESC and considering a Nb target in an atmosphere of Ar and N_2. To couple the change of the sputtering yield with discharge voltage, a semi-empirical equation by Yamamura [2], along with SRIM software simulations [3], was employed to derive sputtering yield expressions both for Nb and N under Ar ion bombardment as a function of discharge voltage.

3. Results and Discussions

Equations for the sputtering yields were obtained from a fitting process of the theoretical data, Figure 1 shows the expression used for data correction. The use of a fitted model allows easy implementation of the dynamic sputtering yields in the calculations. Figure 2 presents three simulated hysteresis curves at constant current, where it can be observed that the required reactive gas flow rate increases with the increase in the discharge voltage, as a consequence of the increased sputtering yield and, consequently, sputtering rate. Furthermore, the implementation of dynamic sputter yields allows for the exploration of the influence of electrical parameters (voltage, current, and power) on the hysteresis phenomenon.

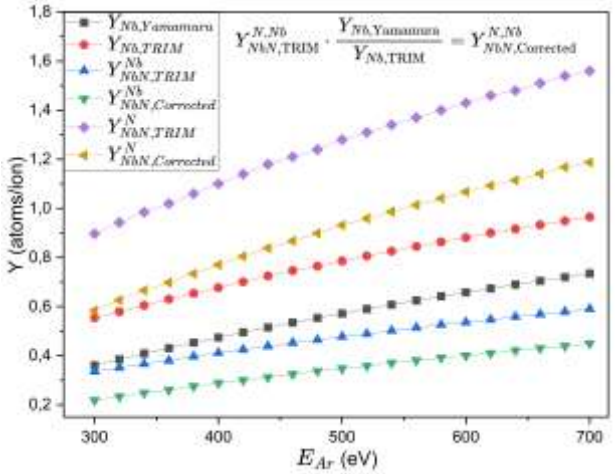


Fig. 1. *The differences between the Sputter Yields values simulated in SRIM and the same coefficients after correction with Yamamura's semi-empirical equation.*

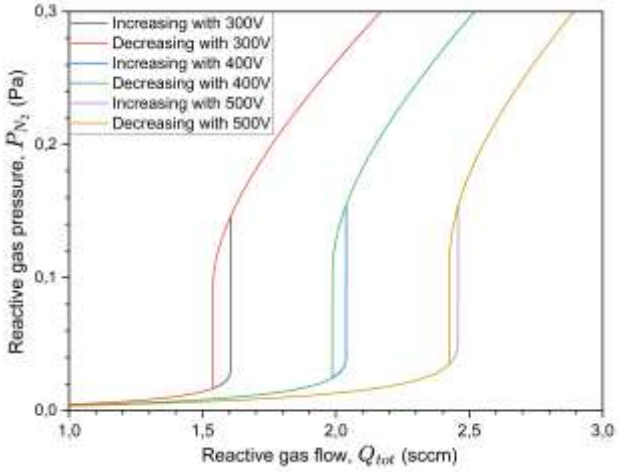


Fig. 2. *The hysteresis curves for a fixed current value of 1.0 A and voltage values of 300 V, 400 V, and 500 V.*

4. References

[1]- S. Berg, E. Särhammar, and T. Nyberg, Thin Solid Films 565, 186 (2014).
[2]- Y. Yamamura, and H. Tawara, J. Nucl. Mater. 233-237, 784 (1996).
[3]- J. F. Ziegler, M. D. Ziegler, and J. P. Biersack, SRIM Co., Chester, MD, USA, (2013).

Acknowledgments

The authors acknowledge financial support from PROBIC/UDESC.

* nathan.silva1251@edu.udesc.br

PLASMA NITRIDING WITH CATHODIC CAGE OF SS 304 ON CORROSION AND WEAR PROPERTIES

Jullia Pironato Amaro[1], Gustavo Gonçalves Forti[2], Gustavo Vinicius Victaliano de Meira[2], Marcos Dorigão Manfrinato[1,2]*
[1]*PPGCM UFSCar – Campus Sorocaba*
[2]*Fatec Sorocaba*

1. Introduction

During plasma nitriding of authentic stainless steels using a DC source, a characteristic defect called edge effect (non-uniform formation of the nitrided layer) occurs. There are several ways to eliminate this defect, including using a high-frequency source (extremely expensive) or using a cathodic cage and isolating the samples in the center. The use of a cathodic cage eliminates this type of defect while maintaining mechanical properties (hardness and fatigue), wear resistance, and corrosion resistance [1]. The objective of this work is to develop a cathodic cage and an isolation system to perform plasma nitriding without edge effect and to characterize the resistance to corrosion and abrasive micro-wear.

2. Experimental

The cathodic cage is shown in Fig. 1, and plasma nitriding was performed at a temperature of 385°C (NIT 385°C) for 6 hours, at a pressure of 3.2 Torr, with a gas mixture of 80% N2 and 20% H2. Metallographic testing was performed to measure the thickness and uniformity of the formed layer. Abrasive micro-wear tests were performed with a 25.4 mm diameter sphere, at 150 RPM, with an 8 N load and a test time of 30 minutes. Corrosion tests were performed with a 3.5% NaCl electrolytic medium, first for 30 minutes at open circuit potential and then a cyclic polarization test with a potential of 1 mV/s. A silver electrode and a saturated Ag/AgCl counter electrode were used. Triplicate tests were performed for both corrosion and abrasive micro-wear to ensure the reliability of the results.

3. Results and Discussions

The nitrided layer formed was uniform along the entire length of the specimen, eliminating the edge effect, with an average thickness of 6 µm. Fig. 2 shows the cyclic polarization curve, and the nitrided specimen exhibited a higher corrosion potential (Ecor = -0.39V) and pitting potential (Epit = 0.55V), thus showing greater corrosion resistance. The tribological behavior (Table 1) of the nitrided layer was superior to the base material, exhibiting a lower wear volume of $3.28x10^{-3}$ mm³ and a lower wear rate of $1.11x10^{-6}$ mm³/Nm, being 10 times more resistant to micro-wear.



Fig. 1. *Plasma nitriding using a cathode cage*

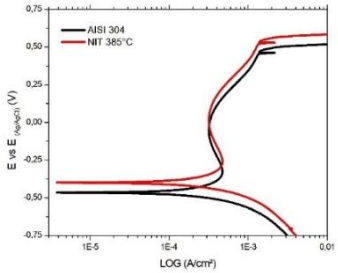


Fig. 2. *Cyclic polarization curves for SS 304: NIT 385°C and BM.*

Tab. 1. Results of micro-abrasive wear using a fixed sphere.

	Wear volume (mm³)	Wear rate (mm³/Nm)
NIT 385°C	$3.28x10^{-3}$	$1.11x10^{-6}$
AISI 304	$6.02x10^{-2}$	$2.05x10^{-5}$

4. References

[1]- T. Borowski, Materials, **14**, 3320-3334, (2021).

Acknowledgments

To the Laboratory of Plasma Technology (LAPTec) as UNESP Sorocaba for providing the potenciostat/galvanostat.

*Corresponding author: marcos.manfrinato@cps.sp.gov.br

STERILIZATION OF DENTAL IMPLANTS USING PLASMA-ACTIVATED WATER (PAW) WITH ANTIMICROBIAL ACTIVITY GENERATED BY NON-THERMAL ATMOSPHERIC PLASMA

Maria Beatriz Sousa Mágulas[1]*, Mikael Regis[2,3], Igor Frederico da Silveira Ramos[2], Marcília Pinheiro da Costa[2, 4], Anderson de Oliveira Lobo[2], Douglas Marcel Gonçalves Leite[1], Rodrigo Sávio Pessoa[1], Fernanda Roberta Marciano[2,3]

[1]*Plasma and Process Laboratory – Aeronautics Institute of Technology (ITA)*
[2]*Interdisciplinary Laboratory for Advanced Materials – Federal University of Piaui (UFPI)*
[3]*Physics Department – Federal University of Piaui (UFPI)*
[4]*Pharmacy Department – Federal University of Piaui (UFPI)*

1. Introduction

Dental implant sterilization is a critical step to prevent peri-implant infections and implant failure. Autoclaving is the current gold standard, but heat and pressure can damage titanium components and face challenges such as protocol deviations and false-positive results [1]. Alternative approaches are therefore needed. Plasma-Activated Water (PAW) is produced by exposing water to non-thermal atmospheric plasma (NTAP), which dissolves reactive oxygen and nitrogen species (RONS), including H_2O_2, NO_2^-, NO_3^- and •OH, into the liquid, yielding a strongly acidic, highly oxidative solution with documented broad-spectrum antimicrobial activity [2]. PAW has demonstrated efficacy against *Enterococcus faecalis* and *Streptococcus mutans* in dental contexts, yet its use for implant decontamination remains unexplored. This work evaluates PAW produced from an NTAP reactor as a non-thermal and non-toxic alternative for the sterilization of Ti6Al4V dental implants.

2. Methodology

Ti6Al4V discs were metallographically prepared and characterised by SEM/EDS. PAW was generated in an ArcAqua LAB reactor (60 W, 3 L/min compressed air) using Milli-Q, distilled and mineral water (80 mL each), activated for 15 and 60 min. Physicochemical characterisation comprised pH, conductivity, RONS (NO_2^-, NO_3^-, H_2O_2), FTIR-ATR and contact-angle measurements. Antimicrobial activity was assessed in 96-well plates against *S. aureus*, *E. coli* and *C. albicans* (630 nm, 24 h, 35 °C). For sterilisation, contaminated discs were immersed in Milli-Q PAW for 30 or 90 min and compared against saline (negative control) and 0.12% chlorhexidine (positive control). Data were analysed by one-way ANOVA with Tukey or Dunnett post-tests ($p < 0.05$).

2. Results and Discussions

SEM/EDS confirmed a homogeneous Ti6Al4V surface (Ti 89.82 %, Al 6.55 %, V 3.63 wt%) free of significant contamination, fulfilling ASTM F136 requirements. PAW characterization showed a sharp pH drop from 6.0 - 2.0 and a conductivity rise from 50 - 300 µS/cm after 60 min activation, consistent with HNO_2 and HNO_3 formation via plasma–gas–water interactions. Milli-Q water reached the lowest pH and highest RONS concentrations (NO_2^- up to 500 mg/L; H_2O_2 = 25 mg/L at 60 min), attributed to its minimal initial ionic content. FTIR-ATR spectra revealed subtle changes in O-H stretching (≈ 3300 cm^{-1}) and H-O-H bending (≈ 1640 cm^{-1}) bands for distilled water, while Milli-Q and mineral waters showed greater structural stability, suggesting complex plasma–matrix interactions. Contact-angle values remained below 90° for all groups, indicating maintained or improved wettability on the implant surface. Microtitration assays demonstrated statistically significant reductions ($p < 0.05$) of *S. aureus* and *E. coli* from 15 min with PAW Milli-Q, and of *C. albicans* from 60 min, reflecting greater fungal resistance to RONS. Colony-count assays on contaminated implants confirmed >99 % inactivation of *S. aureus* after 90 min immersion in PAW Milli-Q ($p < 0.05$ vs. saline), with performance approaching that of 0.12 % chlorhexidine. The combined effect of extreme acidity (pH ≈ 2) and RONS-driven oxidative damage, membrane peroxidation, DNA fragmentation and enzyme inactivation, accounts for the bactericidal outcome. These results establish PAW as a clean, non-thermal, non-toxic sterilization method capable of overcoming the limitations of conventional autoclaving for sensitive titanium implants.

4. References

[1]- Ardeshna, Anil *et al.* Effectiveness of different sterilization methods on clinical orthodontic materials. **Journal of Indian Orthodontic Society**, v. 57, n. 2, p. 98-105, 2023.

[2]- Shambharkar, Akash *et al.* Plasma activated water pre-treatment substantially enhances phage activity against Proteus mirabilis biofilms. **Biofilm**, v. 8, p. 100230, 2024.

Acknowledgments

Interdisciplinary Laboratory for Advanced Materials; Aeronautics Institute of Technology.

*Corresponding author: biamagulas@outlook.com

On the Adhesion of a-C:H Coatings Deposited by PECVD on PDMS for Biomedical Applications

Lidi Astrid Yanez Hernandez[1], Pascale Chevallier[1], Linda Bonilla-Gameros[1], Charlotte Rossi[2], Laurent Houssiau[2], Andranik Sarkissian[3], Diego Mantovani[1]

[1]*Laboratory for Biomaterials and Bioengineering, (CRC-Tier I), Dept Min-Met-Materials Eng., & Regenerative Medicine, CHU de Quebec, Laval University, Quebec City, QC, Canada;*
[2]*Namur Institute of Structured Matter (NISM), University of Namur, 5000 Namur, Belgium;*
[3]*Plasmionique Inc., Varennes, QC, Canada*

1. Introduction

Polydimethylsiloxane (PDMS) is widely used in biomedical devices due to its hemocompatibility, elasticity, and chemical stability [1]. However, its low surface energy and high deformability limit coating adhesion and promote bacterial colonization, which can lead to device failure [2]. Hydrogenated amorphous carbon (a-C:H) coatings have emerged as a promising strategy to functionalize PDMS surfaces while preserving bulk properties [3]. Nevertheless, achieving mechanically stable and adherent coatings on soft substrates remains a critical challenge [4]. The objective of this study is to investigate how substrate bias and hydrogen incorporation during plasma-enhanced chemical vapor deposition (PECVD) influence the adhesion, morphology, and mechanical integrity of a-C:H coatings deposited on PDMS.

2. Experimental

Medical-grade PDMS substrates were first activated by oxygen plasma and subsequently coated using a PECVD process. Four coating configurations were investigated by varying substrate bias (0 V and −300 V) and gas composition (Ar/CH_4 with or without H_2): polymer-like carbon (PLC), diamond-like carbon (DLC), and their hydrogenated counterparts (PLCH and DLCH). Surface and interface characterization were performed using X-ray photoelectron spectroscopy (XPS), Raman spectroscopy, atomic force microscopy (AFM), and time-of-flight secondary ion mass spectrometry (ToF-SIMS). Mechanical performance and adhesion were evaluated through tensile stress-relaxation tests up to 50% strain, combined with crack density analysis. Coating stability was assessed by immersion in phosphate-buffered saline (PBS) under static and dynamic conditions up to 21 days.

3. Results and Discussions

ToF-SIMS depth profiling revealed that non-biased coatings (PLC and PLCH) exhibited greater thickness and well-defined interfaces, whereas biased coatings (DLC and DLCH) were thinner and showed evidence of interfacial intermixing with PDMS components. Hydrogen incorporation led to a reduction in coating thickness and nanoscale roughness, indicating a modification of film growth mechanisms. It also significantly improved mechanical performance, with PLCH showing a ~65% reduction in crack density compared to PLC after tensile deformation. Under mechanical loading, DLC-based coatings exhibited brittle behavior with extensive cracking, while PLC and particularly PLCH coatings demonstrated improved flexibility and resistance to crack propagation. This behavior is attributed to reduced internal stresses and enhanced compliance associated with hydrogen incorporation and the absence of energetic ion bombardment. Immersion tests under pseudo-physiological conditions confirmed that PLCH coatings remained stable for up to 21 days, showing only localized cracking and no significant delamination under both static and dynamic conditions. These results indicate that PLCH coatings can accommodate mechanical deformation while maintaining interfacial integrity.

4. References

[1] A. Victor, J. Ribeiro, F. F. Araújo, *J. Mech. Eng. and Biomech.,* **4**, 1–9, (2019).
[2] L.B. Neves, I.S. Afonso, G. Nobrega, L.G. Barbosa, R.A. Lima, J.E. Ribeiro, *Micromachines (Basel).,* **15**, (2024).
[3] R. Shah, N. Pai, R. Khandekar, R. Aslam, Q. Wang, Z. Yan, A. Rosenkranz, *Surf. Coat. Technol.,* **487**, (2024).
[4] L.A. Yáñez-Hernández, L. Bonilla-Gameros, P. Chevallier, A. Sarkissian, D. Mantovani, *Appl. Sci.,* **15,** 9968, (2025).

Acknowledgments

This work was partially supported by the Natural Science and Engineering Research Council of Canada (Discovery and Alliance funds), the Quebec Ministry of Economy and Innovation (PRIMA funds), and the Research Center of the CHU de Quebec.

*Corresponding author: lidi.yanez-hernandez.1@ulaval.ca

CORRELATION BETWEEN PLASMA CHARACTERISTICS AND OIL-METHANOL EMULSION IN DBD REACTOR FOR BIODIESEL PRODUCTION

Eloisa G. Meinerz, Vinicios E. Pinter, Giorgio E. Testoni, Maíra O. Palm, Diego A. Duarte*, Rafael C. Catapan
Universidade Federal de Santa Catarina, Joinville, 89219-600, SC, Brazil

1. Introduction

Global population growth, coupled with the lifestyle of modern society, suggests a significant increase in energy demand in the coming decades. Alternative fuels, such as biodiesel, play a crucial role in the transition of the transportation sector toward greater sustainability by reducing carbon emissions while maintaining the majority of the current vehicle fleet, where plasma-assisted transesterification has emerged as a promising advanced method for biodiesel production, offering reduced reaction times and enhanced ester yields [1]. In this work, a correlation between plasma optical emission spectra and oil–methanol emulsions during biodiesel production is investigated using optical emission spectroscopy, spectrophotometry, and optical microscopy.

2. Experimental setup

Experiments were carried out in a dielectric barrier discharge (DBD) reactor [2] using different methanol/oil volume ratios (0.25, 0.50, 0.75, and 1.0). During the treatments, plasma optical emissions were monitored by optical emission spectroscopy (OES) using an Ocean Optics SR4 spectrometer. After the treatments, the solution transmittance and the emulsion droplets formed in each sample were analyzed by spectrophotometry (Kasuaki IL-592-LC) and optical microscopy (Zeiss Axio Observer), respectively.

3. Results and Discussions

The OES spectrum for the methanol/oil volume ratio of 0.25 shows the nitrogen second positive system N_2 ($C^3\Pi_u \rightarrow B^3\Pi_g$) with the highest intensity at 337 nm, assigned to the N_2 vibrational line [3,4]. The temporal evolution at 337 nm exhibits a strong correlation with the formation of the oil–methanol emulsion, as illustrated in Figure 2. At the initial stage of the treatment (t = 0), the emission intensity is minimal, corresponding to a system in which oil and methanol remain as two distinct, immiscible phases with no emulsion formation. In this condition, the optical emission is primarily localized within the methanol phase, and both liquids exhibit optical transmittance values close to 100% at 600 nm. As the treatment progresses, methanol droplets begin to disperse into the oil phase, characterizing a non-stationary regime. This process leads to the gradual development of a homogeneous emulsion, in which the DBD optical emission becomes uniformly distributed throughout the reactor volume. Upon reaching the stationary regime, the fully developed oil–methanol emulsion displays a significantly reduced optical transmittance at 600 nm, falling below 2%, in agreement with previous studies [1].

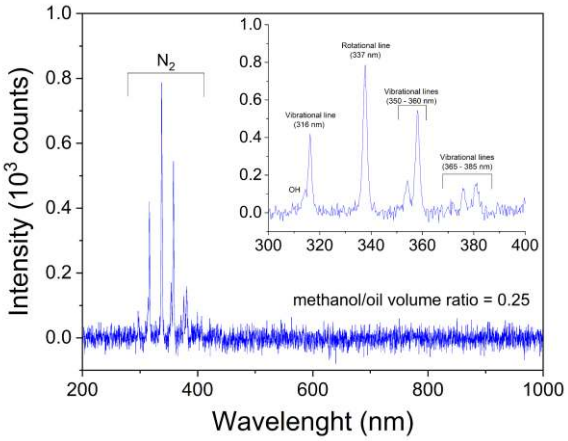


Fig. 1. *OES for methanol/oil volume ratio = 0.25.*

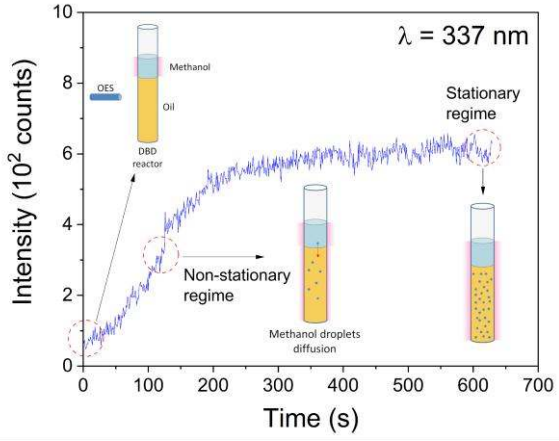


Fig. 2. *OES time evolution (λ = 337 nm).*

4. References

[1] M. O. Palm *et al.*, Fuel, 400 (2025) 135686.
[2] M. O. Palm *et al.*, Plasma Chem. Plasma Process, 44 (2024) 353.
[3] N. Nagarajan *et al.*, J. Phys. D: Appl. Phys., 58 (2025) 405201.
[4] S. Mir and S. Kooshki, Langmuir, 39 (2023) 14459.

Acknowledgments

This work was supported by CNPq (Grant numbers 405818/2022-0 and 406376/2022-0).

*Corresponding author: diego.duarte@ufsc.br

EVALUATION OF DYE-SENSITIZED SOLAR CELLS WITH Nb_2O_5-TiO_2 SINGLE-LAYER PHOTOANODES

Danilo B. Machado[1], Érica Dallastra[1], Alice M. Ramade[2], Diego. A. Duarte[1*]
[1]*Universidade Federal de Santa Catarina, Joinville, 89219-600, SC, Brazil*
[2]*Universidade do Estado de Santa Catarina, Joinville, 8219-710, SC, Brazil*

1. Introduction

Brazil's abundant natural resources such as TiO_2 and Nb_2O_5 position the country for strategic advances in advancing optoelectronic and PV technologies. These include third-generation solar cells, such as dye-sensitized solar cells (DSSCs), which are a promising alternative to Si solar cells widely used in the aerospace industry [1]. In this work, DSSCs were prepared with single-layer Nb_2O_5-TiO_2 photoanodes with different Nb_2O_5 mass concentrations and evaluated through electrical characteristics.

2. Experimental Setup

Nb_2O_5-TiO_2 photoanodes with different Nb_2O_5 mass concentrations (0, 2.5, 5.0, and 7.5%) were prepared on standard microscope slides and FTO glass substrates (7 Ω/sqr.) by spin-coating and doctor-blade, respectively, according to procedures described in ref. [2]. Samples were evaluated by mechanical profilometry, X-ray diffraction (XRD), X-ray photoelectron spectroscopy (XPS), field emission scanning electron microscopy (FESEM), energy-dispersive X-ray spectroscopy (EDS) and two-point probes technique. DSSCs were assembled in a sandwich-type, two-electrode, open-cell configuration, and evaluated through the current-voltage characteristics at the AM 1.5 standard and in dark conditions, following the procedures described in ref. [2].

3. Results and Discussions

Mechanical profilometry indicates film thicknesses ranging from 10 to 20 µm. XRD confirms that all samples exhibit a polycrystalline structure, with an average crystallite size of ~23 nm and a predominant anatase phase (~83%). FESEM, shown in Figure 1, reveals rough and porous film surfaces with an average particle size of (20.5 ± 0.7) nm, in good agreement with the crystallite size estimated using the Scherrer equation. XPS and EDS confirm the presence of Ti, O, and Nb, with Nb showing a non-uniform distribution and atomic concentrations below 1%. Measurements obtained via the two-point probe method demonstrate that Nb incorporation reduces the sheet resistance of the photoanodes, contributing to an overall enhancement in the power conversion efficiency of DSSCs. As illustrated in Figure 2, photoanodes containing 2.5% Nb_2O_5 yield DSSCs with improved current–voltage characteristics and higher global conversion efficiency.

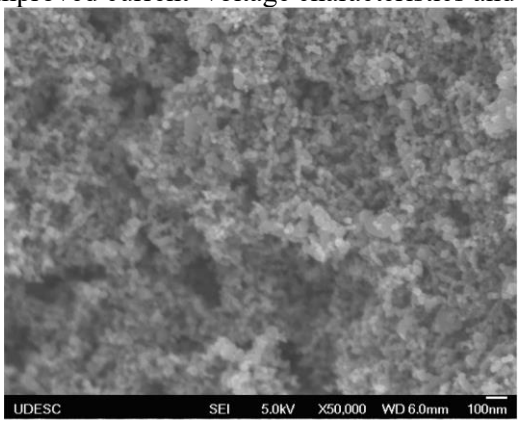


Fig. 2. *FESEM image of photoanode prepared with 2.5% Nb_2O_5 showing the TiO_2 nanoparticle distribution.*

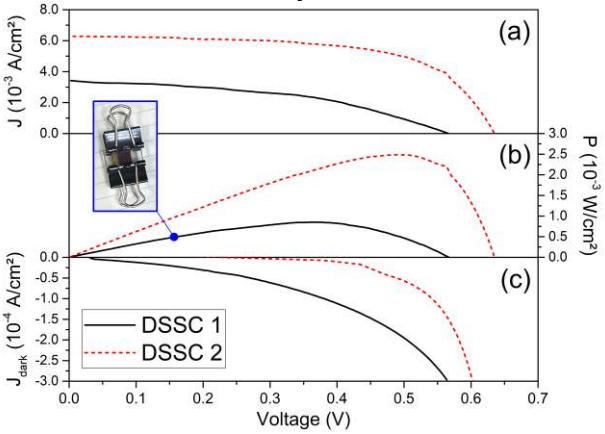


Fig. 1. *(a) J–V, (b) P–V, and (c) dark current curves for DSSCs 1 (undoped) and 2 (prepared with 2.5% Nb_2O_5).*

4. References

[1] R. Sasikumar *et al.* Renew. Sustain. Energy Rev., 199 (2024) 114549.
[2] D. B. Machado *et al.*, Braz. J. Phys., 56 (2026) 65.

Acknowledgments

This work was supported by CNPq (406376/2022-0) and FAPESC (Edital 21/2024).

*Corresponding author: diego.duarte@ufsc.br

TAILORING MG-BASED ALLOYS VIA SURFACE FINISHING AND PLASMA PROCESSING FOR BIOMEDICAL APPLICATIONS

L. Malvestiti[1,2,3], C. Paternoster[1], M. Nonaka[3], D. Krygier[3], M. Kovalsky[3,4], S. Ceré[2,4], D. Mantovani[1*]

[1]Lab. for Biomaterials and Bioengineering, Laval University, Québec, Canada; [2]INTEMA, Mar del Plata National University, Mar del Plata, Argentina; [3]CEILAP-CITEDEF, Villa Martelli, Argentina; [4]CONICET, Buenos Aires, Argentina

1. Introduction

Oxygen plasma immersion ion implantation (O–PIII) technology applied to Mg-based alloys enables the formation of a thin MgO layer [1], improving surface properties for biomedical applications, particularly by reducing the corrosion rate, which remains the main limitation for their use [2]. Although the implantation process strongly depends on the plasma parameters, the impact of the initial surface condition on plasma–material interaction is often overlooked. In this study, O–PIII under different plasma processing was used to modify a Mg-based alloy (AZ31B), and the impact of surface finishing on the MgO formation was evaluated.

2. Experimental

AZ31B alloy (Mg 95–96 wt%, Al 2.5–3.5 wt%, and Zn ~0.6–1.5 wt%) were prepared using two different surface finishing: Chemical polishing (CP), based on an acid-inorganic solution, and mechanical polishing (MP) applying 600– and 1200–grit sandpapers. O–PIII was carried out by PBII-300 system (Plasmionique, Varennes, Canada) varying working pressure (P_W=*5–10 mTorr*), treatment duration (t_D= *60- 300 min*) and pulse frequency (P_F=*200–1000 Hz*). Three plasma conditions (OP1–OP3) were set at a constant implantation dose (P_F/t_D), varying P_W and t_D. OP1 and OP2 were performed at 5 mTorr with t_D of 60 min and 300 min, respectively, while OP3 was carried out at a higher P_W (50 mTorr) with short t_D (60 min). Morphological, chemical and electrochemical characterizations were performed by scanning electron microscopy (SEM), atomic force microscopy (AFM), X-ray photoelectron spectroscopy (XPS), static contact angle, electrochemical impedance spectroscopy (EIS) and polarization curves for corrosion rate determination in Hanks' solution (pH=7 and 37°C).

3. Results and Discussions

CP and MP modified surface topography and chemistry, leading to different plasma–surface interactions during implantation. Plasma parameters further influenced the resulting MgO morphology, promoting the formation of oxide compact layers or nodule-like structures, changing oxide/hydroxide surface composition, wettability, and corrosion behavior. In particular, at low P_W and short t_D (OP1), both CP and MP, generated a homogeneous oxide layer with minor changes in roughness and increased hydrophobicity. Similar surface properties were observed for longer t_D but after MP (MP-OP2), suggesting surface-dependent behavior. These conditions promoted higher MgO content over $Mg(OH)_2$, reduced carbon species, and improved corrosion resistance as shown by higher impedance and lower corrosion rates. Overall, these results demonstrate the critical role of Mg surface finishing prior to applying O–PIII, and the potential of the applied approach to tune MgO layer. Ongoing studies aim to include micromachined laser followed by O–PIII, to further evaluate its effects on oxide layer properties.

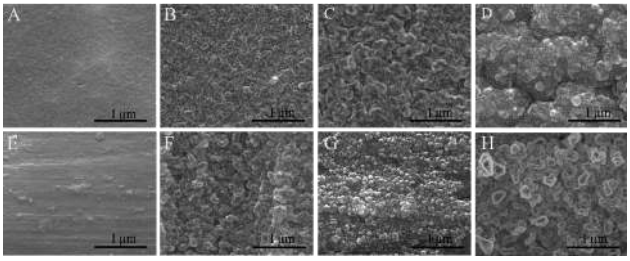


Fig. 1. *SEM images of: AZ31B chemically polished (CP, A); CP-OP1 (B), CP-OP2 (C), CP-OP3 (D);mechanically polished (MP, E), MP-OP1 (F), MP-OP2 (G) and MP-OP3 (H).*

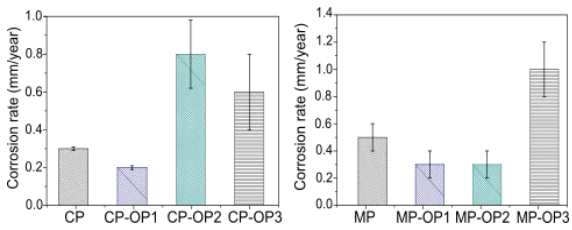


Fig. 2. *Corrosion rate (mm/year) of AZ31B chemically polished (CP), mechanically polished (MP) and after O–PIII treatment (OP1–OP3).*

4. References

[1]- A. Anders, *Handbook of Plasma Immersion Ion Implantation and Deposition*, Wiley, USA, (2000).

[2]- A. Kocijan et col., Materials, 15, 7405, (2022).

Acknowledgments

LBB, NSERC- Canada, and CHU, Quebec Research Centre. CEILAP-CITEDEF and CONICET, Argentina.

*Diego.Mantovani@gmn.ulaval.ca

OPTICAL AND SURFACE PROPERTIES OF Nb2O5 THIN FILMS GROWN BY DC-PULSED MAGNETRON SPUTTERING

R. Ramos[1*], C. Zickenheiner[2], V. Udachin[2], M. P. F. de Godoy[3], S. F. Durrant[1], N. C. da Cruz[1], J. R. R. Bortoleto[1] and C. F. O. Graeff[4]

[1]*Institute of Science and Technology, São Paulo State University (UNESP), Sorocaba-SP, Brazil;*
[2]*Clausthal Center of Materials Technology, Clausthal University of Technology, Clausthal-Zellerfeld, Germany;*
[3]*Department of Physics, Federal University of São Carlos (UFSCar), São Carlos-SP, Brazil*
[4]*School of Sciences, São Paulo State University (UNESP), Bauru-SP, Brazil*

1. Introduction

Perovskite solar cells require transparent and chemically stable electron transport layers (ETLs). Nb2O5 is a wide-band-gap n-type oxide with high optical transmittance and suitable band alignment, making it a promising alternative to TiO2 and SnO2 [1-3]. This work evaluates how pulse length and oxygen partial pressure affect Nb2O5 films deposited by DC-pulsed magnetron sputtering for ETL and optical-coating applications.

2. Experimental

Nb2O5 films were grown at room temperature on glass using a Nb metallic target in a homemade DC-pulsed magnetron sputtering system. Two series were prepared: (i) pulse length from 170 to 600 µs at fixed Ar/O2 pressures of 2/1 mTorr respectively; and (ii) O2 pressure from 0.25 to 1.00 mTorr at fixed 250 µs pulse length and 2 mTorr Ar. Plasma species were analyzed by OES, thickness by profilometry, structure by grazing-incidence X-ray diffraction, wettability by contact angle, and optical properties by UV-Vis-NIR spectroscopy.

3. Results and Discussions

OES revealed Ar I and oxygen-related emissions, and the DC-pulsed discharge showed stronger oxygen-species ionization than RF under comparable conditions (Fig. 1). The deposition rate increased almost linearly with pulse length and decreased as O2 pressure increased (Fig. 2), reaching 17.5 nm min-1 at 600 µs and 12.2 nm min-1 at 0.25 mTorr O2. All films were amorphous. The optical band gap remained nearly constant between 3.41 and 3.54 eV, while the refractive index at 500 nm increased to 2.40 at lower O2 pressure, suggesting denser films and/or partial phase changes [4]. DC-pulsed films also showed more favorable wetting than the RF reference, which is relevant for perovskite deposition [5]. Therefore, DC-pulsed sputtering provides transparent Nb2O5 coatings with tunable growth rate and surface/optical properties.

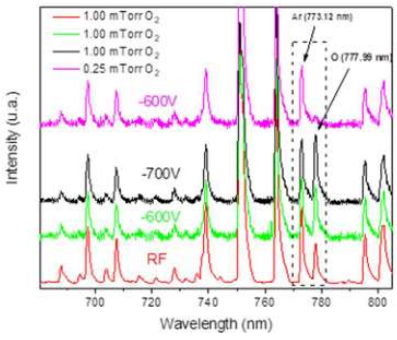


Fig. 1. *OES spectra comparing RF and DC-pulsed plasmas, highlighting stronger oxygen-related emissions in pulsed mode.*

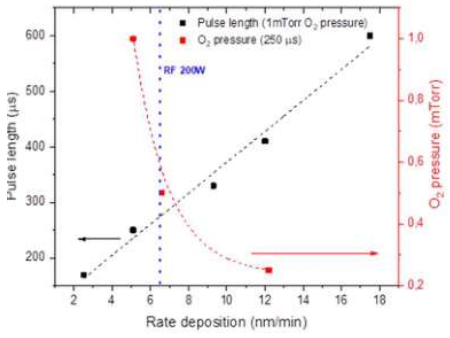


Fig. 2. *Deposition rate as a function of pulse length and O2 pressure; the dashed blue line indicates the 200 W RF reference.*

4. References

[1] J. Feng *et al.*, *Nano Energy*, v. 36, p. 1–8, 2017.
[2] R. Ramos *et al.*, IEEE, p. 166–173, 2025.
[3] K. Valadi, *et al*, *Environ Chem Lett*, v. 19, n. 3, p. 2185–2207, 2021.
[4] N. Hossain *et al.*, *J Mater Sci: Mater Electron*, v. 30, n. 10, p. 9822–9835, 2019.
[5] S. L. Fernandes *et al.*, v. 14, n. 4, p. 043703, jul. 2022.

Acknowledgments

The authors acknowledge MCTI/FINEP (grant 0034/21) and CBMM for support and the metallic niobium target.

*Corresponding author: raul.ramos@unesp.br

POROSITY MEASUREMENTS IN 316L STEEL SINTERED BY ADDITIVE MANUFACTURING

Vitor Hugo Fioravanti Gomes[1], Waldemar Bonventi Jr.[2]*, Marcos Dorigão Manfrinato[1]
[1]*Faculdade de Tecnologia de Sorocaba, Sorocaba, SP, fatecsorocaba.cps.sp.gov.br*
[2]*Mestrado Profissional em Gestão e Tecnologias em Sistemas Produtivos, São Paulo, SP*

1. Introduction

AISI 316L austenitic stainless steel parts, generated by the Selective Laser Melting (SLM) method, show high geometric precision, using a laser beam to melt each layer [1]. 316L exhibits good fusibility, low susceptibility to oxidation, and dense parts with adequate mechanical properties [2]. This work consisted of quantifying the resulting porosity in SLM-manufactured steel, using metallographic analysis and digital image processing, manually and with the assistance of Artificial Intelligence (AI).

2. Methods and Experiments

Samples (10x10x20 mm) were generated on an Omnisint 160/2 printer, using 316L steel powder (40-46 µm), laser powers of 50, 125, 200, 275 and 350 W, one and two passes, keeping other parameters constant. Preparation followed ASTM-E3 standard. Defects revealed by the cut surfaces were analyzed with ImageJ software (manually) and by Driven Watershed [3] (200x magnification).

3. Results and Discussions

In figures 1 and 2, some selected samples: (a) manual ImageJ pore selection (b) and by watershed (c). Watershed with AI resulted in more precise pore selections and did not distinguish pores from sanding and polishing marks. In ImageJ, preparation defects can be discarded by the operator. As future work, train the AI to perform this distinction.

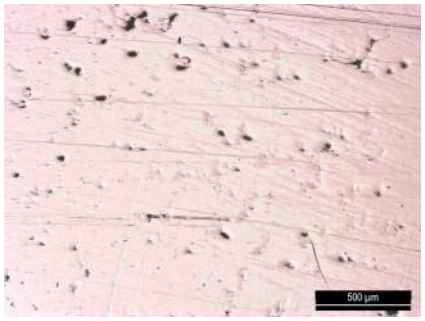
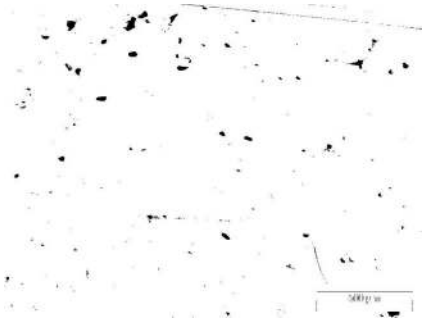


Fig. 1a. Sample 125-1


Fig. 1b. Sample 125-1, Image J

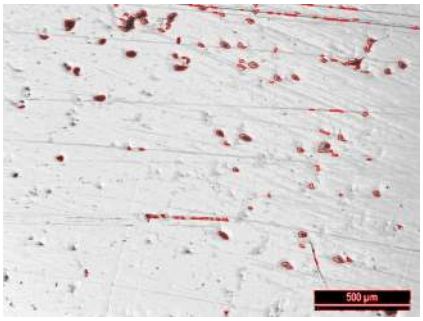


Fig. 1c. Sample 125-1, Watershed

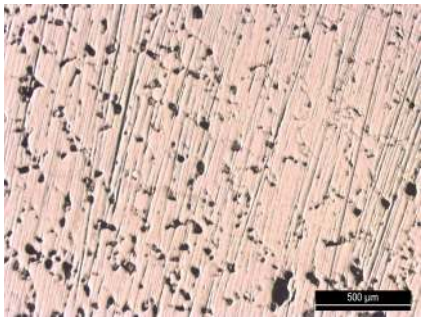
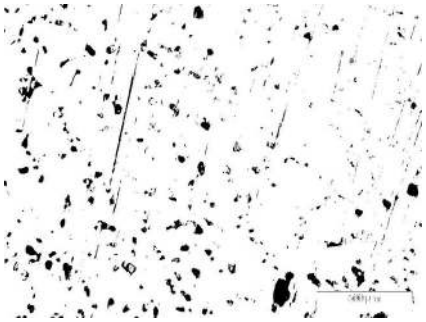


Fig. 2a. Sample 125-2


Fig. 2b. Sample 125-2, Image J

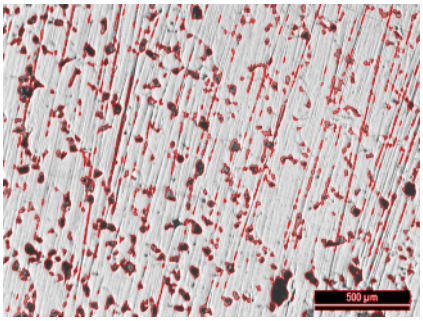


Fig. 2c. Sample 125-2, Watershed

Table 1: Relative area of pores by image with the two methods, highlighting those from Fig. 1.

Sample	**125-1**	**200-1**	**275-1**	**350-1**	**125-2**	**200-2**	**275-2**	**350-2**
ImageJ	1,75 %	1,90 %	3,08 %	3,18 %	4,65 %	3,94 %	6,40 %	0,20 %
Watershed	5,95 %	5,18 %	2,63 %	4,85 %	7,40 %	3,97 %	6,08 %	3,97%

4. References

[1] W. E. Frazier, “Metal additive manufacturing: A review,” J. Mater. Eng. Perform., vol. 23, no. 6, pp. 1917–1928, (2014), doi:10.1007/s11665-014-0958-z.
[2] D. Herzog et al., “Additive manufacturing of metals,” Acta Mater., vol. 117, pp. 371–392, (2016).
[3] I. Levner, H. Zhang, and R. Greiner, “Heterogeneous stacking for classification-driven watershed segmentation,” EURASIP J. Adv. Signal Process., pp. 1–13, (2008), doi:10.1155/2008/485821

*Corresponding author: waldemar.bonventi@cps.sp.gov.br

DESIGN AND CHARACTERIZATION OF A 4 LAYERS TIO2/SIO2 OPTICAL COATING USING THE OPTILAYER SOFTWARE

Marcos H. Morbidelli Jr. [1]*, and Alvaro J. Damião[2]
[1]*National Astrophysics Laboratory, Itajubá, Brazil*
[2]*Institute for Advanced Studies, São José dos Campos, Brazil*

1. Introduction

Multilayer optical thin films produced by vacuum deposition are widely used in industrial and scientific applications, such as antireflective coatings. In this context, OptiLayer is a software platform for the design, optimization, and post-production analysis of optical coatings. Among its synthesis techniques, Needle Optimization and Gradual Evolution are relevant for generating multilayer designs from target spectral requirements while satisfying feasibility demands for manufacture [1].

2. Theory and Experimental Setup

Traditional refinement involves the local optimization of the coating layers thicknesses from a starting design. However, in Needle Optimization, very thin layers are inserted according to a perturbation function. The inserted layer has a different index of refraction than the position in which it is being inserted, therefore its introduction increases the number of coating layers by two and so the number of optimization parameters. Gradual Evolution extends this idea by increasing the total optical thickness of the design after each needle cycle until a termination criteria is met. In this work, the design began with the selection of TiO_2 and SiO_2 as layer materials, soda lime as substrate and zero reflectance as target spectral response. The coating was synthesized using Gradual Evolution and refined under manufacture constraints. After manufacturing by electron-beam deposition, the sample was characterized by multiangle spectroscopy using an Agilent Cary 7000 spectrophotometer. The experimental spectra were analyzed in the post-production module for comparison with the nominal design [2, 3].

3. Results and Discussions

The nominal reflectance of a 4 layers design obtained by Gradual Evolution is presented in Fig. 1 as the solid black lines, one for each angle (4, 10, 20, 30 and 40°), together with its experimental spectra as colored lines. The comparison indicates a discrepancy of 2.78, which represents the root mean square deviation between them. The design thicknesses in nm and post-production analysis of systematic errors is shown in Fig.2.

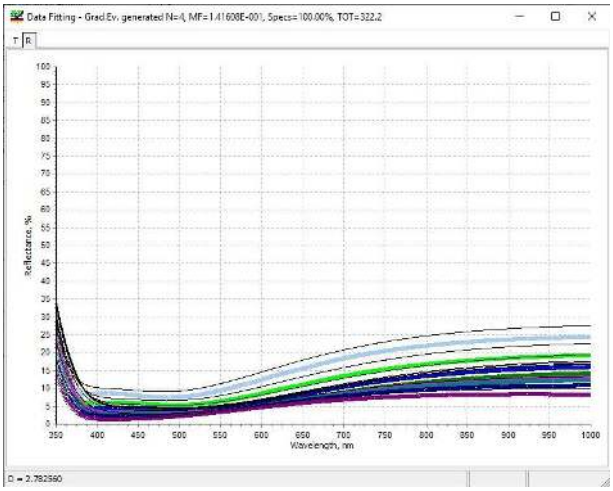
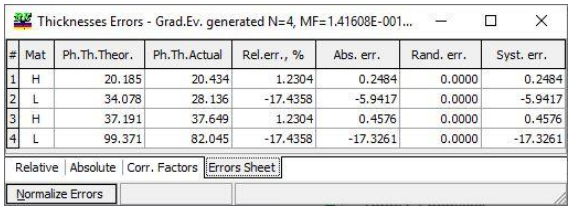


Fig. 1. *Comparison between the nominal reflectance of a 4 layer TiO_2 and SiO_2 coating and its photometric data measured by Agilent Cary 7000 at five different angles.*



#	Mat	Ph.Th.Theor.	Ph.Th.Actual	Rel.err., %	Abs. err.	Rand. err.	Syst. err.
1	H	20.185	20.434	1.2304	0.2484	0.0000	0.2484
2	L	34.078	28.136	-17.4358	-5.9417	0.0000	-5.9417
3	H	37.191	37.649	1.2304	0.4576	0.0000	0.4576
4	L	99.371	82.045	-17.4358	-17.3261	0.0000	-17.3261

Fig. 2. *Design and estimated systematic errors by the OptiLayer post-production characterization module.*

4. References

[1]- M. Trubetskov, *"OptiLayer Thin Film Software"*, OptiLayer, Russia, (2020).
[2]- A. Tikhonravov, *"Optical Coatings"*, SPIE Press, USA, (2024).
[3]- A. Tikhonravov et al., *"Optical characterization and reverse engineering based on multiangle spectroscopy"*, Applied Optics, **51**, 2, (2012).

Acknowledgments
LNA, Jesulino Santos, Vinícius Pimentel, Lais Abreu, Viviane Silva, Alvaro Damião, ITA, IEAv and CNPq.

*Corresponding author: mmorbidelli@lna.br

PROCESS OPTIMIZATION FOR THE DEVELOPMENT OF ZnO THIN FILM RESISTORS WITHOUT PHOTOLITHOGRAPHY

Jhon Franco Vasquez Abad*, Jorge David Reyes Diaz, Marcos Tiago Albuquerque Marques, Everton Bonturim, Marcos Massi, and Mariana A. Fraga
Escola de Engenharia, Universidade Presbiteriana Mackenzie, São Paulo, Brasil

1. Introduction

Zinc oxide (ZnO) is a promising material for thin film resistors due to its tunable electrical properties, thermal stability, and compatibility with low-cost deposition techniques [1,2]. This work explores a lithography-free approach based on sputtering and shadow masks to simplify fabrication and to use them as strain gauges or piezoresistive sensors. Initial processes using acrylic masks at room temperature resulted in poor film quality. By transitioning to stainless steel masks, deposition at 500 °C became feasible, significantly improving film electrical properties. This study focuses on process optimization, highlighting the impact of mask material and substrate temperature on the quality of ZnO thin film resistors.

2. Experimental

ZnO thin films were deposited on Si(100) substrates using radiofrequency (RF) magnetron sputtering. Preliminary depositions at different conditions without masks were carried out and characterized by four-point probe measurements, X-ray diffraction (XRD), and scanning electron microscopy (SEM), indicating that the selected conditions were suitable for ZnO resistor fabrication. An acrylic shadow mask was used for depositions performed at room temperature without active substrate heating, while a stainless steel mask was employed for depositions at 500 °C. A 2-inch ZnO target was sputtered at 150 W (RF), under a working pressure of $1.0x10^{-1}$ hPa, with an $Ar/O_2/N_2$ gas flow ratio of 40:10:10. The deposition time was 60 min. A pre-sputtering step (5-10 minutes) was carried out *in-situ* to clean the target surface prior to film growth. Figure 1 summarizes the development process of the ZnO thin film resistors.

3. Results and Discussions

ZnO thin film resistors fabricated using the steel shadow mask are currently under piezoresistive testing, showing satisfactory performance. The improved film quality obtained at 500 °C contributed to enhanced device response compared to room-temperature depositions. However, alignment issues associated with the masking process were identified, leading to slight variations in geometry and contact definition. Despite these limitations, the results demonstrate the feasibility of the lithography-free approach, with alignment optimization representing a key step for further improving resistor uniformity and reproducibility.

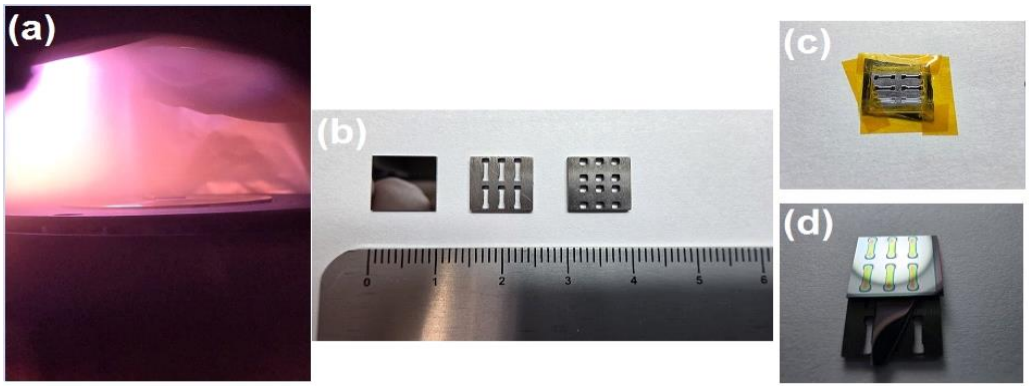


Figure 1. RF magnetron sputtering plasma during ZnO deposition, (b) steel shadow masks used for lithography-free patterning, (c) Sample with acrylic shadow mask positioned prior to deposition and (d) fabricated ZnO thin film resistors.

4. References

[1] M. A. Fraga, et al., "Wide bandgap semiconductor thin films for piezoelectric and piezoresistive MEMS sensors applied at high temperatures: an overview," Microsystem Technologies, vol. 20, no. 1, pp. 9-21, 2013.
[2] G. W. A. Cardoso et al., "Evaluation of piezoresistivity properties of sputtered ZnO thin films," Materials Research, vol. 17, no. 3, pp. 588-592, 2014.

Acknowledgments

The financial support from MackPesquisa, CNPq, Fapesp, and Fundação Cenep.

*Corresponding author: jhon.abad@mackenzista.com.br

AUTOMATED RADIOMETRIC CHARACTERIZATION OF INFRARED SENSORS USING THE RADIOMÉTRICA SOFTWARE

Rafael Vicente Freires dos Santos[1]*, Ruy Morgado de Castro [2], Alvaro José Damião[1,2]
[1]*Instituto Tecnológico da Aeronáutica, São José dos Campos, SP*
[2]*Instituto de Estudos Avançados, São José dos Campos, SP*

1. Introduction

Radiometric characterization ensures the reliability of infrared sensors used in remote sensing, industrial inspection, and scientific applications. The radiometric transfer function is expressed as *"$DN = G \cdot T + O$"*, relating digital number (DN) to scene temperature through gain and offset. Manual workflows often lack reproducibility and traceability. To address these limitations, this work presents *Radiométrica*, a software tool that automates the complete radiometric characterization pipeline, including ROI selection, statistical analysis, temporal noise, spatial uniformity, radiometric regression, and report generation.
Palavras-chave: caracterização radiométrica; sensores térmicos; automação; regressão linear; infravermelho.

2. Experimental Procedure

Two validation campaigns were conducted. The first used a CI Systems SR80012D blackbody and a WIRIS Pro thermal camera. A controlled sweep from 20 °C to 80 °C in 10 °C increments was performed, acquiring 30 images per temperature level (240 TIFF images). The second validation used laboratory data from Salles (2026), obtained with a Parrot Sequoia NIR camera, an integrating sphere, and FieldSpec™ spectroradiometer measurements. Radiance values were computed by trapezoidal integration in the 770–810 nm band. Both saturated and non-saturated datasets were analyzed to evaluate linearity and saturation-detection algorithms.

3. Results and Discussions

Radiométrica processed all datasets without errors. For the blackbody experiment, the calibration curve showed high linearity (R^2 = 0.9965), sensitivity of 0.0248 °C/DN, temporal noise below 2.11 °C, and spatial non-uniformity under 1.7%. The mean $|\Delta T|$ bias was 1.46 °C, with a maximum of 3.3 °C at 80 °C.
For the Sequoia NIR data, the regression using non-saturated datasets yielded $R^2 = 0.999974$, confirming excellent linearity. Differences of 1–2% relative to ImageJ were attributed to ROI geometry rather than algorithmic discrepancies. Saturated datasets were correctly identified, with DN values near 65,472 and proper threshold detection. The software demonstrated numerical stability, robust anomaly detection, and consistent generation of radiometric metrics. These results confirm the suitability of Radiométrica for standardized and automated radiometric characterization.

4. Conclusion

These results indicate that Radiométrica is suitable for standardized and automated radiometric characterization of infrared sensors, providing robust linear regression, reliable saturation detection, and stable computation of temporal noise and spatial non-uniformity. As a conclusion, the software effectively replaces manual spreadsheet-based workflows with a traceable, auditable, and fully integrated pipeline. Future developments will incorporate environmental variables, such as ambient temperature and humidity, into the calibration model to further improve accuracy.

5. References

[1] EMVA 1288 Working Group, EMVA Standard 1288 – Standard for Characterization of Image Sensors and Cameras, Release 4.0 Linear, 2021.
[2] Salles, T. S., Radiometric and Spatial Characterization of a Multispectral Electro-Optical Sensor in Field Conditions, M.Sc. Dissertation, ITA, 2026.

Acknowledgments

The authors thank Thamís da Silva Salles for providing laboratory datasets and the PITER Project at IEAv for equipment support.

*Author: rafael_freiressantos@hotmail.com

INFLUENCE OF ELECTRODEPOSITION TIME OF THE NiCoFeCrMn ALLOY ON THE MORPHOLOGY OF SAE 1020 STEEL

Oliveira, L.S.[1,2*], Correa, O.V.[1], Cotinho, S. P.[1], Rodrigues, D.[1] e Pillis, M.F.[1]
[1]Instituto de Pesquisas Energéticas e Nucleares, *IPEN/CNEN-SP* [2]Fatec Mauá

1. Introduction

High-entropy alloys are used as coatings to increase the wear and corrosion resistance of less noble materials. Electrodeposition stands out for its low cost, but requires rigorous control due to the electrochemical competition between the various elements of the alloy. The electrochemical potential of each element influences the sequence and rate of deposition. In addition, pH and current density are controlled to minimize hydrogen evolution, which generates bubbles and compromises the morphology and performance of the coating.

2. Materials and Methods

SAE 1020 steel samples were polished, washed in running water, pickled, and mounted in a standard ASTM electrochemical cell. The electrolyte was composed of sulfate salts of the elements of interest and complexing agents, presenting pH=2 and electrical conductivity of 70 mS/cm, parameters that allowed a current density of 35 A/dm². Electrodeposition occurred under direct current for periods of 10 and 30 minutes, under constant agitation and temperature of 40 °C. Morphological characterization was performed by scanning electron microscopy (SEM), and the chemical composition by energy dispersive spectroscopy (EDS).

3. Results and Discussion

It was observed that increasing the deposition time promoted changes in the coating morphology, as illustrated in Figures 1 and 2. The deposit presented a cracked appearance, originating from the intense generation of bubbles resulting from the hydrogen evolution reaction. This phenomenon is due to the electrochemical potential of hydrogen, which favors its simultaneous discharge with that of metallic ions. Consequently, the deposition sequence follows the hierarchy of element potentials, resulting in a non-equiatomic composition. Competition between the elements for incorporation into the coating is evident, as discussed in the literature [1,2].

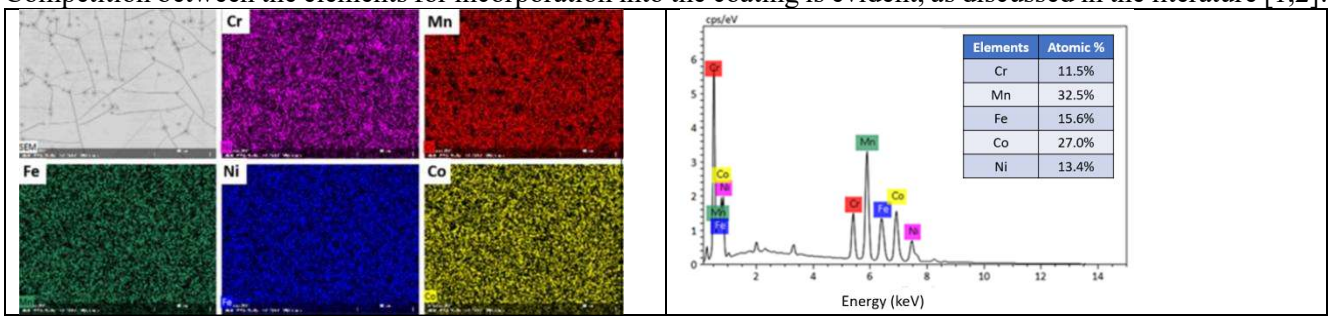


Fig. 1 – *Surface morphology of the NiCoFeCrMn coating electrodeposited for 10 minutes.*

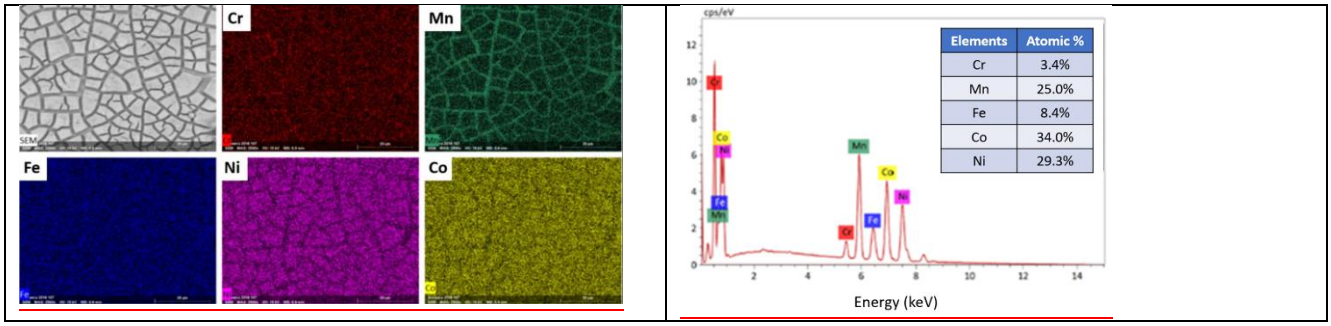


Fig. 2 - *Surface morphology of the NiCoFeCrMn coating electrodeposited for 30 minutes*

References

[1]- Cantor B et al., Mater. Sci. Eng. A, 375–377, 213-218, (2004).
[2]- Nechvoglod O et al., JOM, 77, 1005-1028, (2025).

Acknowledgments

This study was financed in part by the Coordenação de Aperfeiçoamento de Pessoal de Nível Superior - Brasil (CAPES) - Finance Code 001.

*Autor para correspondência: leandro_oliveira@usp.br

STUDY OF DIFFERENT POWDERS FOR THE BORONIZATION OF AISI 304 STAINLESS STEEL

Rogério Varavallo[1]*, Bruno Paes Silva[2], Marcos Dorigão Manfrinato[3]

[1]*Centro Universitario Unica*

[2,3]*Fatec Sorocaba*

1. Introduction

Among the most common problems associated with industrial equipment and machinery are component wear, fatigue, and corrosion, which cause significant losses for industrial facilities. Even though the wear process generally does not occur catastrophically, it reduces operational efficiency due to power losses, which significantly increases energy and lubricant consumption, not to mention the downtime required for maintenance and/or replacement of these components [1].

2. Experimental or Theory

AISI 304 steel was thermochemically treated via solid-state boronizing at a temperature of 950°C for 5 hours and subsequently cooled in the furnace. Two types of solid boronizing agents were used: Mixture 1 consisted of 80% borax dehydrated at 600°C and 20% SiC with a particle size of 5 µm. Mixture 2, on the other hand, is the commercial boriding agent Ekabor 2. Subsequently, the thickness of the formed layer, the microhardness of the layer, and the wear resistance were analyzed.

3. Results and Discussions

Figure 1 shows the layer formed after thermochemical treatment of mixtures 1 and 2. In mixture 1, the layer had a thickness of 4.7 ± 1.1 µm and exhibited cracks between the interface and the boride layer, whereas mixture 2 had a thickness of 16.7 ± 1.7 µm and showed no cracks in the boride layer. Figure 2 shows the results of the wear test on the base metal and the two mixtures studied; it can be observed that mixture 2 exhibited less wear. We performed a microhardness profile on the base material (308 HV) and on mixtures 1 (643 HV) and 2 (1272 HV) studied.

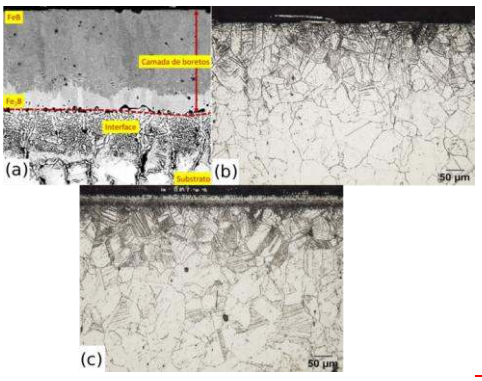


Fig. 1. Microstructure of the boron-doped layer. (a) Regions of the boron-doped layer [2], (b) boron-doped layer with Mixture 1, (c) boron-doped layer with Mixture 2 – EKABOR 2.

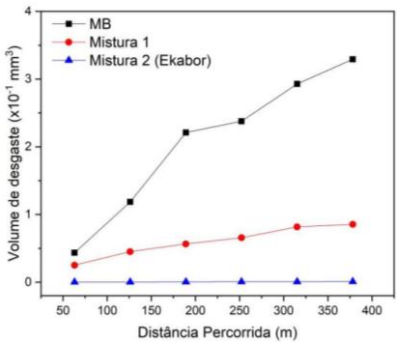


Fig. 2. Vickers surface microhardness.

Both mixtures showed improvements in mechanical properties; mixture 2 was the most efficient, but mixture 1 has the advantage in terms of the cost of producing the powder.

4. References

[1]- B. Venkatesh, K. Sriker, and V. S. V. Prabhakar, "Wear Characteristics of Hardfacing Alloys: State-of-the-art," Procedia Mater. Sci. 10, 527–532 (2015). https://doi.org/10.1016/j.mspro.2015.06.002

[2]- F. E. Mariani et al., "Caracterização de camadas obtidas no aço inoxidável AISI 304 boretado em meio líquido," in 22° CBECIMat - Congresso Brasileiro de Engenharia e Ciência dos Materiais (Natal, 2016).

Acknowledgments

I would like to thank the professors for the opportunity to complete this project and FATEC Sorocaba for making it possible.

*Corresponding author: rogerio.varavallo@gmail.com

DESIGN AND DEVELOPMENT OF A DIDACTIC PLASMA NITRIDING CHAMBER

Arão Ngadi Makiesse Zampassi[1]*, Mauricio Andolfato[2], Mateus Ritter Pasini[3], Mario Wolfart Junior[4], João Pedro Naderer Baptistão[5]
[1,2,3,4,5]*Instituto Federal Catarinense – Campus Luzerna*

1. Introduction

Experimental activities involving gas ionization chambers are highly relevant for both scientific investigation and engineering education. Plasma, recognized as the fourth state of matter, exhibits unique physical and chemical properties governed by the interaction of charged species under electromagnetic fields, playing a key role in materials engineering and surface modification processes. In industrial systems, such as plasma nitriding reactors, plasma visualization is typically limited due to the closed metallic chamber design. In contrast, the use of a translucent ionization chamber in an educational environment enables direct and safe visualization of plasma, allowing the observation of phenomena such as gas ionization, electrical discharge regimes, and light emission.

Plasma consists of electrically charged particles that respond to electromagnetic forces, comprising a gas containing neutral and charged species such as electrons, positive and negative ions, atoms, and molecules, with the degree of ionization being a key plasma parameter [1].

The mixture of ions and free electrons defines plasma as a state of matter in which charged particles interact through electromagnetic forces, which can dominate over gravitational forces under certain conditions [2].

Furthermore, the lack of accessible didactic equipment for plasma demonstration often limits the effective teaching of gas ionization concepts. In this context, the development of a dedicated experimental platform aligned with research-based learning strategies represents an important contribution to engineering education [3].

2. Experimental

This work presents the design, fabrication, and validation of a didactic plasma nitriding chamber intended for the study of gas ionization phenomena. The system consists of a cylindrical reactor incorporating a translucent tube, allowing real-time plasma visualization during operation.

The internal configuration includes a central cathode and the chamber base acting as the anode. The system is equipped with a vacuum pump for pressure control, a vacuum gauge for monitoring, and valves for regulating gas inlet and composition. Electrical parameters (voltage and current) are continuously monitored using appropriate instrumentation, while temperature is measured using a type K thermocouple coupled to a data acquisition system. Experimental tests were performed using hydrogen (H_2) and nitrogen (N_2) gases under reduced pressure conditions. The theoretical framework is based on plasma physics principles, including ionization mechanisms, electrical conduction in gases, and plasma stability behavior.

3. Results and Discussions

Preliminary results demonstrate the successful operation of the developed chamber, with stable plasma formation observed under different operating conditions. The translucent design enabled clear visualization of plasma structure and color variation as a function of gas composition and electrical parameters.

It was observed that the use of hydrogen (H_2) resulted in a comparatively more stable discharge during the initial operation stages, particularly for chamber cleaning via sputtering, contributing to improved plasma uniformity. Nitrogen (N_2), on the other hand, showed distinct light emission characteristics and discharge behavior, consistent with its role in nitriding processes. Despite the successful operation, some limitations were identified, including challenges related to sealing efficiency, discharge stability under certain conditions, and the need for improvements in the electrical insulation system to enhance safety and reproducibility. Overall, the system demonstrated strong potential as a didactic and experimental platform. Ongoing improvements aim to enhance operational reliability, safety, and process control, consolidating the setup for applications in plasma-assisted surface engineering and engineering education.

4. References

[1]- C. Alves Junior *"Nitretação a plasma: fundamentos e aplicações"*, 7th edition, Natal, Brazil, (1998).
[2]- A. L. Perrant *"Physics of the plasma universe"*, 7th edition, Los Alamos, USA, (1992).
[3]- J. Pinho Alves *"Atividade experimental: Uma alternativa na concepção construtiva"*, Florianópolis, Brazil, (2000).

Acknowledgments
The authors acknowledge the Instituto Federal Catarinense (IFC) – Luzerna Campus for the financial support provided for the development of this project.

*Corresponding author: araozampassi9@gmail.com

HIGH-HEAT-FLUX PERFORMANCE OF THERMAL BARRIER COATINGS FOR ATMOSPHERIC REENTRY

Nazir M. Santos[1*], Roberson J. Silva[1], Agatha C. Corrêa[1],Vera L. O. Brito[1]
[1]*Institute of Advanced Studies (IEAv),São José dos Campos, São Paulo,Brasil*

1. Introduction

Thermal barrier coatings (TBCs) are widely investigated for aerospace applications involving severe thermal environments, especially high heat fluxes associated with atmospheric reentry [1,2]. Typically composed of ceramic top coats and metallic bond coats, these systems reduce heat transfer to the substrate while preserving structural integrity under rapid heating and steep thermal gradients [3,4]. Therefore, evaluating microstructural stability, interfacial integrity, and thermal protection capability is essential to assess their suitability for aerospace systems. This study investigates APS-deposited TBCs subjected to extreme thermal loading produced by an atmospheric plasma flow, focusing on the relationship between heat-flux exposure, coating degradation, and implications for atmospheric reentry applications.

2. Experimental

Thermal barrier coating systems were deposited by atmospheric plasma spraying onto Ti-6Al-4V substrates. The coating system consisted of a NiCrAlY bond coat and a yttria-stabilized zirconia ceramic top coat. The coated specimens were exposed to high heat fluxes generated by an atmospheric plasma torch under conditions selected to simulate severe reentry-relevant heating environments. After thermal exposure, the samples were characterized in terms of surface condition, cross-sectional microstructure, coating thickness variation, interfacial damage, and evidence of ablation or delamination. Optical microscopy, scanning electron microscopy, and X-ray diffraction were used to identify degradation features and assess the structural integrity of the coating system after ablation testing.

3. Results and Discussions

Atmospheric plasma exposure promoted significant microstructural changes in the TBC system, particularly under higher heat fluxes and longer exposure times. Degradation was mainly observed in the ceramic top coat and near the coating/substrate interface, where localized cracking, partial material loss, and adhesion degradation occurred. Ablation tests showed that the TBC maintained structural integrity at heat fluxes up to 2.0 $MW \cdot m^{-2}$ for 27 s, with minimal mass loss. These findings indicate that the YSZ/NiCrAlY coating system provided effective thermal protection by delaying direct damage to the Ti-6Al-4V substrate. Nevertheless, coating integrity progressively decreased under the most severe conditions, highlighting the importance of coating design, bond coat composition, and thermal cycling resistance for reentry applications. Overall, APS TBCs are promising candidates for aerospace thermal protection, although further optimization is required.

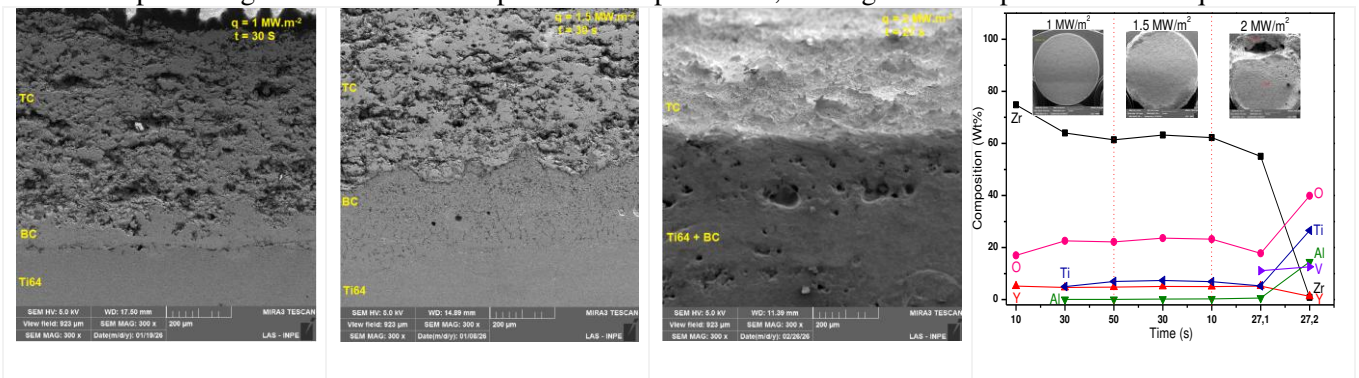


Fig. 1. Cross-sectional SEM images of the YSZ-TC/NiCrAlY-BC/Ti64 interface after ablation at 1.0 $MW \cdot m^{-2}$ for 30 s (a), 1.5 $MW \cdot m^{-2}$ for 30 s (b), and 2.0 $MW \cdot m^{-2}$ for 27 s (c); surface composition versus exposure time under different heat fluxes (d).

4. References

[1] Miller RA. Cleveland: NASA; 2009.
[2] Clarke DR, Phillpot SR. 2005;8(6):22-29. doi:10.1016/S1369-7021(05)70934-2
[3] Liu Q, et al. Journal of Thermal Spray Technology. 2024;33:2723-2733. doi:10.1007/s11666-024-01782-0
[4] Jaworski R, et al. Journal of the European Ceramic Society. 2020;40:3745-3762.

Acknowledgments

COMAER - Ed. CAPA IEAV- PropHiper (Proc. 67720.009933/2024-93) and CNPq (Proc. 157898/2025-3).

*nazirmonteiro@gmail.com

SMART CHITOSAN FILMS WITH ALGINATE NANOPARTICLES FOR ON-DEMAND GENTAMICIN RELEASE

Cecilia Zorzi Bueno[1]*, Helton José Wiggers[1], Pascale Chevallier[2], Francesco Copes[2] and Diego Mantovani[1,2]
1Associação de Ensino, Pesquisa e Extensão Biopark (Laboratório de Biomateriais e Bioengenharia)
2Université Laval (Department of Min-Met-Materials Engineering and CHU de Quebec Research Center, Division Regenerative Medicine)

1. Introduction

Skin wounds are highly prone to infection, often requiring prolonged antibiotic use, which can reduce patient compliance and contribute to antimicrobial resistance. To overcome these challenges, smart wound dressings with controlled and stimuli-responsive drug release have been increasingly explored. Natural polymers such as chitosan and alginate stand out due to their biocompatibility, biodegradability, and responsiveness to environmental conditions. In this context, the study proposes a system based on alginate nanoparticles embedded in chitosan films to enable controlled, pH-responsive release of gentamicin.

2. Experimental

Alginate–gentamicin nanoparticles were prepared via ionic gelation under magnetic stirring. The nanoparticles were then incorporated into chitosan-based films crosslinked with tannic acid and iron [1,2]. Nanoparticles were characterized for size, morphology, drug loading, release behavior and antimicrobial activity. Films were thoroughly characterized for morphology, swelling and mass loss under physiological conditions, mechanical, thermal, and chemical properties, as well as release behavior at different pHs. Biological performance was evaluated through antibacterial assays and cytocompatibility tests using human dermal fibroblasts.

3. Results and Discussions

Alginate–gentamicin nanoparticles were successfully synthesized, presenting an average size of ~86 nm, narrow size distribution, and high drug loading efficiency (~100%). The incorporation of nanoparticles into chitosan-based films reduced swelling capacity and decreased the initial burst release of gentamicin by up to 57% at physiological pH (7.4), indicating improved control over drug delivery. The system also exhibited clear pH-responsive behavior, with up to 50% higher antibiotic release under mildly acidic conditions (pH 5.5), maintaining drug concentrations above the minimum inhibitory level for up to 14 days. Additionally, the films showed effective antibacterial activity against both Gram-positive and Gram-negative bacteria while remaining cytocompatible and mechanically robust. Overall, this strategy shows promising potential for the development of smart wound dressings with controlled, stimuli-responsive antibiotic release, enhancing infection management and promoting improved healing.

4. References

[1] P. Chevallier, H. J. Wiggers, F. Copes, C. Z. Bueno, D. Mantovani. Nanomaterials **13(3)**, 484 (2023)
[2] C.Z. Bueno, H.J. Wiggers, P. Chevallier, F. Copes, D. Mantovani. Polymers **17**, 2261(2025)

Acknowledgments

BIOPARK, Prati–Donaduzzi Pharmaceutical Industry, the Natural Science and Engineering Research Council of Canada and CNPq 408919/2023-0. Thanks to Carmen Donaduzzi, Ph.D., and Luiz Donaduzzi, Ph.D. for guidance.

*Corresponding author: cecilia.bueno@bpkedu.com.br

SUBSTRATE-DEPENDENT WETTABILITY AND HYDROPHOBIC RECOVERY OF PE AND PDMS UNDER IDENTICAL PLASMA TREATMENT

Vinicius Luiz Ruschel*, Francisco Alfaro[1], Diego Mantovani[2]
[1] *Associação de Ensino, Pesquisa e Extensão Biopark (Laboratory for Biomaterials and Bioengineering)*
[2]*Université Laval (Min-Met-Materials Eng, Lab Biomaterials & Bioengineering)*

1. Introduction

Polyethylene (PE) and polydimethylsiloxane (PDMS) are hydrophobic polymers widely used in biomaterials, coatings, and microfluidic systems. Plasma treatment is a clean and effective strategy to increase polymer wettability by introducing polar groups and increasing surface energy [1]. However, the induced hydrophilicity may decrease over time due to hydrophobic recovery, which is strongly dependent on the polymer structure [2]. Because PE and PDMS differ in chemical structure and chain mobility, we hypothesized that both the polymer substrate and plasma power would influence the initial wettability response and the time-dependent hydrophobic recovery under identical Ar/O_2 plasma conditions.

2. Experimental

PE and PDMS samples were treated simultaneously in a PECVD reactor (Flarion, Plasmionique). Plasma was generated using Ar (5 sccm) and O_2 (25 sccm). The chamber was evacuated (~1 h), followed by purge and stabilization steps. Treatments were performed for 1 min at powers ranging from 50 to 300 W. Wettability was evaluated by water contact angle (WCA) measurements using a goniometer (OCA 11, DataPhysics). WCA was measured using 3 µL water droplets at three points per sample for untreated surfaces, immediately after plasma treatment, and after 10 min, 30 min, and 24 h.

3. Results and Discussions

Plasma treatment significantly reduced the WCA of both materials. Untreated PE and PDMS showed hydrophobic behavior, with WCA values of ~102–105°. Immediately after treatment, PDMS reached ~25–30°, whereas PE showed higher values of ~38–47°, indicating a stronger initial hydrophilic response for PDMS. However, both materials exhibited progressive hydrophobic recovery over time, as shown in Figs. 1 and 2.

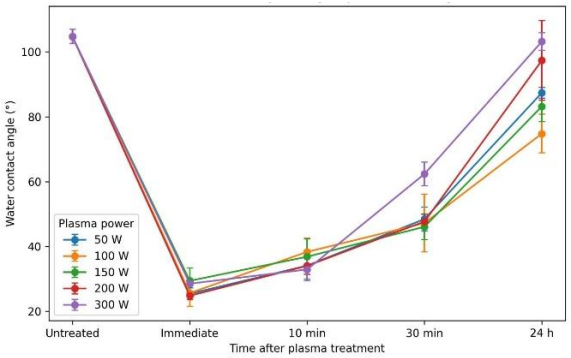


Fig. 1. *Water contact angle evolution of PDMS surfaces as a function of time after plasma treatment performed at different applied powers.*

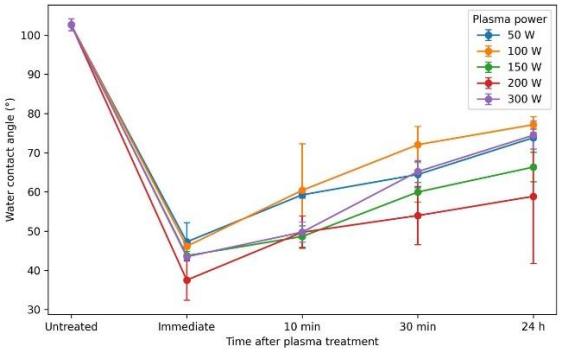


Fig. 2. *Water contact angle evolution of PE surfaces as a function of time after plasma treatment performed at different applied powers.*

PDMS exhibited a more pronounced hydrophobic recovery, reaching ~75–103° after 24 h and approaching its untreated state. In contrast, PE showed only partial recovery (~59–76°), remaining more hydrophilic and indicating better temporal stability. Plasma power affected the substrates differently: PDMS recovery was more power-dependent, with the lowest 24 h WCA at 100 W, whereas PE showed greater overall stability, with 200 W producing the lowest immediate WCA. These results confirm that wettability evolution under identical Ar/O_2 plasma conditions is substrate-dependent.

4. References

[1]- C. Ma, A. Nikiforov, D. Hegemann, N. De Geyter, R. Morent and K. Ostrikov, *Int. Mater. Rev.*, 68, (2023).
[2]- M. Mozetič, *Polymers*, 15, 4668, (2023).

Acknowledgments

BIOPARK, Prati–Donaduzzi Pharmaceutical Industry, the Natural Sciences and Engineering Research Council of Canada, and CNPq 408919/2023-0. The authors also thank Carmen Donaduzzi, Ph.D., and Luiz Donaduzzi, Ph.D.

EXPLORING THE POTENTIAL OF OIL AND GAS DRILLING TECHNOLOGIES IN NATURAL HYDROGEN EXTRACTION

Gustavo Henrique Romeu da Silva[1,2,*] and Andreas Nascimento[1,2,3]
[1]*School of Engineering and Sciences, São Paulo State University, Guaratinguetá, Brazil*
[2]*Institute of Drilling Engineering and Fluid Mining, TU Bergakademie Freiberg, Freiberg, Germany*
[3]*Institute of Engineering and Mechanics, Federal University of Itajubá, Itajubá, Brazil*

1. Introduction

One of the major challenges today is to meet the global energy demand sustainably by developing clean fuels and renewable energy sources, amid increasing pressure to reduce emissions and combat global warming [1][2]. Natural hydrogen is a promising and sustainable alternative for diversifying the energy mix and reducing carbon emissions [3][4]. The objective is to identify research trends, technological approaches, and knowledge gaps, particularly regarding the challenges related to hydrogen's physical properties. The results are intended to support future experimental research and contribute to the development and transfer of appropriate technologies.

2. Material and method

This research was conducted through a bibliometric analysis of scientific publications indexed in the Scopus database, focusing on articles and reviews published between 2020 and 2024 in English. The search includes articles related to the following keywords: natural hydrogen, drilling technology, oil and gas technology, hydrogen exploration, and technology adaptation, in order to identify meaningful connections and trends within literature.

3. Results and Discussions

This analysis allows us to observe trends in academic interest and the growing relevance of the subject. Fig. 1 and 2 illustrate a steady increase in the number of publications from 2020 to 2024, indicating a continuous expansion of research activities. The network, created with VOSviewer software, version 1.6.20, includes 50 selected keywords grouped into four clusters, with a minimum co-occurrence threshold of four.

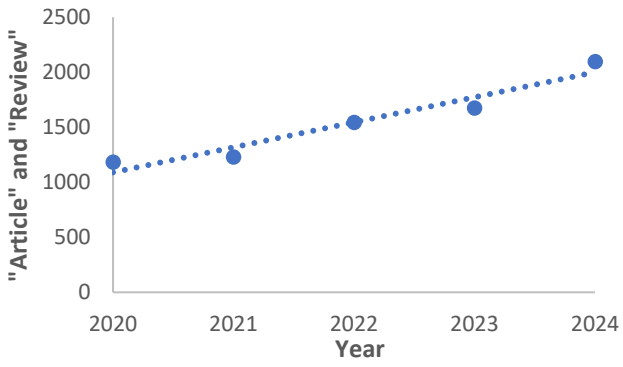


Fig. 1. Publications on Natural Hydrogen and Drilling Technologies Published per Year.

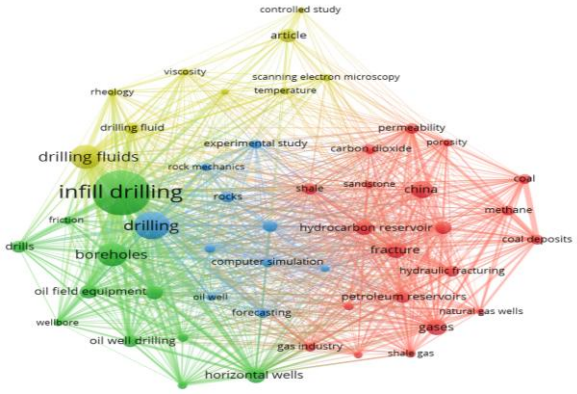


Fig. 2. Keyword co-occurrence network based on Scopus articles.

4. Conclusions

This study evaluates the adaptation of oil and gas drilling technologies for natural hydrogen extraction, highlighting efficiency gains, safety improvements, and existing knowledge gaps, while emphasizing the relevance of natural hydrogen for future energy systems.

5. References

[1] G.H.R. Silva, A. Nascimento, C. D. Baum, and M. H. Mathias, "Renewable Energy Potentials and Roadmap in Brazil, Austria, and Germany," **Energies**, vol. 17, Article ID 1482, March 2024.
[2] G.H.R. Da Silva et al. "Renewable energy perspectives: Brazilian case study on green hydrogen production," **AIMS Energy**, vol. 13, pp. 449-470, April 2025.
[3] E. C. Gaucher, "New Perspectives in the Industrial Exploration for Native Hydrogen," **Elements**, vol. 16, pp. 8–9, February 2020.
[4] V. Zgonnik, "The occurrence and geoscience of natural hydrogen: A comprehensive review," **Earth-Science Reviews**, vol. 203, Article ID 103140, April 2020.

Acknowledgments

This work was supported by the MCTI, CNPq and CAPES – 001, Brazil; and AvH, Germany.

*Corresponding author: gustavo.romeu@unesp.br

EFFECT OF APPLIED FREQUENCY ON THE FORMATION OF REACTIVE SPECIES AND THE PHYSICOCHEMICAL PROPERTIES OF PLASMA-ACTIVATED WATER

Gabriel Nunes[1]*, Júlia Karnopp[2], Julio César Sagás[3]

[1]*Universidade do Estado de Santa Catarina (Udesc), Graduate Program in Physics, Laboratory of Plasmas, Films and Surfaces, Joinville, SC, Brazil*

1. Introduction

The possibility of species generating reactive oxygen and nitrogen RONS, associated with alterations in their physicochemical properties, shows the importance of plasma-activated water (PAW) in the development of new technologies for applications in the biomedicine field, microbial inactivation, seed germination and plant growth [1-3]. Thus, investigating its properties, as well as its operational parameters, it is fundamental for the optimization of PAW. In this context, this work analyzes the influence of applied frequency on PAW production through the analysis of its parameters under different experimental conditions.

2. Experimental

For the production of (PAW), 50 mL of distilled water was activated using a DBD plasma jet system with a fixed compressed air flow at 2 L/min during 30 minutes. Three conditions were selected with applied frequency at 8, 12, and 20 kHz under the same applied voltage, 16.2 ± 0.2 kV. After the activation, the physicochemical parameters pH, oxidation-reduction potential (ORP), total dissolved solids (TDS) and conductivity (EC) were measured using a HANNA HI3512 multiparameter instrument. The composition of each PAW was determined using an AKSO MICRO 20 multiparameter instrument to measure the concentration of the RONS peroxide, nitrite, and nitrate .

3. Results and Discussions

The results indicate an influence of the applied frequency on the physicochemical properties of PAW, according to the results in Tab. 1.

Frequency	pH	ORP (mV)	EC (µS)	TDS (ppm)	Peroxide (ppm)	Nitrite (ppm)	Nitrate (ppm)
Control	6.33	33.7	2.135	1.068	0	0	0
20 kHz	3.58	185.8	83.4	41.71	0.9	1.73	27.6
12 kHz	3.19	208.4	223.3	111.7	2.2	1.16	<30.0
8 kHz	3.66	182.6	82.15	41.06	1.0	1.04	26.4

Tab 1. Results of physicochemical parameters and RONS concentrations for distilled water (control) and plasma-activated water at different applied frequencies.

The 12 kHz frequency showed the most variations on the PAW chemistry , with a reduction in pH from 6.33 to 3.19 and an increase in ORP from 33.7 mV to 208.4 mV, suggesting greater acidification and oxidizing capacity of the PAW due the increase in production of RONS as can be confirmed analyzing the TDS (111.7 ppm) and concentration of peroxide and nitrate species.Under this same condition, it was observed the highest values of electrical conductivity (223.3 µS) which is directly associated with the presence of ionic species in the solution as nitrate and H+ produced due the dissolution of nitric acid produced in the plasma. For the frequencies of 20 and 8 kHz, even if the pH values are close to those obtained at 12 kHz, the other parameters are significantly lower. These results show us that the 12 kHz frequency is more favorable to the generation of reactive species which is a consequence of the plasma operation. The results provided relevant information regarding the system operation for future applications of PAW.

4. References

[1]- D. Xu, S. Wang, B. Li, M. Qi, R. Feng and Q. Li, Microorganisms, 8, 1091, (2020).
[2]- L. Guo, R. Xu, L. Gou, Z. Liu, Y. Zhao, D. Liu, L. Zhang, H. Chen and M. G. Kong, Appl. Environ. Microbiol., 84, (2018).
[3]- M. Bafoil, A. Jemmat, Y. Martinez, N. Merbahi, O. Eichwald, C. Dunand and M. Yousfi, PLoS One, 13, (2018).

Acknowledges FAPESC for the financial support and UDESC for the infrastructure and support provided.

*Corresponding author: nunesg920@gmail.com

POTENTIAL ANTIMICROBIAL ACTIVITY OF MULTI-WALLED CARBON NANOTUBES (MWCNTs) OBTAINED BY DIFFERENT SYNTESIS METHODS: A COMPARATIVE STUDY

Hilda Geovana Alves Pinto[1]*, Antônio Marcos Fonseca[3], Larissa Solano De Almeida[2], Luciano do Nascimento Batista[4], Luciana Sgarbi Rossino[1], Silvia Pierre Irazusta[1,3]

[1]*Faculdade de Tecnologia de Sorocaba (FATEC)*

[2]*Universidade Federal de São Carlos (UFSCar) - Campus Sorocaba*

[3]*Mestrado Profissional em Gestão e Tecnologia em Sistemas Produtivos, CEETEPS*

[4]*Instituto Nacional de Metrologia, Qualidade e Tecnologia (INMETRO)*

1. Introduction

Microbial resistance caused by the inappropriate use of antibiotics and antifungals represents a global threat to public health, requiring new antimicrobial approaches. Nanomaterials, due to their unique physicochemical and mechanical properties, have shown promise in combating microorganisms. Among them, carbon nanotubes stand out for their antimicrobial action based on mechanical interaction with cell membranes. Studies indicate that multi-walled carbon nanotubes (MWCNTs) can damage microorganisms in a way that inhibits their growth [1]. Thus, this work aims to compare the antimicrobial activity of MWCNTs produced by PECVD method, comertials MWCNT-HELIX, and MWCNT-CARBON EXPLORER, both obtained by CVD method in the microbiological control of surfaces.

2. Experimental methodology

Microbial suspensions were prepared from standardized fungal cultures of *Fusarium spp.* according to the 0,5 MacFarland scale. Serial dilutions of MWCNTs (10–50 mg/L). were prepared and 1 mL of each one was spread in petri dishes contained solid medium with a Fusarium sp. Inoculum. The results were expressed in number of Colony Unit Forming.

3. Results and Discussions

The present study demonstrated that the PECVD-MWCNTs exhibited effective antifungal activity in 10 and 50 mg/L concentrations (Figure 1 A and B, C). This result is in agreement with other studies in the literature [2], where the *Fusarium spp*. was inhibited by a tenfold higher concentration of CNT. The commercial HELIX-MWCNTs did not affect the growth in any concentration and the CARBON EXPLORER-MWCNTs, caused an increase in culture proliferation, probably acting as a carbon support for enhanced fungal growth after 48 hours of incubation. This property probably is related to the quantity of graphene sheets present in the CNTs (Figure 1 D and E, F).

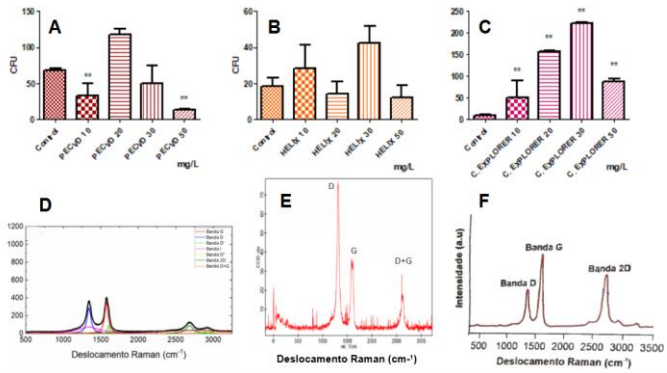


Figure 1. A: PECVD Colony Forming Unity. B: HELIX Colony Forming Unity. C: CARBON EXPLORER Colony Forming Unity. D: RAMAN of PECVD. E: RAMAN of HELIX. F: RAMAN of CARBON EXPLORER.

4. References

[1]DE ANDRADE, L. R. M.; *et al*. Biomedical applications of carbon nanotubes: A systematic review of data and clinical trials. **Journal of Drug Delivery Science and Technology**, [*s. l.*], v. 99, n. July, 2024.

[2]MANZOOR, Sadia et al. Elucidating the mechanisms of *Fusarium oxysporum f. sp. tuberosi* inhibition using functionalized multi-walled carbon nanotubes: A comprehensive analysis of biophysical and molecular interactions. **Journal of Integrative Agriculture**, [s. l.], v. 25, n. 4, p. 1544-1555, 2026.

Acknowledgments

We thank CNPq for the scientific initiation scholarship, and Luciano do Nascimento Batista from INMETRO for sponsorship.

*hildasgeoalves@gmail.com

Modification of the Structure and Properties of TiN_x Films with Nitrogen Concentration

Josieli Honorato[1,*], Ana Júlia Schneider Garcia[1], Abel André Cândido Recco[1], Felipe Carneiro da Silva[2], Diao Xungang[3], Luis César Fontana[1], Julio César Sagás[1]

[1] *Universidade do Estado de Santa Catarina (UDESC), Laboratório de Plasmas, Filmes e Superfícies, Joinville-SC, Brazil*[2] *Faculdade de Tecnologia (FATEC), Centro Estadual de Educação Tecnológica Paula Souza, Cotia-SP, Brazil*
[3] *Beihang University, School of Energy and Power Enginnering, Beijing, China*

1. Introduction

Titanium nitride (TiN) thin films stand out and have been widely studied due to their properties [1]. Parameters such as nitrogen concentration, temperature, and substrate bias influence both film growth and its final properties [2-4]. Another approach to achieve outstanding performance is functionally graded deposition, in which the film composition is controlled along with its thickness by adjusting the flow of the reactive gas during film growth [4]. This work investigates the evolution of TiN_x films, including systems with a functional gradient along the thickness.

2. Experimental

TiN_x films were deposited using the GAMS (grid-assisted magnetron sputtering) technique. The depositions were carried out at a fixed discharge current of 2.00 A, a substrate bias of −100 V, and a temperature of approximately 300 °C. Seven depositions were performed at different N_2 flow rates, as defined by the hysteresis curve, covering the range from the metallic phase to TiN formation. The deposition time to obtain a film thickness of approximately 1.5 µm was adjusted according to the previously determined deposition rate. Additionally, a film was deposited using a gradient N_2 flow throughout the film growth.

3. Results and Discussions

Fig. 1 shows cross-sectional scanning electron microscopy images of the deposited films. The structural variation of the samples observed in Fig. 1 is driven by the increase in nitrogen content. As the nitrogen concentration increases, the typical columnar morphology is gradually replaced by a less well-defined structure. The $TiN_{0.95}$ sample, in particular, exhibits a fibrous morphology, while the graded film shows a continuous structural evolution along the thickness, reflecting the progressive change in deposition conditions during growth.

The film morphology has an impact on both corrosion resistance and interfacial contact resistance (ICR), as it directly affects film density and surface morphology. As shown in Figure 2, which presents the ICR results, both the graded film and the $TiN_{0.95}$ sample exhibited values closer to the requirements for fuel cell applications (ICR < 10 mΩ·cm² at 138 N/cm²), as established by the U.S. Department of Energy.

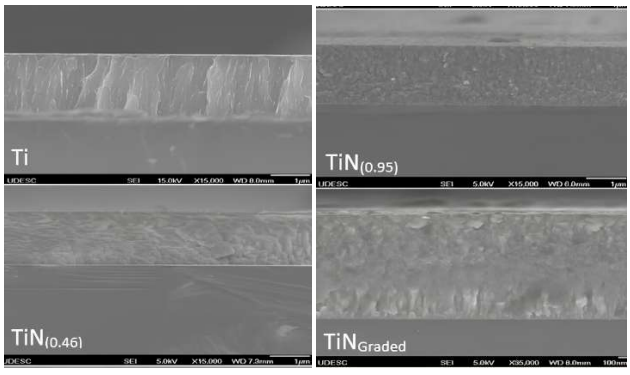


Fig. 1. *The cross-section of the TiN coatings, SEM.*

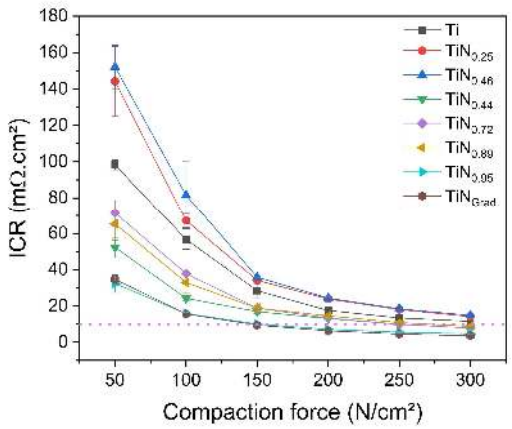


Fig. 2. *Interfacial contact resistance (ICR) between samples with different nitrogen concentrations.*

4. References

[1]- BELIAEV, L. Y. et al. Optical Materials (Amsterdam), v. 143, (2023).
[2]- CHOU, W. J.; YU, G. P.; HUANG, J. H. Surface & Coatings Technology, v. 149, n. 1, p. 7–13, (2002).
[3]- DA SILVA, F. C. et al. SN Applied Sciences, v. 2, n. 5, (2020).

Acknowledgments

The authors are thankful for the Multi-User Facility infrastructure from Santa Catarina State University's Technological Sciences Center, CNPq (grant 305330/2024-1), and finally, to the Graduate Monitoring Scholarship Program (PROMOP) for the financial support, which was essential for carrying out this research.

*Corresponding author: josielihonorato@gmail.com

COMPARATIVE EFFICIENCY OF PIN AND DBD PLASMA REACTORS IN THE DEGRADATION OF RHODAMINE B AND METHYLENE BLUE

Jade Helena Campos Augstroze[1]*, Felipe Souza Miranda[1], Argemiro Soares da Silva Sobrinho[1], Rodrigo Sávio Pessoa[1]

[1]*Laboratório de Plasmas e Processos - Instituto Tecnológico de Aeronáutica (LPP-ITA)*

1. Introduction

Synthetic dyes like methylene blue (MB) and rhodamine B (RhB) found in industrial wastewater present significant environmental risks because they are highly stable chemically, toxic, and difficult to break down through biological processes. These dyes are widely used in textile, pharmaceutical, and food industries, and their improper disposal can lead to significant ecological and health impacts [1].

Advanced oxidation processes (AOPs) have been extensively studied as effective alternatives for the removal of persistent organic pollutants. Among these, non-thermal plasma technologies stand out due to their ability to generate highly reactive species at atmospheric pressure and near room temperature [2].

Dielectric Barrier Discharge (DBD) and Pin-to-Water (PIN) plasma reactors are two commonly employed configurations. The DBD system is known for producing homogeneous plasma over a larger area, while the PIN reactor generates highly localized plasma with strong electric fields.

This study aims to compare the degradation efficiency of MB and RhB solutions at an initial concentration of 300 ppm using DBD and PIN plasma reactors over a treatment time of 90 min and 75 min, respectively, focusing on degradation kinetics and reactor performance.

2. Experimental

Aqueous solutions of methylene blue and rhodamine B (300 ppm) were prepared using deionized water and treated without additives. The experiments were performed using two atmospheric-pressure plasma reactors: a DBD and a PIN. The DBD reactor operated for 90 min, while the PIN reactor operated for 75 min under similar electrical conditions. Aliquots were collected during treatment, and the degradation was monitored by UV-Vis spectroscopy at 664 nm (MB) and 555 nm (RhB). Dye concentrations were determined from calibration curves.

3. Results and Discussions

The degradation of MB and RhB was evaluated using UV-Vis calibration curves with high linearity ($R^2 = 0.995–0.999$), ensuring reliable quantification. Considering an initial concentration of 300 ppm, the final concentrations were 1.452 ppm (RhB) and 0 ppm (MB) for the DBD reactor after 90 min, and 4.617 ppm (RhB) and 12.536 ppm (MB) for the PIN reactor after 75 min.

The DBD reactor exhibited superior performance, achieving complete removal of MB and near-complete degradation of RhB, despite the longer treatment time. This higher efficiency is attributed to the homogeneous discharge and enhanced plasma-liquid interaction, which increases the generation and distribution of reactive oxygen species such as •OH, O_3, and H_2O_2 [3,4]. In contrast, the PIN reactor, characterized by localized filamentary discharges, showed lower efficiency due to limited interaction volume and reduced mass transfer [5]. Additionally, MB showed faster degradation compared to RhB, consistent with its simpler molecular structure and higher susceptibility to oxidative attack. RhB, with its more stable xanthene structure, required longer exposure and higher oxidative capacity for degradation. In general, the results confirm that while both reactors are effective for high-concentration dye removal, the DBD system provides higher degradation efficiency highlighting its potential for advanced wastewater treatment applications.

4. References

[1]- S. R. Sousa, M. A. A. Schoeps and L. F. Silva, J. Environ. Chem. Eng., 9, 105899, (2021).
[2]- P. Bruggeman, C. Leys, J. L. Walsh, et al., Plasma Sources Sci. Technol., 30, 053001, (2021).
[3]- M. Magureanu, N. B. Mandache and V. I. Parvulescu, Plasma Chem. Plasma Process., 40, 1-25, (2020).
[4]- B. Sun, M. Sato and J. S. Clements, Chem. Eng. J., 426, 131821, (2021).
[5]- X. Lu, M. Laroussi and V. Puech, Phys. Rep., 101, 1-62, (2022).

Acknowledgments (bold face Times New Roman 11 pt)

The authors gratefully acknowledge the financial support provided by the Fundação de Amparo à Pesquisa do Estado de São Paulo (FAPESP), Coordenação de Aperfeiçoamento de Pessoal de Nível Superior (CAPES), and Conselho Nacional de Desenvolvimento Científico e Tecnológico (CNPq).

*Corresponding author: jadeh.rede@gmail.com

BIOPOLYMER NANOPARTICLES WITH HIGH MUCOADHESION TO IMPROVE ANTIBIOTIC RETENTION IN MUCOSAL INFECTIONS

Leonardo Cristiano Dahmer[1] , Helton José Wiggers[1] , Diego Mantovani[2] , Cecilia Zorzi Bueno[1]
[1]*Associação de Ensino, Pesquisa e Extensão Biopark (Laboratório de Biomateriais e Bioengenharia),*
[2]*Université Laval (Min-Met-Materials Eng, Lab Biomaterials & Bioengineering)*

1. Introduction

Bacterial infections can lead to significant damage, and conventional therapies present limitations, such as poor antibiotic retention and limited permeation across mucosal surfaces, resulting in reduced bioavailability [1]. To address this issue, nanoparticles based on biopolymers were explored for the development of mucoadhesive systems. Specifically, alginate, a biocompatible polysaccharide mainly derived from brown algae, and chitosan, obtained through the deacetylation of chitin, were investigated [2].

2. Experimental

Biopolymer nanoparticles were produced by the dropwise addition of an antibiotic solution into a polymer solution under magnetic stirring. For chitosan-based nanoparticles, a TPP solution was also incorporated. Subsequently, the suspensions were maintained under constant stirring for 5 minutes, centrifuged for 20 minutes at 3500 rpm, and the supernatant was collected. The systems were characterized in terms of number-based size, zeta potential, PDI, and mucoadhesive properties through interaction studies with mucin. Measurements were performed using Dynamic Light Scattering (DLS).

3. Results and Discussions

Nanoparticles and mucin formed aggregates, resulting in an increase in particle diameter [3]. Chitosan nanoparticles exhibited a 430% increase in diameter, whereas alginate nanoparticles showed only a 34% increase. Alginate nanoparticles were subsequently coated with chitosan to enhance mucoadhesion, leading to a 253% increase in diameter. Zeta potential also showed notable changes after incubation with mucin. For chitosan nanoparticles, it decreased from +22.1 to +2.5 mV, while for chitosan-coated alginate nanoparticles, it decreased from +31.9 to +4.9 mV. In contrast, alginate nanoparticles showed no significant variation. These findings indicate that nanoparticles containing chitosan exhibited greater mucoadhesiveness, suggesting prolonged residence time upon direct mucosal administration. Further characterization will be conducted regarding irritation potential and permeability, aiming to develop new systems for the treatment of mucosal infections.

4. References

[1] Y. Zheng et al. Journal of Controlled Release, 114046 (2025).
[2] C. Zorzi Bueno et al. Polymers, 17, 2261 (2025).
[3] S. Eliyahu, A. Aharon and H. Bianco-Peled, Polymers, 10, 106 (2018).

Acknowledgements

BIOPARK, Prati–Donaduzzi Pharmaceutical Industry, the Natural Science and Engineering Research Council of Canada and CNPq 408919/2023-0. Thanks to Carmen Donaduzzi, Ph.D., and Luiz Donaduzzi, Ph.D. for guidance.
*Corresponding author: leonardocdahmer@gmail.com

CONTROLLING ANTIBIOTIC RELEASE IN CHITOSAN FILMS: FROM MOLECULAR INTERACTIONS TO LONG-TERM PERFORMANCE

Nathalia Fernanda Sczesny[1,2], Isabela Tavares Rampim[1], Cecilia Zorzi Bueno[1], Pascale Chevallier[2], Francesco Copes[2], Diego Mantovani[2] Helton José Wiggers[1*]

[1]*Laboratório de Biomateriais e Bioengenharia (LBB-BPK), Biopark Educação, Toledo, PR, Brazil*
[2] *Laboratory of Biomaterials and Bioengineering (LBB-ULaval), Laval University, Quebec, Canada*

1. Introduction

Biomaterial-associated infections continue to compromise the performance and longevity of medical devices, underscoring the need for coatings capable of delivering localized and sustained antimicrobial activity. Chitosan-based systems offer a versatile platform in this context, given their tunable physicochemical properties and capacity to regulate drug release.

2. Experimental hypothesis

In this study, we demonstrate how rational control over film formulation governs antibiotic release kinetics and, consequently, the duration of antibacterial efficacy, enabling coatings tailored for medical devices with different implantation times. An initial strategy focused on engineering crosslinked networks using naturally derived compounds, including quercetin and tannic acid–iron complexes. In parallel, catechol oxidation to quinone functionalities enabled covalent stabilization via Schiff base formation and Michael-type addition.

3. Results and Discussions

These approaches yielded films with controllable antibacterial lifetimes spanning from days to approximately one month, highlighting the role of network chemistry in diffusion and retention mechanisms. Building on this framework, key formulation parameters within tannic acid–iron–chitosan systems were systematically investigated. The incorporation of structurally distinct antibiotics revealed a strong dependence of release behavior on molecular features such as polarity, size, and interaction potential with the polymeric matrix. This enabled the development of a modular delivery platform capable of spanning short- to long-term release regimes, from a few days to up to six months. Additionally, comparative analysis of chitosan sources indicated that crosslinking density and chemistry exert a more dominant influence on release kinetics than intrinsic variability in polymer origin, while preserving consistent antibacterial performance.

To assess translational potential, the formulation exhibiting the most prolonged release profile was applied as a coating onto polyethylene substrates. The resulting system demonstrated robust adhesion for up to 35 days and sustained antimicrobial activity for approximately six months, reaching or surpassing the performance typically reported for commercial antimicrobial coatings.

Collectively, these results establish structure–property–function relationships that enable the design of chitosan-based antimicrobial coatings with finely tunable release kinetics, next steps include integration onto medical-device materials via plasma surface activation and spray coating.

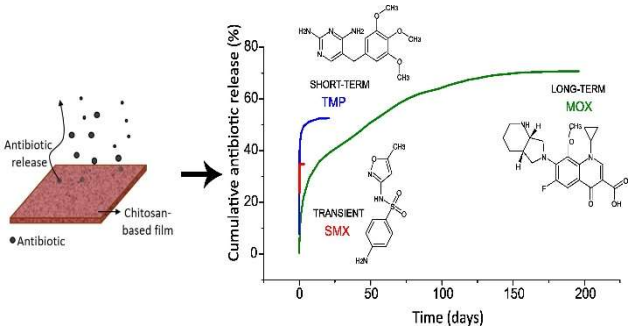


Figure 1*. Schematic cumulative release profiles of antibiotics from chitosan-based films, highlighting the influence of molecular structure on release kinetics and duration, ranging from transient to sustained release (days to months).*

4. References

[1] H. J. Wiggers, N. F. Sczesny, P. Chevallier, C. M. Silva, C. Z. Bueno, F. Copes and D. Mantovani, RSC Adv., 16, 5758 (2026).
[2] I. T. Rampim, H. J. Wiggers, C. Z. Bueno, P. Chevallier, F. Copes and D. Mantovani, Polymers, 17, 884 (2025).
[3] N. F. Sczesny, H. J. Wiggers, C. Z. Bueno, P. Chevallier, F. Copes and D. Mantovani, Antibiotics, 13, 1055

Acknowledgments

Biopark, Prati-Donaduzzi, CNPq 408919/2023-0, Natural Science and Engineering Research Council of Canada (Discovery and Alliance programs), Carla C. Joner and Claudia M da Silva for technical assitance, Dr. Carmen Donaduzzi and Dr. Luiz Donaduzzi for guidance throughout the project.

*Corresponding author: helton.wiggers@bpkedu.com.br

CHARACTERIZATION OF A REMOTE PLASMA JET USING LISSAJOUS FIGURES

Lais Bastos da Silva Lima, Kleber Alexandre Petroski, Julio César Sagás*
Universidade do Estado de Santa Catarina (UDESC), Programa de Pós-Graduação em Física (PPGF), Laboratório de Plasmas, Filmes e Superfícies, Joinville-SC, Brazil

1. Introduction

Dielectric Barrier Discharge (DBD) reactors are a well-established method for generating non-thermal plasmas at atmospheric pressure. A transferred (or remote) cold atmospheric plasma jet is a DBD plasma device where a discharge is produced in a DBD reactor between a high voltage electrode (covered with a dielectric) and a floating metal wire. The wire is inside a plastic tube where the gas flows. The charging of the wire ignites a plasma jet at the other tip of the wire. Due to the features of the device, it can be easily maneuvered to adjust distance and direction from the plasma jet to a targeted surface, which is useful for applications as 3D printing assisted by plasma. DBD reactors have active and passive phases – without plasma– within a period of applied voltage. In this work, the capacitances of the systems were obtained by means of analyses of Lissajous figures, allowing also the determination of the dissipated power.

2. Experimental

The experimental setup is described elsewhere [2]. A known 10 nF capacitor was inserted between the electrode and the ground. By measuring the voltage values across the capacitor, we can obtain the Lissajous figures (QV-plots) (Figures 1 and 2), obtaining information about the average discharge power by integrating the area of the figure. We can also measure the capacitances of the system through the slope of the tangent lines to the Lissajous figure: cell capacitance C_{cell} (when the plasma is off) and discharge capacitance C_d (when the plasma is on).

3. Results and Discussions

A slight increase in discharge power is observed with increased frequency. For the plots in figures 1 and 2, the average discharge power was 0.87 W for 9 kV and 8 kHz, while for 10 kV and 20 kHz, it is 2.18 W. The cell capacitance is close to 0.55 pF, while the C_d is close to 3 pF. A “deformation” of QV-plots is observed for frequencies lower than 10 kHz due to a distortion in the voltage waveform that is erased for frequencies higher than 10 kHz.

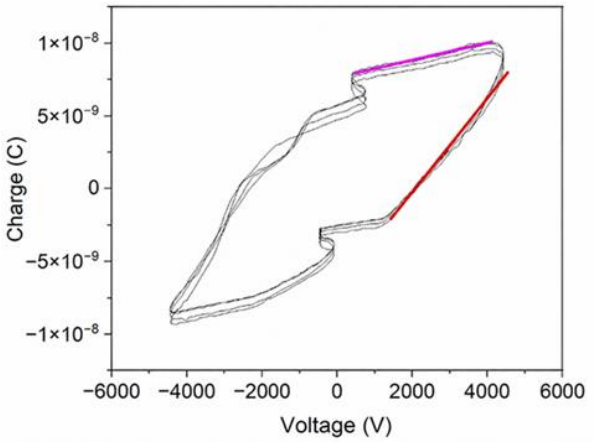


Fig 1. *Lissajous figure (QV-plot) for 9 kV and 8 kHz.*

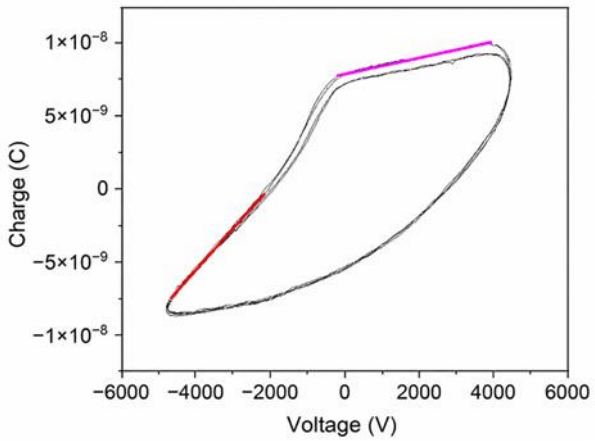


Fig 2 *Lissajous figure (QV-plot) for 10 kV and 20 kHz.*

4. References

[1] Kostov KG, Machida M, Prysiazhnyi V, Honda RY. Transfer of a cold atmospheric pressure plasma jet through a long flexible plastic tube. Plasma Sour Sci Technol 24(2), 025038, 2015.
[2] Fernandes, AC, Lima, LS, Krol, M. *et al.* Surface modification of 3D-printed PLA using an integrated remote plasma JET: in situ enhancement of wettability and functionalization without post-processing. Prog Addit Manuf 11, 2123–2139, 2026.

Acknowledgments

This study was financed in part by the Coordenação de Aperfeiçoamento de Pessoal de Nível Superior - Brasil (CAPES) - 88887.202065/2025-00.

*Corresponding author: julio.sagas@udesc.br

INFLUENCE OF HEAT FLUX AND EXPOSURE TIME ON SURFACE ROUGHNESS OF YSZ THERMAL BARRIER COATINGS

Agatha C. Corrêa[1,2], Roberson J. Silva[1], Lucas Caetano[3], Nazir M. dos Santos[1*]
[1]*Institute of Advanced Studies (IEAv), São José dos Campos, São Paulo, Brasil*
[2]*FATEC Prof. Jessen Vidal, São José dos Campos, São Paulo, Brasil*
[3]*ICT/UNIFESP/LCMM, São José dos Campos, São Paulo, Brasil*

1. Introduction

Thermal Barrier Coatings (TBCs) are widely used in aerospace components exposed to severe thermal conditions, often above 1000°C. These systems typically consist of a ceramic top coat (TC), commonly yttria-stabilized zirconia (YSZ), and a metallic bond coat (BC), such as MCrAlY alloys, deposited on a Ti6Al4V substrate [1]. The YSZ layer provides low thermal conductivity and thermal stability, while the bond coat improves adhesion and oxidation resistance. However, TBCs may degrade under high heat fluxes and thermal gradients through sintering, cracking, oxidation, and interfacial delamination [2], which can modify surface topography and affect coating performance. Surface roughness is therefore an important parameter for evaluating plasma-sprayed coatings, as it is associated with porosity, splat morphology, and surface degradation [3]. In this context, this study evaluates the effects of heat flux and exposure time on the surface roughness of YSZ-based TBCs subjected to ablation tests.

2. Experimental

TBC samples consisting of an atmospheric plasma-sprayed (APS) YSZ top coat, an APS CoNiCrAlY bond coat, and a Ti6Al4V substrate were subjected to ablation tests at heat fluxes from 1.0 to 2.0 MW/m² and exposure times of 10 and 30 s. Before testing, cross-sectional metallographic preparation was performed to determine coating thicknesses, which ranged from 406 to 487 µm for the YSZ top coat and from 123 to 176 µm for the CoNiCrAlY bond coat. Three samples were tested for each condition. Ablation tests were conducted using a tornado-type plasma torch, with heat fluxes defined according to standardized conditions previously reported by the research group [4, 5]. Surface roughness was measured using a Mitutoyo Surftest SJ-210 profilometer, following ISO standards. The arithmetic mean roughness (Ra) was evaluated from five measurements per sample, using $\lambda c = 0.8$ mm, an evaluation length of 4.0 mm, and Gaussian filtering.

3. Results and Discussions

The surface roughness parameters showed limited variation after ablation exposure, with Ra ranging from 6.1 to 7.4 µm. These results indicate that the YSZ top coat largely retained the characteristic surface morphology of APS coatings, even under severe thermal loading. For heat fluxes of 1.0 and 1.5 MW/m², increasing exposure time led to a reduction in Ra. At 1.0 MW/m², Ra decreased from 7.2 µm at 10 s to 6.1 µm at 30 s, while at 1.5 MW/m² it decreased from 7.4 to 6.9 µm. This behavior is attributed to thermally induced surface densification and partial smoothing of asperities. Optical microscopy of cross sections supports this interpretation, showing a relatively compact YSZ top coat after ablation, with the multilayer structure preserved at 10s. The measured top-coat thicknesses after 10 s exposure were 552.18, 483.97, and 505.08 µm for 1.0, 1.5, and 2.0 MW/m², respectively. In contrast, at 2.0 MW/m², Ra increased from 6.9 to 7.4 µm, suggesting that more intense thermal loading promoted localized surface roughening and microstructural heterogeneity. Overall, exposure time influenced roughness more clearly under moderate heat flux, whereas the highest heat flux intensified surface degradation effects.

4. References

[1] Sezavar A, Sajjadi SA. Journal of the European Ceramic Society. 2025; 45:117274. doi:10.1016/j.jeurceramsoc.2025.117274
[2] Tahir M, et al. Ceramics International. 2024; 50:53976-53986. doi:10.1016/j.ceramint.2024.10.253
[3] Rodrigues BC, Brito VLO, Fazan LH, Barbosa CWS, Takahashi RJ, Reis DAP. Tecnologia em Metalurgia, Materiais e Mineração. 2025; 22:e3238. doi:10.4322/2176-1523.20253238
[4] Silva RJ, Reis RI, Pardini LC, Sias DF, Petraconi Filho G. International Journal of Thermophysics. 2019; 40:88. doi:10.1007/s10765-019-2525-7
[5] Loureda OB, et al.. Materials Research Express. 2020; 7:015619. doi:10.1088/2053-1591/ab6c87

Acknowledgments
CNPq (Proc. 157898/2025-3), COMAER - Ed. CAPA IEAV/PropHiper (Proc. 67720.009933/2024-93), UNIFESP and ITA for the experimental infrastructure.

*Corresponding author: nazirmonteiro@gmail.com

INFLUENCE OF THERMAL ANNEALING ON THE MORPHOLOGICAL AND OPTICAL PROPERTIES OF Nb_2O_5 THIN FILMS DEPOSITED BY PULSED DC MAGNETRON SPUTTERING

Paulo S. Oliveira[1, 2], Raul Ramos[1], Luiz H. C. Monteiro[1]*, Elidiane C. Rangel[1] and José R. R. Bortoleto[1]
[1]*São Paulo State University (UNESP), Institute of Science and Technology, Sorocaba/SP, Brazil*
[2]*Federal Institute of Education, Science and Technology of São Paulo (IFSP), Itapetininga/SP, Brazil*

1. Introduction

Niobium pentoxide (Nb_2O_5) thin films are increasingly prominent in the development of next-generation optoelectronic devices, including electrochromic windows and gas sensors, due to their high refractive index, chemical stability, and tunable bandgap [1]. This study investigates the properties of films synthesized via reactive Pulsed DC Magnetron Sputtering, focusing on how post-deposition processing influences the material's final characteristics [2]. The research specifically examines how thermal annealing at 500°C affects the internal organization and surface topography of the films [3]. By correlating lattice expansion and structural reorganization with variations in optical constants and surface roughness, this work provides essential insights into tailoring Nb_2O_5 properties. Such optimization is fundamental for enhancing the efficiency and reliability of these films in advanced technological applications.

2. Experimental

Nb_2O_5 thin films were deposited by reactive Pulsed DC Magnetron Sputtering using a metallic Nb target in an Ar/O_2 atmosphere. The deposition was performed for 20 minutes at a voltage of 700 V, using a 1 kHz pulsed DC source, with the substrate heated to 250°C. One sample was subjected to thermal treatment at 500°C for 1 hour in an atmospheric environment. The surface morphology and roughness were characterized by Atomic Force Microscopy (AFM), while the physical thickness was measured via profilometry. Optical properties were analyzed by UV-Vis-NIR spectroscopy, with the spectra processed using PRISA software to calculate the refractive index (n) and the energy bandgap (E_g).

3. Results and Discussions

The thermal treatment at 500°C promoted significant structural and optical changes in the films. The physical thickness increased from 178 nm to 223 nm, while the refractive index decreased from 2.34 to 2.16, indicating lattice expansion and changes in material density. Fig. 1 (AFM) reveals an increase in surface roughness (RMS) from 1.42 nm to 3.05 nm, suggesting grain growth. The transmittance spectra (Fig. 2) show a shift in the absorption edge, resulting in an energy bandgap (E_g) broadening from 3.3 eV to 3.5 eV. These variations indicate that thermal reorganization reduces structural defects, optimizing the Nb_2O_5 thin films for optoelectronic applications.

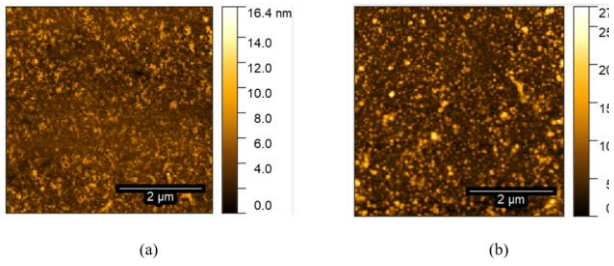


Fig. 1. *AFM surface images of Nb_2O_5 thin films: (a) as-deposited sample and (b) sample after thermal annealing at 500°C.*

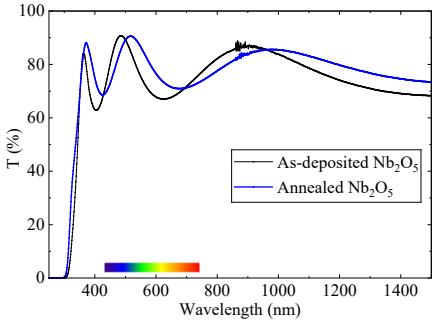


Fig. 2. *UV-Vis-NIR transmittance spectra of the as-deposited and annealed Nb_2O_5 thin films.*

4. References

[1]- Y. Zhao et al., Micromachines, 15, 1453, (2024).
[2]- F. Lai et al., Thin Solid Films, 488, 314-320, (2005).
[3]- M. Mazur et al., Appl. Surf. Sci., 301, 63-69, (2014).

Acknowledgments

The authors thank the technical staff of the Plasma Laboratory (UNESP-Sorocaba) and the Materials Laboratory (IFSP-Itapetininga) for experimental support, and CAPES for financial assistance.

* Corresponding author: lh.monteiro@unesp.br

PLASMA-ASSISTED SURFACE FUNCTIONALIZATION OF THERMOPLASTIC STARCH FILMS FOR NISIN-BASED ANTIMICROBIAL APPLICATIONS

Emily Clara Aguiar Welter[1,2]*, Francisco Alfaro[1], Cecilia Zorzi Bueno[1], Diego Mantovani[3], Helton José Wiggers[1,2]

[1]*Associação de Ensino, Pesquisa e Extensão Biopark*
[2]*Universidade Tecnológica Federal do Paraná, UTFPR – Campus Toledo*
[3]*Laboratory of Biomaterials and Bioengineering (LBB – ULaval), Laval University, Quebec, Canada*

1. Introduction

Global plastic pollution is a pressing environmental challenge, with the food and beverage sector being one of the main contributors due to its extensive use of disposable packaging. Bioplastics, such as thermoplastic starch (TPS) films, have emerged as sustainable alternatives; however, their bactericidal functionality still requires improvement. The incorporation of antimicrobial agents – particularly peptide-based compounds such as nisin – is a promising strategy to reduce food contamination by pathogenic microorganisms [1,2]. Among these, nisin stands out as a naturally occurring bacteriocin with well-established efficacy against Gram-positive bacteria and approvement by FDA (Food and Drug Administration) as Generally Regarded As Safe (GRAS) for several food application, making it especially attractive for active food packaging applications [2]. In this context, the central hypothesis of the present work is that low-pressure cold plasma surface modification enhances the anchoring of bioactive agents onto TPS films, improving their antimicrobial performance [3].

2. Experimental

Based on a formulation widely described in the literature, a homogeneous TPS film was produced from potato starch and subjected to low-pressure cold plasma treatment. The process comprised a vacuum pre-treatment step followed by sequential argon and oxygen plasma exposure, aiming to functionalize the film surface and enhance the anchoring of the antimicrobial agent. After treatment, nisin was loaded onto treated and untreated TPS films by dip-coating. Antimicrobial activity was evaluated through microbiological assays against *Staphylococcus epidermidis*. Swelling and mass loss analysis were also assessed to compare plasma-treated and non-treated films regarding water-related structural properties.

3. Results and Discussions

Plasma-treated TPS films exhibited notably enhanced antimicrobial performance when combined with nisin. This result can be attributed to the improved surface interaction promoted by plasma treatment, which introduces oxygen based polar functional groups on the TPS surface. However, to explain and have sure about the better antibacterial performance of plasma-treated TPS films, adhesion and release based on time assays must be done.

Regarding water-related properties, plasma treatment did not cause expressive changes in film stability. Mass loss measurements yielded 18.9 ± 3.5% for treated films and 22.3 ± 5.1% for untreated films, while swelling capacity was 99.2 ± 6.0% and 88.0 ± 7.7%, respectively – with no statistically significant differences between groups. These results indicate that plasma treatment, as expected, effectively modifies the TPS film surface in nanoescale, that enhance antimicrobial agent incorporation, without compromising the structural integrity of the material. Overall, low-pressure cold plasma stands as a promising and green technology for producing active biopolymer packaging films.

4. References

[1]- Jayarathna, S., Andersson, M., & Andersson, R. Polymers, 14, no. 21 (2022).
[2]- Leelaphiwat, Pattarin, et al. Food chemistry, 369, 130956 (2022).
[3]- Sifuentes-Nieves, I. et al. Carbohydrate Polymers, 237, 116103 (2020).

Acknowledgments

Biopark Educação, Biomaterials and Bioengineering Laboratory team, Fundação Araucária (Convênio nº 175/2024), NAPI Alimentos Saudáveis, Biopark, Prati-Donaduzzi, CNPq 408919/2023-0, Dra. Carmen Donaduzzi and Dr. Luiz Donaduzzi for guidance throughout the project.

*Corresponding author: emily.welter@bpkedu.com.br

Optimization of $CaCl_2$ Concentration in Edible Film Formation

Jaqueline Portes Pagnoncelli Martins[1]*, Bianca dos Reis Santana Caldeira[2], Maia Godoy da Luz,[2] Renato Eising[2]

[1]*UNIOESTE - Universidade Estadual do Oeste do Paraná - Toledo*

[2]*UTFPR - Universidade Tecnologia Federal do Paraná – Toledo*

1. Introduction

Edible films based on alginate and whey protein have emerged as sustainable alternatives to conventional materials; however, they still present structural limitations. Ionic crosslinking with $CaCl_2$ stands out as a key strategy to enhance these matrices by promoting the formation of more stable three-dimensional networks. This process leads to significant improvements in mechanical and barrier properties. In this context, optimizing $CaCl_2$ concentration is crucial to achieving high-performance films.

2. Experimental

Film formulations were developed based on a mixture design approach, in which component proportions (alginate, protein, and plasticizer) were expressed as percentages while maintaining a constant total. The $CaCl_2$ crosslinking solution was applied at different stages of the film drying process (20–80% of water evaporation), allowing the evaluation of how the timing of ionic crosslinking influences the final properties of the films.

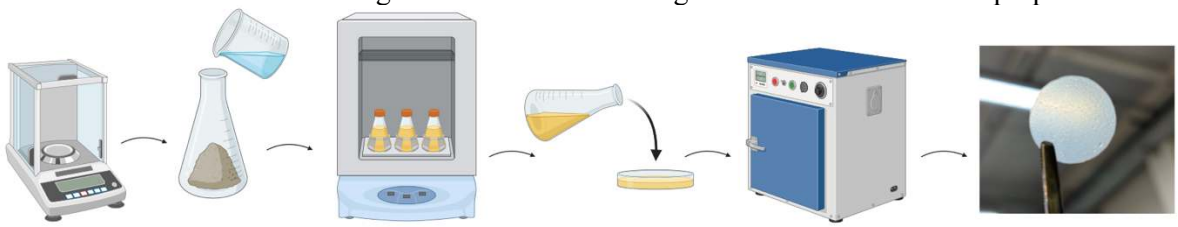


Fig 1. *Diagram of the preparation of film-forming solutions and obtaining films using the casting method.*

3. Results and Discussions

Edible films were successfully obtained and evaluated under different $CaCl_2$ crosslinking conditions, varying the drying stage (20–80% water loss), $CaCl_2$ concentration (0.01–1.00 mol/L), and added volume (0.5–5.2 mL). The best performance was achieved at 60% water loss during drying, using 0.3 mol/L and 3.2 mL of $CaCl_2$. This result indicates that crosslinking efficiency is strongly governed by the structural state of the polymer matrix at the moment of $CaCl_2$ addition. At 60% mass loss, polymer organization favors effective interactions between Ca^{2+} ions and alginate carboxyl groups, promoting the formation of a more cohesive network (egg-box model) [1,3]. Lower concentrations result in insufficient crosslinking, while higher concentrations may lead to over-crosslinking, increasing rigidity and structural heterogeneity [2]. Thus, the optimal condition reflects a balance between ion availability and matrix organization, being crucial for achieving films with improved properties.



Fig. 2. *Film without $CaCl_2$*

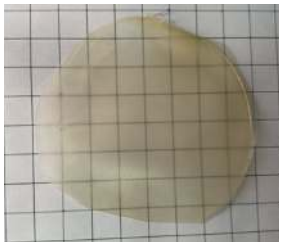


Fig. 3. *Film with $CaCl_2$*

4. References

[1] Rhim, J. W. Physical and mechanical properties of water resistant sodium alginate films. *LWT - Food Science and Technology*, 37, 323–330 (2004).

[2] Sothornvit, R.; Krochta, J. M. Plasticizer effect on mechanical properties of β-lactoglobulin films. *Journal of Food Engineering*, 50, 149–155 (2001).

[3] Olivas, G. I.; Barbosa-Cánovas, G. V. Alginate–calcium films: Water vapor permeability and mechanical properties. *Food Research International*, 41, 359–366 (2008).

The authors gratefully acknowledge the financial support from CNPq and CAPES. The authors also thank UNIOESTE, UTFPR, and Fundação Araucária - NAPI Abelhas for providing infrastructure and technical support essential to this work.

*Corresponding author: Jaqueline.martins7@unioeste.br

CONTROLLED SYNTHESIS OF SILVER NANOPARTICLES VIA DIELECTRIC BARRIER DISCHARGE PLASMA–LIQUID INTERACTION

Marina Clara Ribeiro dos Santos[1]*, Eduardo Ferreira Martins[1], Clodomiro Alves Junior[2], Rodrigo Savio Pessoa[1]

1. *Plasmas and Processes Laboratory (LPP), Aeronautics Institute of Technology (ITA),12228-900, São José dos Campos-SP, Brazil*
2. *Federal Rural University of the Semi-arid Region, 59625-900, Mossoro-RN, Brazil*

1. Introduction

The synthesis of silver nanoparticles (AgNPs) has attracted significant attention due to their unique optical, antimicrobial, and catalytic properties. Conventional chemical methods rely on reducing agents that may introduce contaminants and limit environmental sustainability. In this context, plasma–liquid interaction has emerged as a alternative, enabling the in-situ generation of reactive species capable of reducing metal ions without additional chemical reagents [1,2]. Plasma systems operating at atmospheric pressure produce reactive species such as solvated electrons and reactive oxygen species, which promote reduction processes in aqueous media. This work investigates the synthesis of AgNPs using a plasma-based approach, aiming to evaluate the influence of plasma parameters on nanoparticle formation and to assess its effectiveness as a clean and controllable method.

2. Experimental

Silver nanoparticles were synthesized from aqueous solutions of $AgNO_3$ (1.2 mM) and sodium citrate (34 mM) in a 1:3 ratio, subjected to plasma treatment using a dielectric barrier discharge (DBD) system under atmospheric pressure with helium as the working gas. Different plasma conditions were investigated by varying voltage (5–12 kV), frequency (15 kHz, AC), current (2.4 A, pulsed DC), and exposure time (1–15 min), as well as reactor geometry. The evolution of the synthesis process was evaluated across multiple samples produced under those distinct conditions. The synthesized materials were characterized using UV–Vis spectroscopy, X-ray diffraction (XRD), scanning electron microscopy (SEM) coupled with energy-dispersive spectroscopy (EDS), and contact angle measurements, enabling optical, structural, and surface characterization.

3. Results and Discussions

The formation of AgNPs was strongly dependent on plasma parameters. Under lower-energy conditions (samples 3–6), no significant colour change or surface plasmon resonance (SPR) band was observed, indicating the absence of nanoparticle formation. In contrast, initial evidence of AgNP formation was observed in sample 2, which exhibited a yellow coloration and a plasmonic band near 400 nm after a short plasma exposure.

Optimized conditions, particularly using 12 kV, 2.4 A pulsed DC, and longer exposure times (3–15 min), resulted in consistent nanoparticle formation (samples 7–9). UV–Vis spectroscopy revealed a well-defined SPR band centred at 402 nm, characteristic of silver nanoparticles. The analysis of peak position and full width at half maximum (FWHM) indicated the formation of nanoscale metallic structures with relatively consistent optical response. The two-phase behaviour in sample 7 suggests non-uniform nucleation dynamics. Under extended treatment conditions, this behaviour was not observed, indicating improved system stability. XRD analysis showed diffraction features around ~38°, consistent with the Ag (111) reflection of face-centred cubic silver. However, partial overlap with substrate-related peaks was observed, particularly in Ti-containing samples, requiring cautious interpretation. EDS analysis confirmed the presence and distribution of silver in the analysed regions, supporting the successful formation and deposition of AgNPs. SEM analysis revealed surface-modified regions and aggregated nanoscale structures, consistent with plasma-assisted synthesis in the absence of stabilizing agents. Contact angle measurements indicated changes in surface wettability after plasma treatment, suggesting modifications in surface energy associated with plasma activation and nanoparticle deposition. Overall, the results demonstrate that plasma–liquid interaction enables controlled synthesis of AgNPs, with plasma parameters playing a critical role in nanoparticle formation and stability.

4. References

[1] A. Nikiforov, C. Leys and R. Morent, Synthesis of silver nanoparticles by atmospheric pressure plasma jet, *Nanotechnology*, 33, 255603, (2022).

[2] S. Barcikowski, A. Hahn and G. Rehbock, Generation of nanoparticles by laser ablation in liquids and plasma-based methods, *Nanoscale Adv.*, 2, 5021–5038, (2020).

Acknowledgments

The authors thank CNPq (178682/2025-0).

marinaclara@ita.br

GRAPHENE: NANOMATERIAL SYNTHESIS IN CONNECTION WITH THE LOCAL PRODUCTIVE ARRANGEMENT

João Pedro Naderer Baptistão[1]*, Mateus Ritter Pasini [2], Mario Wolfart Junior [3], Mauricio Andolfato [4], Arão Ngadi Makiesse Zampassi [5]
[1,2,3,4,5]*Instituto Federal Catarinense – Campus Luzerna*

1. Introduction

The discovery of graphene by Geim and Novoselov, awarded the Nobel Prize in Physics in 2010 [1], marked a decisive advance in materials science, highlighting the potential of two-dimensional structures with exceptional properties, such as high electrical and thermal conductivity and remarkable mechanical strength [2]. These characteristics make the material promising for various technological applications.

However, large-scale production still faces challenges, particularly regarding control, reproducibility, and economic viability. Traditional methods such as chemical vapor deposition (CVD), although widely used, require high temperatures and significant energy costs, limiting their industrial application [3].

In this context, the PECVD technique emerges as a more efficient alternative, enabling graphene synthesis under milder conditions and with greater process control, favoring the production of films with tunable properties [3]. Thus, the development of a PECVD reactor for graphene synthesis aims to optimize operational parameters and enable its production, contributing to both scientific advancement and strategic industrial applications.

The present project involves the construction of a graphene synthesis chamber in partnership with the local productive arrangement, as well as with the company Odeme Dental Research [4], which has expressed formal support for this project through a letter of consent and is interested in the promising properties of graphene for dental applications.

2. Experimental

The construction of a plasma reactor involves the acquisition, fabrication, and integration of the various components that make up the system, as well as the implementation of the necessary connections for its proper operation. In this context, the plasma reactor is structured into three main subsystems: (i) the electrical system, which includes a transformer, VARIAC, current and voltage controllers, a current rectifier, and resistances; (ii) the mass flow control system, consisting of a vacuum pump, vacuum gauge, and gas inlet lines (Ar and CH_4); and (iii) the temperature control system, composed of a FieldLogger and a thermocouple. The chamber is being developed in partnership with the local productive arrangement, with its design and configuration conceived within the institution.

However, the effective validation of the system will only occur after the analysis and characterization stage using Raman spectroscopy and X-ray diffraction (XRD), techniques that allow the evaluation of structural integrity, degree of crystalline organization, and homogeneity of the hexagonal carbon atom network.

3. Results and Discussions

The plasma reactor has been fabricated and assembled and is currently operating properly, meeting the design requirements. At present, the work focuses on the analysis and adjustment of synthesis parameters. It should be noted, however, that the project is still ongoing, and therefore the results obtained so far are preliminary.

4. References

[1] - Universidade Estadual do Centro-Oeste (UNICENTRO) "*Prêmio Nobel em Física – 2010*", Grupo PET Física, Brazil, (2026).

[2] - J. Vieira Segundo; E. Vilar "*Grafeno: uma revisão sobre propriedades, mecanismos de produção e potenciais aplicações em sistemas energéticos*", Revista Eletrônica de Materiais e Processos, Brazil, (2017).

[3] - N. Woehrl; O. Ochedowski; S. Gottlieb; K. Shibasaki; S. Schulz "*Plasma-enhanced chemical vapor deposition of graphene on copper substrates*", AIP Advances, USA, (2014).

[4] - Odeme "*Home – Odeme Dental Research*", Brazil, (2025).

Acknowledgments

The authors acknowledge the Instituto Federal Catarinense (IFC) – Luzerna Campus for the financial support provided for the development of this project.

*Corresponding author: jpnaderer0@gmail.com

ENGINEERING ELECTROSPUN PVA NANOFIBERS WITH PORCINE LIVERBIOACTIVES FOR ANTIMICROBIAL DRESSINGS AND CHRONIC WOUND HEALING

Calisto Nonato Silva Junior[1]*, Mônica Lady Fiorese[1], Douglas Cardoso Dragunski[1], Edson Antônio da Silva[1]

[1]*Universidade Estadual do Oeste do Paraná – UNIOESTE – Programa de Pós-Graduação em Engenharia Química – Toledo – PR*

Abstract

The healing of hard-to-heal wounds, such as chronic ulcers and infected lesions, represents a significant challenge for healthcare systems, requiring the development of advanced wound dressings capable of providing physical protection, microbial control, and stimulation of tissue regeneration. In this context, electrospun nanofibers have emerged as promising platforms for wound dressing engineering due to their high surface area, high porosity, and ability to mimic the extracellular matrix. Poly(vinyl alcohol) (PVA) is widely employed in these applications due to its biocompatibility, hydrophilicity, and ease of processing, as well as its ability to incorporate bioactive compounds.

In this study, a system of electrospun PVA nanofibers functionalized with porcine liver protein hydrolysate and extract was developed for application in wound healing dressings. The precursor solutions were prepared in a final volume of 10 mL containing 8% PVA and previously defined additives, with hydrolysate concentrations ranging from 0 to 50% (w/w). The experimental evaluation considered critical parameters for obtaining nanofibers suitable for biomedical applications, including solubility, viscosity, jet stability, needle clogging, and uniform fiber formation. The formulation containing 30% hydrolysate showed the best overall performance, combining high bioactive incorporation with adequate processability and the formation of continuous and homogeneous nanofibers, with reduced bead formation.

Additionally, the incorporation of porcine liver extract was investigated, and a concentration of 3% (w/w) was selected, which exhibited bactericidal and bacteriostatic activity against Staphylococcus aureus, Escherichia coli, and Pseudomonas aeruginosa, as well as fungicidal and fungistatic activity against Candida albicans. These results are particularly relevant for the treatment of chronic wounds, where microbial infection is one of the main factors impairing the healing process.

The results indicate that solution rheological properties, such as viscosity and conductivity, are key determinants of electrospinning stability and nanofiber morphology, directly influencing dressing performance. Therefore, the optimized formulation developed in this study demonstrates strong potential for application as a bioactive wound dressing, combining suitable structural properties with antimicrobial activity, contributing to innovative strategies for the treatment of hard-to-heal wounds.

Keywords: wound dressings; wound healing; electrospinning; nanofibers; PVA; bioactives; antimicrobial activity.

Acknowledgments

The authors acknowledge the financial support provided by Coordenação de Aperfeiçoamento de Pessoal de Nível Superior – Brasil (CAPES). The authors also thank the Sustainable Engineering Laboratory (LES – UNIOESTE), the Laboratory of Process Systems (LPS – UNIOESTE), Agritech Symbiosis Lab– UNIOESTE, the Analytical Center of UNIOESTE (Toledo campus), Universidade Tecnológica Federal do Paraná (UTFPR – Toledo), Institute of Chemistry (Leiden Universiteit – The Netherlands) and Universidade Federal do Paraná (UFPR) for infrastructure and technical support.

*Corresponding author: caliston@utfpr.edu.br

FROM PATENT TO PRODUCTION: THE CIMENT COMPOSITE DEVELOPMENT CASE

Limad, Waltson Gomes Neto[1,2]*, Silva, Maria Lúcia Pereira[1,2]
[1] *Paula Souza State Centre for Technological Education (CEETEPS), São Paulo, SP, Brazil*
[2] *Polytechnic School, University of São Paulo (EPUSP), São Paulo, SP, Brazil.*

1. Introduction

Surface main issue on big structures, such as wind towers, is the composite formation and stability. Several different attempts to solve this puzzle have already been reported, most of them through the generation of relevant international patents [1]. However, the critical step is the path from patent and the correspondent tests, usually on lab stage only, to use on site. Thus, this work shows the real case of building wind towers with the use of new reinforced concrete formulation and the correspondent tests for feasibility approval.

2. Experimental

This work uses the design previously developed for analysis of wind turbines malfunctions, which consider the whole situation in three perspectives: *macro-meso-micro* i.e. *macro* attends to structure design, *meso* to the environmental conditions whereas *micro* evaluates the material itself, specifically on site. The main steps for production of wind tower are on site, as follows: receipt of raw material and respective physical-chemical evaluation, formation of several layers of composites in pre-established molds, and on site, evaluation of material characteristics and, on the last step, reinforced concrete fills the entire body of voussoirs towers.

3. Results and Discussions

The patent that should be adapted for Brazilian conditions faces two main characteristics: the innovative structure (*macro* aspect) and respective assembly (*meso* aspect). On this case, the adaptations show less problems that could be expected since all the manufacturing occurred without drawbacks. However, the micro aspect shows to be the main root cause, since the lab essays initial processing indicated that the reported results were quite different from the design specifications (according to the patent).

Considering Pareto Diagram, the 80:20 analysis shows the concrete quality, due to its variability, as the main issue. This unexpected property is due to the raw material variability, such is a natural material, and the adaptation to the patent required several tests and steps, especially due to surface interactions, as SWOT shows:

- Concrete-iron interactions required prefabricated reinforcement cages that were assembled on dedicated jigs outside the formwork, inspected by pacometry, and installed as single units, eliminating in-formwork bar adjustments and reducing reinforcement placement time from 4.5 to 2.8 hours per voussoir.
- The low humidity in Brazilian NE climate led to easiness on water depletion and increase concrete formation, however, the higher water depletion kinetic velocity means higher thermal gradients in the walls, which locally hinder aggregate formation and the ultimate result, can be the mechanical failures. In other words, a surface interaction problem was induced.
- Surface cracking due to plastic shrinkage occurred on peak temperature hours for voussoirs cast and the solution was embedded thermocouples, which revealed peak temperatures of 72 – 78°C.

After a two-year period test, some main procedures were established, and the patent was considered completely adapted. Thermal control and curing procedures were enhanced by shifting casting operations to 04:00 – 10:00, limiting fresh concrete temperature to ≤ 30°C through ice-cooled mixing water, shaded aggregate stockpiles, and insulated cement silos, while an automated fog-misting system maintained curing conditions for at least 72 hours whenever ambient temperature exceeded 30°C or relative humidity dropped below 60%. As result of compressive strength at 3 days (fc,3) under conventional curing demonstrated a mean value of 18.4 MPa with a coefficient of variation of 22.3%, surpassing the target value of 15 MPa. Nevertheless, the elevated coefficient of variation indicates inadequate process control, with 8.7% of specimens falling below the 15 MPa limit established for demoulding.

This work also shows not only the importance of SWOT analysis but also the establishment of Milestones that allows the process optimization. Thus, a Roadmap was obtained and remained in place throughout the production of these towers.

4. References

[1] Assembly structure and procedure for concrete towers used in wind turbines, EUROPEAN PATENT SPECIFICATION, EP 1 889 988 B1, 08.11.2006.

*Corresponding author: wlimad@alumni.usp.br

TRANSESTERIFICATION REACTION CATALYZED BY NANOPOWDER CALCIUM OXIDE ASSISTED BY PLASMA

Vinicios E. Pinter, Maíra O. Palm, Diego A. Duarte, Rafael C. Catapan*
Federal University of Santa Catarina, Joinville, 89219-600, SC, Brazil

1. Introduction

Plasma-assisted transesterification reaction was investigated as an alternative process for biodiesel production, since it allows for milder conditions, decreasing both reaction temperature and time [1]. Conventional high-conversion processes commonly employ homogeneous base catalysts such as metal alkoxides or hydroxides for better reaction efficiency. However, heterogeneous base catalysts have advantages over homogeneous ones from both economic and environmental standpoints [2]. Therefore, this article proposes the use of plasma discharge for the transesterification of soybean oil catalyzed by calcium oxide nanocatalyst.

2. Experimental

For catalyst synthesis, waste eggshells were collected, washed, and ground (<400 mesh) and calcined at 1000 °C for 90 minutes to produce CaO. Based on commonly reported conditions for CaO-catalyzed methanolysis, the operating point was 3 wt% of CaO (relative to oil), a 9:1 methanol:oil molar ratio and 180 minutes [3]. Conventional reactions were performed at 65 °C under vigorous stirring, while the plasma-assisted runs were carried out at room temperature without stirring for the same duration, with the DBD system operated at 7.8 kV and 60 Hz (fig. 1). Post-reaction procedures included phase-separation, washing, and drying steps for further analysis. FAME (Fatty Acid Methyl Ester) yield was quantified by gas chromatography (Agilent 8860 GC coupled to an Agilent 5977C MS) according to the European Standard EN 14103.

3. Results and Discussion

The transesterification reactions performed in the DBD plasma reactor showed a maximum yield of 89.84%, slightly higher than the 87.23% achieved using the conventional method under identical feed composition. Those results show the potential use of plasma technology for biodiesel production, in agreement with previous studies [1]. The successful conversion observed in both systems confirms that the catalyst synthesis route was effective in producing an active material from a low-cost waste source. A key distinction of the plasma system is the absence of mechanical stirring, meaning that mass transfer relies on plasma-induced effects rather than conventional mixing. Interestingly, during plasma operation, the initially undissolved catalyst progressively dissolved in the reaction medium, indicating enhanced dispersion or possible formation of reactive species promoted by plasma activation (fig. 2).

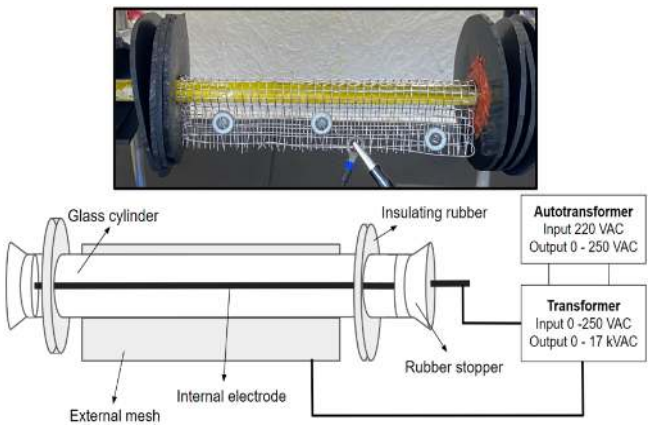


Fig. 1. *DBD reactor setup*

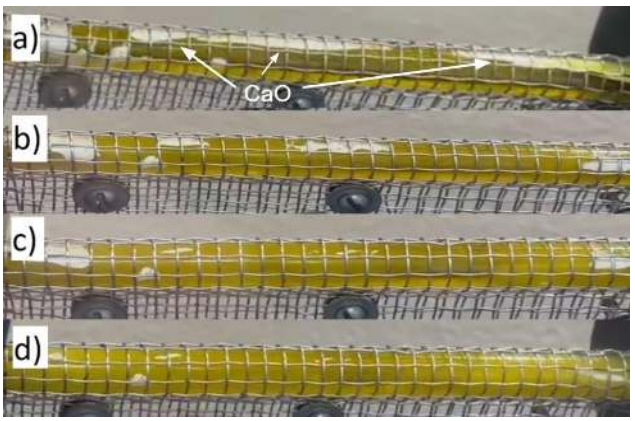


Fig. 2. *Catalyst dispersion under DBD plasma: (a) 0 s, (b) 20 s, (c) 1 min, and (d) 2 min.*

4. References

[1] M. O. Palm *et al.*, Fuel, 400 (2025) 135686.
[2] S. M. Farouk *et al.* Environmental Science and Pollution Research (2024) 31:12722–12747
[3] Z. Wei *et al.,* Bioresource Technology 100 (2009) 2883-2885.

Acknowledgments

This work was supported by CNPq (Grant numbers 405818/2022-0)
*Corresponding author:

ELECTROSTATIC STUDY OF CAPACITIVE COUPLING IN REMOTE PLASMA JET SYSTEMS

Júlia Karnopp[1]*, Julio César Sagás[1]

[1]*Universidade do Estado de Santa Catarina (Udesc), Graduate Program in Physics, Laboratory of Plasmas, Films and Surfaces, Joinville, SC, Brazil*

1. Introduction

Atmospheric pressure plasma jets (APPJs) have attracted significant attention due to their ability to generate reactive species at near-ambient conditions. In particular, remote plasma jet configurations [1], where a secondary plasma is ignited downstream from a primary dielectric barrier discharge (DBD) through a floating metallic wire, offer enhanced flexibility and safety for applications such as in situ functionalization during 3D printing [2]. However, the physical mechanisms governing the electrical coupling between the primary and secondary plasmas, especially the role of the floating wire potential, remain not fully understood. This work aims to investigate the electrical behavior of such systems as a preliminary step toward fully coupled plasma modeling.

2. Methodology

The system under study consists of a primary dielectric barrier discharge (DBD) operating at atmospheric pressure, where the plasma is generated between an energized electrode in contact with a dielectric layer and a metallic wire. The metallic wire, electrically floating and inserted along the gas flow path, connects the primary discharge region to a secondary (remote) plasma can be ignited. A multi-stage numerical approach was developed using COMSOL Multiphysics. A two-dimensional electrostatic model was implemented to analyze the electric field distribution and estimate the floating potential of the metallic wire under different applied voltages.

3. Results and Discussions

The electrostatic analysis shows that the floating wire potential follows the applied sinusoidal voltage, reaching approximately 48% of its peak value. This behavior is consistent with a capacitive coupling mechanism, in which the primary and secondary discharge gaps act as a series capacitor system, and the wire potential is established through displacement currents. As shown in Fig. 1, increasing the applied voltage amplitude leads to a proportional increase in the floating potential, while preserving a nearly sinusoidal waveform.

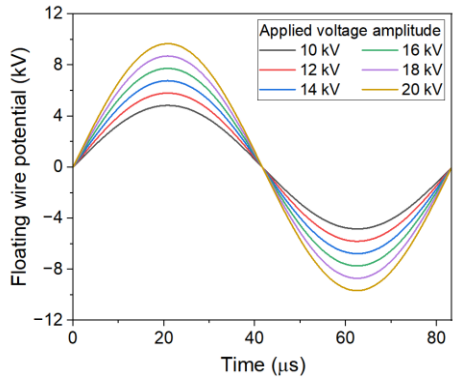


Fig. 1. *Floating wire potential as a function of time for different applied voltage amplitudes.*

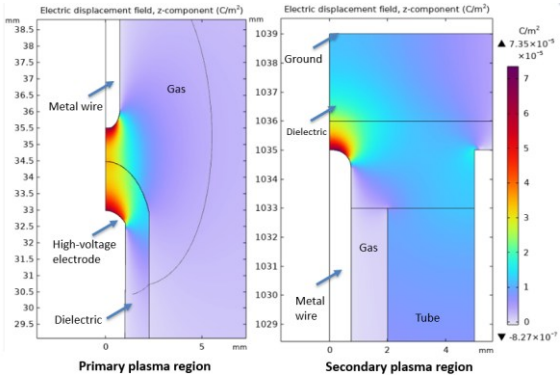


Fig. 2. *Electric displacement field (z-component) distribution in the plasmas regions.*

The electric displacement field distribution (Fig. 2) further confirms that field enhancement occurs near electrode edges and dielectric interfaces, identifying the regions where plasma ignition is most likely. These results demonstrate that, in the absence of plasma, the system behavior is governed by capacitive coupling and displacement currents, providing a consistent basis for predicting the conditions required for remote plasma ignition.

4. References

[1]- K. G. Kostov, *et al*. Plasma Sources Sci. Technol. **24**, 025038 (2015).
[2]- A. C. Fernandes, *et al*. Progress In Additive Manufacturing, **11,** 2123-2139 (2025).

Acknowledgments

The authors are grateful for the financial support provided CNPq, process number 176717/2023-4.

*Corresponding author: julia_karnopp@outlook.com

PLASMA-SUBSTRATE INTERACTIONS DURING LOW-VACUUM PLASMA TREATMENT OF THERMOPLASTIC STARCH FILMS FOR CHITOSAN COATING RETENTION

Diuly Effgen[1]*, Francisco Alfaro[1], Helton José Wiggers[1], Diego Mantovani[2]
[1]*Associação de Ensino, Pesquisa e Extensão Biopark, Laboratory for Biomaterials and Bioengineering*
[2]*Université Laval, Laboratory for Biomaterials and Bioengineering*

1. Introduction

Polysaccharide-based films are promising sustainable materials for biodegradable packaging [1,2]. Thermoplastic starch (TPS) is low-cost and abundant, chitosan coatings can add functional value, although stable retention remains challenging. Low-vacuum plasma treatment may improve TPS wettability and introduce reactive groups, enhancing coating adhesion [3]. We hypothesize that TPS also alters plasma chemistry through the release of volatile species. This study investigates plasma-treated TPS films by OES, correlating plasma–substrate interactions with wettability and chitosan retention.

2. Experimental

TPS films were treated in a low-vacuum reactor using argon and oxygen plasmas. The system was evacuated for ~1 h, followed by argon purge (90 sccm, 10 min). Argon plasma was applied at 15 sccm and 30 W for 30 s, and oxygen plasma at 15 sccm and 30 W for 45 s. After treatment, films were coated with 1% chitosan and rinsed. Wettability was evaluated by water contact angle, and chitosan retention by the Orange II method. OES spectra were recorded 10 s after ignition, with and without TPS, and emission line ratios (OH, O, N_2, Hα, Ar) were used to assess plasma chemistry and excitation changes.

3. Results and Discussions

Low-vacuum plasma treatment increased TPS wettability, reducing WCA from ~90° to 25°, and enhanced chitosan retention (19.4 to 50.8 µg/mL, ~2.6×) (Figure 1). OES showed that TPS modified plasma emission even under identical conditions. In oxygen plasma, OH/O(777) and OH/O(844) ratios increased by 62% and 114%, while N_2(337)/OH decreased by 51%. In argon plasma, OH/O ratios increased by 82% and 121%, and Ar(750)/Ar(811) increased by 36%, indicating changes in excitation.

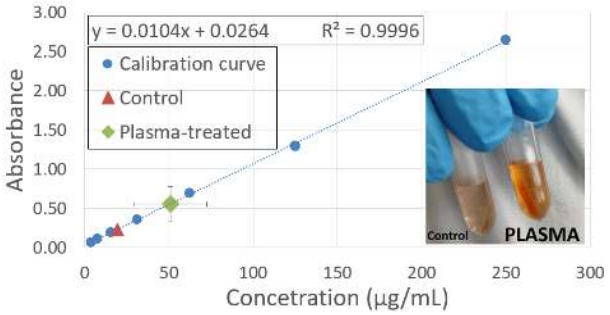


Fig. 1. *Orange II calibration curve and visual comparison between control and plasma-treated TPS films after reaction with Orange II dye.*

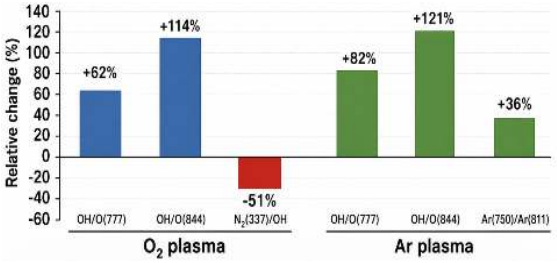


Fig. 2. *Values represent the relative variation observed with TPS films inside the reactor compared with plasma without TPS.*

These results suggest that TPS releases volatile species, increasing hydrogen-related emissions and actively influencing plasma chemistry. Overall, plasma treatment improves wettability and coating retention, while OES reveals plasma–substrate interactions.

4. References

[1]- S. Siciliano, C. G. Lopresto, O. Mileti and M. G. De Paola, Food Bioscience, 73, 107652, (2025).
[2]- C. L. Luchese, J. M. F. Pavoni, N. Z. Dos Santos, L. K. Quines, L. D. Pollo, J. C. Spada and I. C. Tessaro, J. Food Sci. Technol., 55, 2963, (2018).
[3]- G. Primc and M. Mozetič, Materials, 17, 1494, (2024).

Acknowledgments

BIOPARK, Prati–Donaduzzi Pharmaceutical Industry, the Natural Sciences and Engineering Research Council of Canada, and CNPq 408919/2023-0. The authors also thank Carmen Donaduzzi, Ph.D., and Luiz Donaduzzi, Ph.D., for support and guidance.

*Corresponding author: diulysearch@gmail.com

MODELING OF A HIGH-VACUUM SYSTEM WITH CUBOID GEOMETRY USING THE MONTE CARLO METHOD

Samuel da Silva Lima[1]*, Regina Maria Ricotta[2] and Francisco Tadeu Degasperi[2]
[1]*Polytechnic School of the University of São Paulo*
[3]*São Paulo College of Technology – CEETEPS – São Paulo – SP*

1. Introduction

Numerous modern technologies and scientific experiments rely on environments with extremely low particle concentrations, making vacuum science fundamental to both academic and industrial development. [1,2] While tubular systems are extensively studied and modeled, there is a growing need to validate simulation methods for non-tubular geometries. The objective of this work is to model a high-vacuum system with cuboid geometry (2D) to verify whether the Monte Carlo method is capable of modeling multidimensional systems. [1,2]

2. Experimental

The computational modeling was conducted using Molflow+ software, developed at CERN, which employs the Test-Particle Monte Carlo (TPMC) method to simulate gas behavior in the molecular flow regime. The modeled system features a cuboid geometry with dimensions of 30 cm in length, 20 cm in width, and 0.5 cm in height, including a 1 cm diameter pumping orifice. Input parameters included a temperature of 293 K and an outgassing rate of $1 \times 10^{-8}\ mbar.L.s^{-1}.cm^{-2}$. The simulation tracks virtual particle trajectories based on the Maxwell-Boltzmann distribution and Knudsen's law for particle emission from surfaces.

3. Results and Discussions

The simulation results obtained in Molflow+ yielded the pressure field and a comprehensive map of the pressure distribution within the cuboid system. The minimum-recorded pressure was approximately $2.6 \times 10^{-6}\ mbar$, while the maximum pressure reached $4.1 \times 10^{-6}\ mbar$. The visualization of the pressure field demonstrated a physically and mathematically consistent behavior for the proposed geometry, validating the use of the Monte Carlo method for two-dimensional vacuum systems. These results will serve as a foundation for future analytical comparisons using the multidimensional diffusion equation.

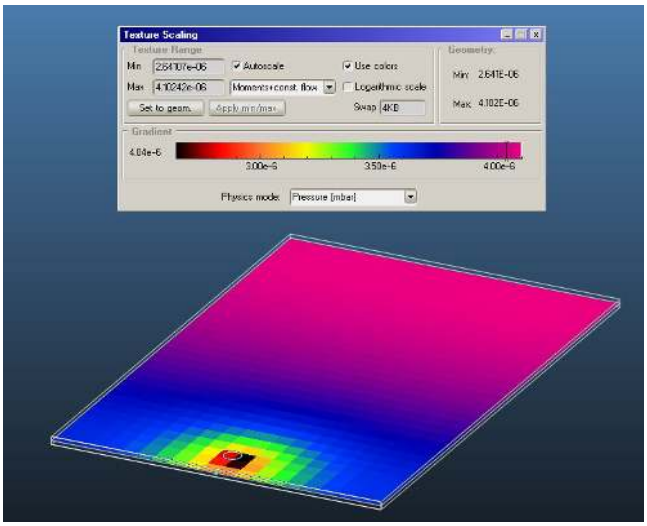


Fig. 1. *Molflow+ simulation of the high-vacuum system featuring a cuboid geometry.*

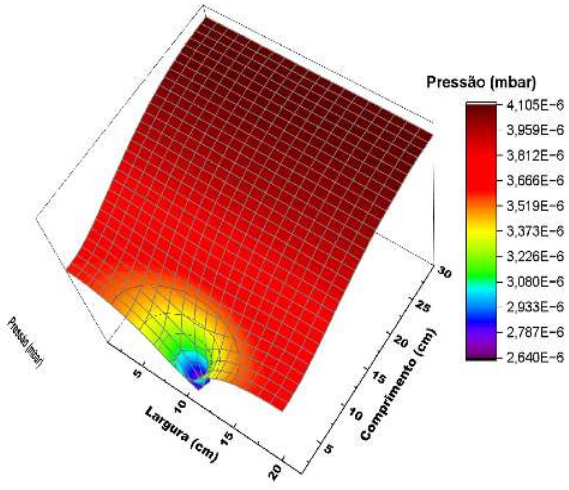


Fig. 2. *Pressure field of the high-vacuum system with cuboid geometry.*

4. References

[1] - F. T. Degasperi, "Contribuições para a Análise, Cálculo e Modelagem de Sistemas de Vácuo," PhD Dissertation, University of Campinas (UNICAMP), (2006).
[2] - S. S. Lima, "Método de Monte Carlo Aplicado a Modelagem de Sistemas Tubulares de Alto Vácuo," Undergraduate Thesis, São Paulo College of Technology (Fatec-SP), (2025).

Acknowledgments

The author would like to thank CNPq for the awarded PIBIC scholarship.

*samuellima09@usp.br

METHOD-DEPENDENT ANTIMICROBIAL EVALUATION OF PLASMA-TREATED SURFACES

Carla Catharina Joner Heck[1]*, Francisco Alfaro[1], Diego Mantovani[2], Helton José Wiggers[1]
[1]*Laboratório de Biomateriais e Bioengenharia (LBB-BPK), Biopark Educação, Toledo, PR, Brazil;*
[2]*Laboratory for Biomaterials and Bioengineering (LBB-Ulaval), Laval University, Quebec, Canada*

1. Introduction

Over the years, antibacterial surfaces have gained importance due to the prevalence of microorganisms, their role in disease, the rise of antibiotic resistance, and the ability of surfaces, especially in medical devices, to support biofilms that increase microbial tolerance [1]. Plasma-based surface modification techniques have gained considerable attention for the development of functional surfaces, these treatments can alter surface chemistry, roughness, wettability, and energy without affecting the bulk properties of the material. Consequently, plasma-engineered surfaces have emerged as promising strategies for biomedical devices, coatings, and advanced materials requiring controlled antibacterial activity [2]. Usually, plasma-based surface modifications affect only nanometric depths, which makes the microbiological evaluation of these materials particularly challenging, since small variations in testing conditions may significantly influence the observed antibacterial performance. In this context, the standardization of protocols is of utmost importance to ensure reproducibility and reliable comparison between studies.

2. Experimental

The objective of this study is to establish a microbiological evaluation framework for plasma-engineered antibacterial surfaces, emphasizing how surface functionalization and the choice of testing methodology influence the observed antimicrobial performance. To this end, chitosan films treated with cold plasma treatment (CPT) were evaluated using standard methods, such as disk diffusion and ASTM E2922-23, as well as an alternative method, named droplet method. Untreated chitosan films were used as control surfaces and paper disk were used as negative controls, while argon/oxygen plasma-treated samples (Sample 1) and nitrogen plasma-treated samples (Sample 2) were comparatively investigated.

3. Results and Discussions

Preliminary results showed that the samples produced no inhibition halo in disk diffusion tests and no detectable antimicrobial activity in ASTM assays. However, the droplet method revealed distinct behaviors depending on the plasma treatment applied. Compared to the untreated control, chitosan films treated with $Ar + O_2$ plasma exhibited a noticeable reduction in bacterial colonies, corresponding to an approximate reduction of 49% relative to the untreated surface. In contrast, chitosan films treated with N_2 plasma showed an increase in bacterial growth compared to the control. These findings demonstrate the method-dependent nature of antimicrobial assessment, where confined and high-contact conditions in the droplet assay amplify the effectiveness of contact killing mechanisms compared to diffusion- or transfer-based methods. Further experiments are ongoing to complete the evaluation and validate the proposed framework.

4. References

[1] T.A. De Vries and M.A. Hamilton, Quant. Microbiol. 1, 29 (1999)
[2] I. Niedźwiedź et al., Pol. J. Microbiol. 68, 153 (2019)
[3] ASTM E2922-23, ASTM International (2023)

Acknowledgments

Biopark, Prati-Donaduzzi, CNPq 408919/2023-0, Natural Science and Engineering Research Council of Canada (Discovery and Alliance programs), Dr. Carmen Donaduzzi and Dr. Luiz Donaduzzi for guidance throughout the project.

*Corresponding author: place the e-mail of the corresponding author here (bookman old style 9 pt)

ANTIMICROBIAL ACTIVITY OF CARVACROL AND ZINC NANOPARTICLES IN POLYLACTIC ACID AND STARCH BLENDS

Maria Clara Hasper de Souza[1]*, Cecilia Zorzi Bueno[1], Diego Mantovani[2], Helton José Wigger[1]
[1]*Laboratory of biomaterial and bioengineering, BIOPARK*
[2]*Laboratory of biomaterial and bioengineering, Laval University*

1. Introduction

The environmental impact of petroleum-based plastics has driven the development of biodegradable materials for food packaging. Polylactic acid (PLA) exhibits good mechanical properties, while thermoplastic starch (TPS) is low-cost and biodegradable, thus, their combination aims to balance performance and sustainability [1]. However, their immiscibility limits interfacial adhesion and overall properties. In this study, Pluronic F127 was used as a compatibilizer [2] and zinc oxide nanoparticles (ZnO) [3] and carvacrol as an antimicrobial agent in PLA/TPS films.

2. Experimental

Blends containing 50:50 of starch and PLA were compatibilized with Pluronic F127 as control and prepared by casting. Three different formulations were produced: 10% of carvacrol (C10), 10% of zinc oxide (Z10) and 10% carvacrol and 10% zinc oxide combined (CZ10), to promote antimicrobial activity. The films were characterized by swelling, mass loss and antimicrobial activity against *S. aureus* by direct contact determining the log reduction. The data were expressed as mean ± standard deviation and analyzed using one-way analysis of variance (ANOVA), followed by Tukey's post hoc test for multiple comparisons. Differences were considered statistically significant when $p < 0.05$.

3. Results and Discussions

Mass loss was not significantly affected by the incorporation of the active compounds, as the samples did not differ statistically from each other, maintaining values close to 16%. In contrast, swelling behavior was strongly influenced by the formulation composition. C10 films exhibited the highest swelling percentage (46.50% ± 4.77), while Z10 showed the lowest value (23.14% ± 3.41). Interestingly, CZ10 films demonstrated that the combination of both actives resulted in the swelling similar to the control groups, presenting intermediate swelling value (30.59 ± 3,12). These findings demonstrate that combining the actives may contribute to improved physicochemical stability while maintaining controlled hydration properties. Z10 films did not show antimicrobial activity, C10 films performed great antimicrobial results against gram positive bacteria, *S. aureus*, with a log reduction of 4,07 corresponding to 99,99% growth inhibition and CZ10 films promoted a log reduction of 7,39 being able to inhibit 100% of bacteria growth. The enhanced antibacterial effect observed for CZ10 suggests a synergistic interaction between the active compounds, leading to greater bacterial susceptibility and improved film functionality. Therefore, the combined formulation proved to be the most promising system, as it associated controlled swelling behavior with superior antimicrobial efficiency, indicating potential applicability as an active packaging.

4. References

[1] K. Hamad, M. Kaseem, F. Deri "Polylactic acid blends: The future of green, light and tough", Progress in Polymer Science, 85, 83–127, (2018).
[2] A. Fonseca-García, B. Hernández Osorio, R. Y. Aguirre-Loredo, H. L. Calambas and C. Caicedo, Carbohydr. Polym. 293, 119744 (2022).
[3] G. Kasi, K. Sadeghi, S. Thanakkasaranee and J. Seo, *Polymers* 11, 1427 (2019).

Acknowledgments

The authors would like to thank Biopark Educação,CNPq 408919/2023-0, the Biomaterials and Bioengineering Laboratory team at Biopark, and the Biomaterials and Bioengineering Laboratory at Université Laval for their support and contributions to this work.

*e-mail: maria.hasper.bpk@gmail.com

METROLOGICAL PRESSURE SYSTEM: MERCURY MANOMETER, VACUSTAT™, BOURDON PRESSURE GAUGE, CAPACITIVE MEMBRANE PRESSURE AND MICRO PIRANI™VACUUM TRANSDUCER.

Caroline Mendes da Silva[1], Francisco Tadeu Degasperi[2]
[1] [2]*Faculdade de Tecnologia de São Paulo - FATEC-SP – CEETEPS São Paulo - SP*

1. Introduction

Pressure metrology is essential in vacuum systems, where precise measurements ensure process control and equipment performance[1]. This work presents the assembly of a metrological bench for vacuum pressure measurement, using a mercury manometer, Vacustat™, capacitive membrane pressure gauge and Bourdon gauge, covering a range from range from 1.33×10^{-3} Pa to 7×10^{7}Pa.

2. Experimental

The metrological bench was assembled with five pressure measuring instruments, covering different operating ranges. The mercury manometer, used as a primary standard, operates from 10^{2} Pa to 10^{5} Pa. The Vacustat™ covers the medium vacuum range, from 4 Pa to 4×10^{-2} Pa. The Bourdon gauge operates from 6×10^{4} Pa to 7×10^{7}Pa, for pressures above atmospheric. The capacitive membrane gauge ranges from $1x10^{-4}$ Pa to 1×10^{5} Pa. The Micro Pirani™ transducer operates from 1.33×10^{-3} Pa to atmospheric pressure ($\sim 1,013 \times 10^{-5}$ Pa). To date, two instruments have been tested: the mercury manometer and the Vacustat™. For the mercury manometer, a mechanical pump was used to reduce pressure, and a digital ruler was employed to accurately measure the meniscus position. Atmospheric pressure reference data were obtained from the IAG/USP Meteorological Station (www.estacao.iag.usp.br), and application Meteum tempo, used to validate the measurements. The Vacustat™ was tested for mercury leakage using a pump vacuum.

3. Results and Discussions

After assembling the bench structure, the mercury columns were cleaned with isopropyl alcohol and all necessary seals were applied. A leakage and tightness test was performed without mercury to verify the system integrity. After that, mercury was added to the columns and the first measurements were performed. Five or more readings were taken on each side of the column to establish a reliable baseline. Column I presented a relative error ranging from -0.23% to +1.26% against the IAG-USP reference and from -0.47% to +0.91% against INMET. For Column II, the relative error ranged from -0.92% to +1.57% and from -1.07% to +1.21%, respectively. The mean of both reference stations was used for graphical comparison, as they are independent stations with a difference below 5 hPa. Observed variations may be attributed to weather conditions during the experiment. The relative error was adopted as the comparison method between measured values and meteorological references, following the GUM guidelines [2]. The Vacustat™ was tested using a Pfeiffer Alcatel 2005 SD pump, yielding 6.67 Pa.

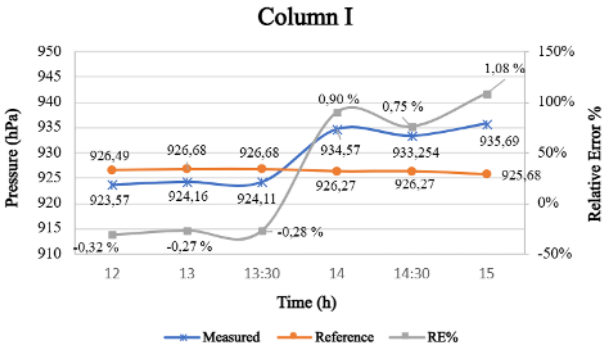


Fig.1. *Pressure Comparison — Column I*

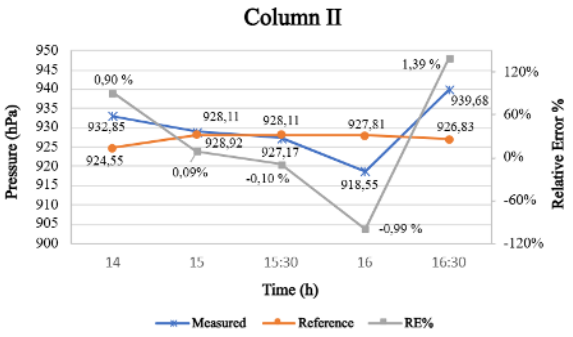


Fig.2. *Pressure Comparison — Column II*

4. References

[1]- JOUSTEN, Karl.Handbook of Vacuum Technology. 2ª ed.Weinheim:Wiley-VCH, 2008.1050 p.
[2]- BIPM et al. Guia para a Expressão de Incerteza de Medição — GUM. 1. ed. brasileira. Rio de Janeiro: INMETRO, 2012.

Acknowledgments
I would like to thank CNPq for the PIBIC scholarship granted.

caroline_silva72@hotmail.com

CUSTOM-DESIGNED PERMEABILITY APPARATUS FOR GAS BARRIER CHARACTERIZATION UNDER CONTROLLED VACUUM-ATMOSPHERE CONDITIONS

Hugo Alexandre Garrido Aguiar[1], Rondes Ferreira da Silva Torin[1,2*], Carlos Fernandes da Silva[2], Silvia Pierre Irazusta[1,3],Francisco Tadeu Degasperi[1,4].

[1]Postgraduate Program in Management and Technology in Productive Systems, (CGPEP), State Center for Technological Education Paula Souza (CEETEPS), São Paulo, Brazil.; [2]Faculty of Technology of Mauá – CEETEPS; [3]Faculty of Technology of Sorocaba - CEETEPS; [4] Faculty of Technology of São Paulo – CEETEPS

1. Introduction

Gas barrier performance is a critical parameter in dense and semi-permeable membranes, directly governing mass transfer resistance to O_2, CO_2, H_2O, and other gaseous species. Reliable permeability measurements are therefore essential for the development, qualification, and optimization of membrane materials for several applications, including packaging films for food, pharmaceutical, and industrial uses [1]. Accurate assessment of this behavior requires experimental systems capable of maintaining controlled pressure gradients, leak-tight sealing, thermal stability, and reproducible test conditions. In this context, the developed system enables the determination of gas transport parameters using a manometric pressure-difference approach with a calibrated downstream volume, consistent in general with the principles established in ASTM D1434. The proposed apparatus was developed as a cost-effective and versatile alternative for laboratory-scale gas barrier evaluation of membranes and films, particularly packaging films, with emphasis on mechanical robustness and operational reliability.

2. Theory and experimental set up of permeability

Theory of permeability is based on diffusion phenomena, which are governed by the diffusion equation derived from Fick's law. The permeability apparatus consists of a dual-chamber cell separated by the test film, hermetically sealed between metallic flanges to define the effective permeation area. Figure 1 shows the schematic of the permeability apparatus. The transport process follows Fick's law and the diffusion equation, $J(x,t)=-D\cdot\partial C(x,t)/\partial x$ and $\partial C(x,t)/\partial t=D\cdot\partial^2 C(x,t)/\partial x^2$. The upstream chamber was pressurized with the test gas, while the downstream chamber, with a calibrated internal volume, was connected to a pressure monitoring system. Prior to testing, the downstream side was evacuated to ensure leak-tight conditions and minimize residual gases. Gas transmission through the film was quantified from the pressure increase recorded over time under controlled temperature conditions.

3. Results and Discussions

Figure 1 shows the vacuum-assisted gas permeation apparatus, composed of a dual-chamber membrane cell connected to a mechanical pre-vacuum system, pressure control valves, and vacuum gauges. Preliminary tests indicated low leakage and stable vacuum conditions during operation. Experimental measurements showed satisfactory sealing and repeatable pressure behavior. Figure 2 shows part of the vacuum-assisted configuration improved baseline stability and enhanced the detection of low gas transmission rates.

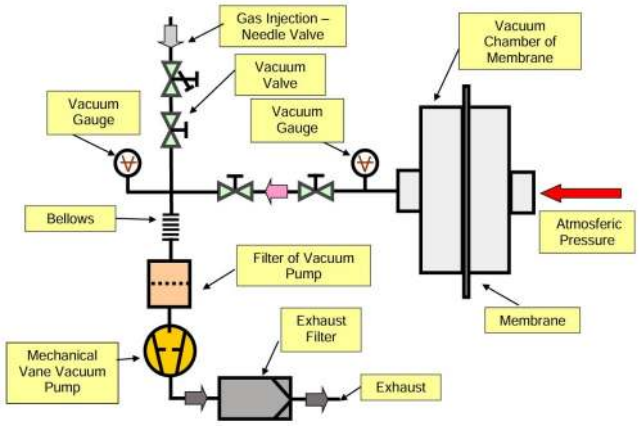


Fig. 1. ***Schematic set up of the permeability apparatus.***

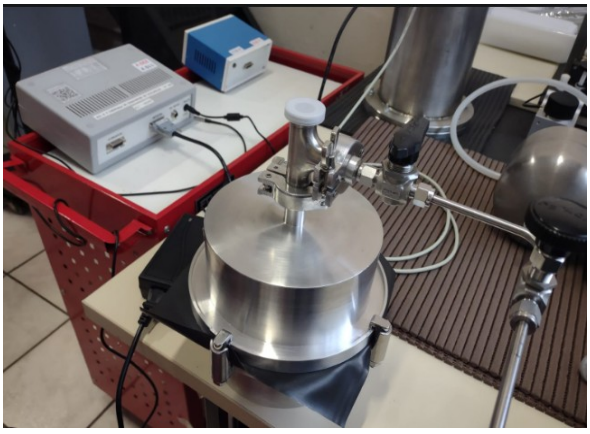


Fig. 2 Vacuum chamber s*et up of the permeability apparatus.*

4. References

[1] - P. Favia and R. D'Agostino, Surf. & Coat. Tech., **98**, 1102-1106, (1998).
[2] – Jousten, K. Editor. Handbook of Vacuum Technology. Second Edition. Wiley Book. 2015.

*rondes.torin@cps.sp.gov.br

LOW PRESSURE PLASMA FOR FABRIC DESINFECTION

Letícia Garrido Lorenz[1*], Alana Maria Corá[1], Tânia Aguiar Passeti[2] and Elidiane Cipriano Rangel[1]
[1]*Instituto de Ciência e Tecnologia – UNESP Campus Sorocaba*
[2]*Municipal University of São Caetano do Sul, R. Santo Antônio, 50, 09521-160, São Caetano do Sul, SP, Brazil*

1. Introduction

The search for efficient disinfection methods for fabrics remains a critical challenge. Low-pressure plasma has emerged as a promising, sustainable, and low-energy dry technique for this purpose. In this work it evaluated the effects of low-pressure plasma parameters, specifically working pressure and electrical configuration of the treatment, on the of N95 respirators fiber integrity.

2. Experimental

Blue and white N95 respirator layers were cut into 2 cm x 1 cm samples and treated in a capacitively coupled plasma at 13.56 MHz. The process was conducted with a 60% SF_6 and 40% O_2 gas mixture for 10 minutes, with working pressures ranging from 5 to 60 x 10^{-2} Torr. System base pressure ranged from 1.0 x 10^{-2} to 3.0 x 10^{-2} Torr. Samples were positioned on both grounded (upper) and driven (lower) electrodes to evaluate the effects of different electrical configuration of the treatment on the properties of the fibers. Surface morphology and elemental composition were respectively analyzed by scanning electron microscopy (SEM) and energy dispersive spectroscopy (EDS). The chemical structure of the fabric fibers was inspected by Fourier Transform Infrared spectroscopy (FTIR) whereas wettability was assessed by contact angle measurements.

3. Results and Discussions

SEM micrographs suggest that the structural integrity of the N95 polymeric fibers treated on the grounded electrode was preserved at all working pressures. The compositional maps shown in Figures 1 and 2 reveal a highly homogeneous elemental distribution across the treated surfaces. Carbon remained the predominant element, confirming that polymer degradation was not significant. Fluorine (F) functionalization was observed, with the fluorine content being influenced by both the plasma pressure and the electrical configuration. Regarding wettability, both fabrics exhibited a tendency toward increased hydrophobicity after treatment; however, the extent of this modification depended on the working pressure and the electrical configuration and evolved during aging under atmospheric conditions.

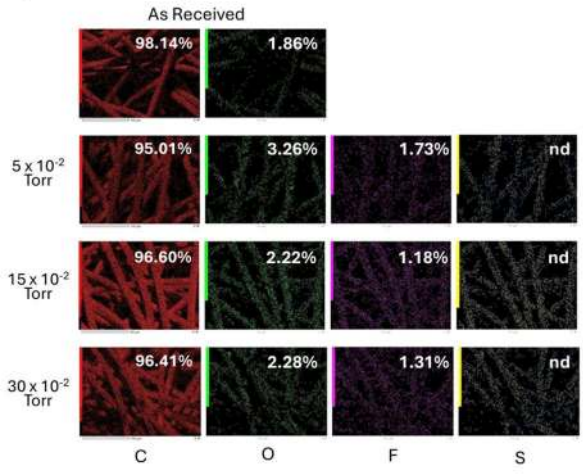


Fig. 1. *EDS compositional maps of the white N95 fabric treated on the grounded electrode as a function of working pressure.*

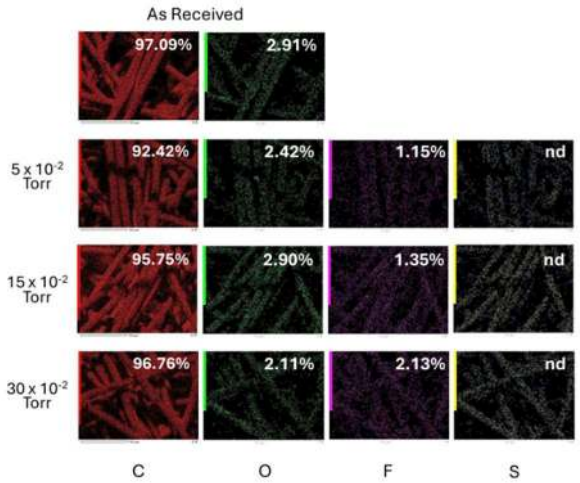


Fig. 2. *EDS compositional maps of the blue N95 fabric treated on the grounded electrode as a function of working pressure*

4. References

[1] - BERGMAN, M. S. ET AL. Evaluation of multiple (3-Cycle) decontamination processing for filtering facepiece respirators. Journal of Engineered Fibers and Fabrics, v. 5, n. 4, p. 33–41, (2010)

Acknowledgments

The authors thank LNNano/CNPEM, FAPESP (2025/05217-5), CNPq-PQ (306302/2021-7), CAPES (88887977646/2024 00), and rectory UNESP/PROPe—Call Process 08/2025 (22469) for financial support.

*Corresponding author: leticia.lorenz@unesp.br

POTENTIAL DISINFECTION OF FABRICS IN LOW-PRESSURE PLASMAS USING SODIUM CHLORITE AS A CHLORINE SOURCE

Maria Cláudia S. Batista[1], Alana M. Corá[1]*, Hilda G. A. Pinto[2], Silvia P. Irazusta[2], Tânia A. Passeti[3], Elidiane C. Rangel[1]

[1]Instituto de Ciência e Tecnologia – UNESP Campus Sorocaba, [2]Faculdade de Tecnologia de Sorocaba – FATEC/SO, [3]Universidade Municipal de São Caetano do Sul

1. Introduction

Respirators are widely used as protective barriers against contamination but are predominantly single-use devices, generating significant waste and environmental impact. This work proposes a new low-pressure plasma sterilization route for fabrics using sodium chlorite as a chlorine donor, aiming to enable their safe reuse.

2. Experimental

Face mask samples (2.0 cm × 1.0 cm) from the blue and white layers were contaminated with *Saccharomyces cerevisiae* and treated in a low-pressure plasma reactor using Ar/O_2 mixtures with Ar proportions of 2%, 20%, 40%, 50%, 60%, and 100%, while maintaining the O_2 proportion constant. Sodium chlorite ($NaClO_2$) was used as a chlorine donor in the plasma phase. Treatments were performed at 150 W for 10 min using a grounded upper electrode and a driven lower electrode, with the mask samples placed on the upper electrode and $NaClO_2$ on the lower electrode. Disinfection efficiency was evaluated by comparing fungal colony-forming units (CFUs) before and after treatment through serial dilution, agar plating, incubation at 25°C for 48 h, and CFU counting. Optical emission spectroscopy (OES) was used to identify plasma species, and cytotoxicity assays were performed under the same experimental conditions to evaluate potential plasma-induced cytotoxic effects on colony formation.

3. Results and Discussions

The OES spectra (Fig. 1) showed the formation of oxygenated, chlorinated, and hydrogenated species during plasma treatment. Species such as OH (519.4 nm), CO (483.0 nm), and H (434.0, 591.9, and 657.1 nm) were associated with interactions between the plasma and the polymeric constituents of the fabrics, while Cl (790.0 nm) and Cl^+ (482.0 nm) indicated the release of $NaClO_2$ fragments into the plasma phase. At lower Ar proportions, a higher relative concentration of oxygenated and chlorinated species, including O (614.6 nm), O_2^+ (526.4 nm), and O_2 (560.5 nm), was observed, indicating a more oxidizing environment and stronger surface etching effects. As the Ar proportion increased, the relative concentration of most reactive species decreased, modifying the plasma–surface interaction mechanisms. Despite these variations, the cell viability assays (Fig. 2) demonstrated high viability under all conditions, indicating that the treatment promoted surface modifications without inducing significant cytotoxic effects. CFU viability remained close to the positive control for both blue and white mask fabrics at all Ar/O_2 proportions tested.

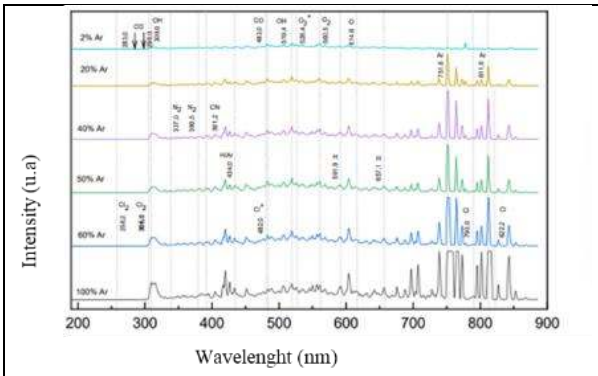


Fig. 1. OES of plasmas excited with Ar proportions ranging from 2 to 100%, acquired during the treatment.

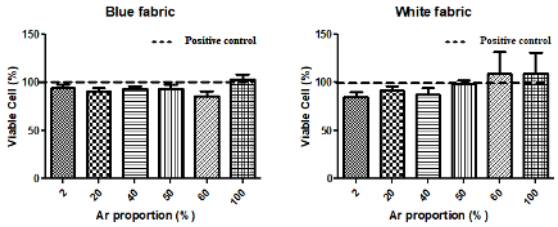


Fig. 2. Percentage of viable cell in function of argon proportion for blue and white fabrics

4. References

[1] HADDAD, M. B. et al. Science of The Total Environment, **798**, (2021)

Acknowledgments

The authors thank FAPESP (2025/05217-5), CNPq-PQ (306302/2021-7), CAPES (88887977646/2024 00), and rectory UNESP/PROPe—Call Process 04/2025 (1005/2025) for financial support.

*Corresponding author: alanacora@gmail.com


CBrAV
REALIZAÇÃO E ORGANIZAÇÃO
Sociedade Brasileira de Vácuo
BIOPARK EDUCAÇÃO
FINANCIAMENTO
ARAUCÁRIA
CIÊNCIA, TECNOLOGIA E INOVAÇÃO PARA O PARANÁ
CNPq
PATROCÍNIO
FCA BRASIL
SOLUÇÕES EM VÁCUO
HSENSOR
Inergiae
NITRETAÇÃO A PLASMA
ohmini
Quantum Design
Advancing Plasma-Based Technologies
PLASMIONIQUE
À l'Avant-Garde de Technologies Plasma